Scuola Dottorale in Scienze Matematiche e Fisiche

Dottorato di Ricerca in Fisica - XXVIII Ciclo

CKM matrix elements from K and D decays on the lattice

Dissertation submitted in partial fulfillment of the requirements for the degree of Doctor of Philosophy in Physics

by

Paolo Lami

Program Coordinator

Prof. Roberto Raimondi

Dissertation Advisor

Prof. Vittorio Lubicz

Prof. Silvano Simula

A Sandro

Acknowledgements

First of all I'd like to thank all the professors who followed me during my PhD, namely Vittorio Lubicz, Silvano Simula and Cecilia Tarantino for their irreplaceable support and their patience. I would also like to thank my colleagues and friends Lorenzo Riggio and Nuria Carrasco Vela for their precious collaboration.

A specific mention must go to my friend Eleonora Picca, who brought me down to Earth and showed me that there is something else beside academia. I should also thank my dear friend Mirko Poggi and my family, namely my parents and Andrea. I feel also thankful towards all the people who shared with me this long journey, namely Dr. Federico Brazzi, Dr. Alessandro Pilloni, Dr Gaia Camisasca, Dr. Margherita De Marzio, Dr. Alessandro Di Cicco, Dr. Francesca Paolucci and Dr. Gaia Silli.

Lastly, I really have no words to express the kind of support and help my boyfriend Sandro gave me during this year.

Contents

Introduction **iii**

1 The CKM matrix and how to calculate its elements **1**
The Cabibbo Kobayashi Maskawa Matrix 1
Leptonic decays of pseudoscalar mesons 6
Semileptonic decays of pseudoscalar mesons 7

2 Lattice QCD **11**
2.1 Lattice regularization 11
2.1.1 Gauge action 11
2.1.2 Fermionic action 13
2.1.3 Quenched approximation and dynamical fermions . . . 15
2.1.4 Monte Carlo Simulations 17
2.1.5 Hybrid Monte Carlo 18
2.2 Improvement 19
2.2.1 Symanzik procedure 20
2.2.2 Twisted Mass 21
2.2.3 Automatic improvement 22
2.2.4 Non-degenerate quarks 24
2.3 What to compute in Lattice QCD 24
2.3.1 Two-point correlation functions 25
2.3.2 Three-point correlation functions 27
2.4 The non-perturbative renormalization method RI-MOM . . . 28
2.5 Twisted boundary conditions 30
2.6 Simulation details 31
2.7 Lattice setup used in this analysis 32

3 Leptonic decay constants **37**
3.1 Calculation of the kaon decay constant 37

3.1.1 Mistuning of the strange and charm sea quark masses 41
3.1.2 Isospin breaking effect on the kaon decay constant . . 42
3.1.3 Determination of $|V_{us}|$ 47
3.2 Calculation of f_D, f_{D_s} and f_{D_s}/f_D 47

4 Vector and scalar form factors of K and D semileptonic decays 53
4.1 Vector and scalar form factors of $K_{\ell 3}$ decay 53
4.1.1 Preliminary analysis 53
4.1.2 Global fits 58
4.1.3 FSE evaluation 60
4.1.4 Discretization effects evaluation 62
4.1.5 Dispersive parametrization and experimental results . 63
4.2 Smearing with heavy quark masses 68
4.2.1 Gaussian Smearing 70
4.3 Vector and scalar form factors of the D semileptonic decay . . 72
4.3.1 The "fishbone" problem 73
4.3.2 Global fits 74
4.3.3 Calculation of V_{cd} and V_{cs} 77

Conclusions 81

Introduction

The Standard Model (SM) is the modern theory that best describes the fundamental interactions among particles. So far the SM has allowed physicists to obtain outstanding agreement between experimental data and theoretical predictions, the latest example being the discovery at ATLAS and CMS of a new particle [1, 2], which turned out to be the Higgs Boson [3].

Despite the success in describing fundamental particle physics, we know that the SM is not the final theory of interactions, but just a low-energy approximation of a more general theory. The fact that the SM doesn't provide a description of gravitational interaction is probably the most evident of its limits. Other problems in the SM are the hierarchy problem, the lack of a mechanism explaining the bariogenesis, the hierarchy of quark masses, the absence of a candidate for dark matter, the dark energy and finally its failure to precisely unify the strong and the electroweak forces together.

Many of these problems involve flavor physics, i.e. the branch of physics that studies the transitions between quarks of different flavors. It is thus of crucial importance to determine the fundamental parameters of flavor physics, which in the quark sector are the quark masses and the CKM matrix elements. These quantities, being quarks confined into the hadrons, are non directly measurable in the experiments. On the other hand, being fundamental free parameters of the SM, they aren't even predictable from theory alone. Therefore, a combination of experimental and theoretical inputs is required in order to determine these parameters.

The experimental inputs needed to calculate the elements of the CKM matrix are the decay rates of leptonic and semileptonic decays of pseudoscalar mesons. The theoretical expressions for these decay rates in fact depend on hadronic quantities and on the CKM matrix element. In the case of leptonic decays the relevant hadronic quantity is the decay constant, while in the case of semileptonic decay it is the vector form factor at zero 4-momentum transfer. Calculating numerically with lattice QCD (LQCD) these hadronic quantities and comparing with the experimental measurements allows us to

determine the CKM matrix elements. In the determination of these quantities, LQCD plays a primary role, being a non-perturbative approach based only on first principles. It consists in simulating QCD itself by formulating the action on a discrete and finite Euclidean space-time which allows for a numerical computation of the path integrals via Montecarlo methods.

In this thesis we present an accurate determination of the CKM matrix elements V_{us}, V_{cd} and V_{cs}, through the leptonic and semileptonic decays of K and D mesons. To this purpose we used the gauge configurations produced by the European Twisted Mass (ETM) Collaboration with four flavors of dynamical quarks ($N_f = 2 + 1 + 1$), which include in the sea, besides the light up and down quarks, assumed to be degenerate, also the strange and the charm quarks with masses close to their physical values. These gauge configurations were generated using the Iwasaki gauge action and the Twisted Mass action at maximal twist. We considered three different values of the lattice spacing and pion masses as low as $\simeq 210$MeV. The plan of this thesis is as follows:

- in Chapter 1 we will provide a brief description of the CKM matrix and of the pseudoscalar mesons decays studied to extract V_{us}, V_{cd} and V_{cs}.

- In Chapter 2 we will provide a brief description of Lattice QCD, and then we will describe the Twisted Mass action used in this work.

- In Chapter 3 we will descibe the first part of the original work of this thesis, namely the computation of leptonic decay constants f_K^+, f_{D_s} and f_{D_s}/f_D. Lattice data of decay constants was extracted from the two-point correlation functions of the mesons at rest. We then performed a chiral and continuum extrapolation of f_K, f_{D_s}/M_{D_s} and $(f_{D_s}/f_D)/(f_K/f_\pi)$ to get to the physical point. By combining these results we found

$$\begin{aligned} f_{K^+} &= 154.4(2.0)\,\text{MeV}, \\ f_{K^+}/f_{\pi^+} &= 1.184(16), \\ f_{D_s} &= 247.2(4.1)\,\text{MeV}, \\ f_{D_s}/f_D &= 1.192(22), \\ f_D &= 207.4(3.8)\,\text{MeV}. \end{aligned}$$

  This quantities are then combined with the experimental results for K and D mesons leptonic decays in order to calculate $|V_{us}|$, $|V_{cd}|$ and

$|V_{cs}|$. For the CKM matrix elements we obtain

$$\begin{aligned} |V_{us}|_{\text{lep}} &= 0.2271(31), \\ |V_{cd}|_{\text{lep}} &= 0.2221(67), \\ |V_{cs}|_{\text{lep}} &= 1.014(24). \end{aligned}$$

- In Chapter 4 we will descibe the second part of the original work of this thesis, namely the computation of semileptonic decay form factors of K and D mesons as functions of the 4-momentum transfer q^2. The main novelty of the analysis is the fact that we didn't limit ourselves to study the vector form factor at zero 4-momentum transfer, i.e. $f_+(0)$, instead we managed to study the whole dependence on q^2 of both f_+ and f_0 for all the decays we studied. Lattice data of the form factors was extracted from a combination of three-point correlation functions of the vector and scalar currents in the case of the $K_{\ell 3}$ decay, while we used only the vector current in the case of $D \to \pi \ell \nu$ and $D \to K \ell \nu$ decays. We then performed global fits of the form factors, analyzing their dependence on the lattice spacing, the light quark mass and the 4-momentum transfer in order to have a determination at the physical point of the form factors throughout the physical cinematical range accessible in experiments. Specifically, at $q^2 = 0$ we found the following results:

$$\begin{aligned} f_+(0)^{(K\to\pi)} &= 0.9684(66), \\ f_+(0)^{(D\to\pi)} &= 0.610(23), \\ f_+(0)^{(D\to K)} &= 0.747(22). \end{aligned} \tag{1}$$

  This quantities are then combined with the experimental results for K and D mesons semileptonic decays in order to calculate $|V_{us}|$, $|V_{cd}|$ and $|V_{cs}|$, for which we found

$$\begin{aligned} |V_{us}|_{\text{semilep}} &= 0.2234(16), \\ |V_{cd}|_{\text{semilep}} &= 0.2336(93), \\ |V_{cs}|_{\text{semilep}} &= 0.975(29). \end{aligned} \tag{2}$$

- In the conclusive chapter we will summarize our work and present some future perspectives.

Chapter 1

The CKM matrix and how to calculate its elements

The Cabibbo Kobayashi Maskawa Matrix

In this section we will describe the CKM matrix, and explain why it plays a crucial role in flavor physics.

In the Standard Model, we can easily see the necessity of the CKM matrix by studying the Lagrangian terms of the interaction between the Higgs field and the quark fields (expressed as interaction eigenstates):

$$\mathcal{L}_Y = -\lambda_d^{ij} \bar{Q}_L^i \phi d_R^j - \lambda_u^{ij} \bar{Q}_L^i \bar{\phi} u_R^j + h.c. \tag{1.1}$$

where Q_L^i represents the left-handed up-down quark doublet for a given generation, u_R^i and d_R^i are respectively the up and down right-handed spinors, λ_u and λ_d are the Yukawa couplings and ϕ is the higgs doublet, which in the unitary gauge is of the form

$$\phi(x) = \frac{1}{\sqrt{2}} \begin{pmatrix} 0 \\ v + h(x) \end{pmatrix}, \tag{1.2}$$

where v is the vacuum expectation value of the field and $h(x)$ is the field responsible for the excitation corresponding to the physical Higgs boson. The complex-valued matrices λ_u and λ_d are not necessarily hermitian and $i, j = 1, 2, 3$ are generation indices; unless one don't ask for a flavor conserving symmetry, the interactions with Higgs field are flavor changing.

It is always possible to diagonalize λ_u and λ_d by means of a redefinition

of the quark fields: a generic, complex valued matrix can be rewritten as

$$\begin{aligned} \lambda_u &= U_u D_u W_u^\dagger, \\ \lambda_u &= U_d D_d W_d^\dagger, \end{aligned} \tag{1.3}$$

where the matrices D are diagonal with positive eigenvalues while U and W are unitary matrices. By rescaling the left-handed and the right-handed quark fields with the relation

$$\begin{aligned} u_L^i &\to U_u^{ij} u_L^j \\ d_L^i &\to U_d^{ij} d_L^j \\ u_R^i &\to W_u^{ij} u_R^j \\ d_R^i &\to W_d^{ij} d_R^j \end{aligned} \tag{1.4}$$

the Yukawa lagrangian becomes

$$\mathcal{L}_Y^{(q)} = -m_d^i \bar{d}_L^i d_R^i \left(1 + \frac{h}{v}\right) - m_u^i \bar{u}_L^i u_R^i \left(1 + \frac{h}{v}\right), \tag{1.5}$$

where

$$m_{u,d}^i = \frac{1}{\sqrt{2}} D_{u,d}^{ii} v. \tag{1.6}$$

Proceeding this way, we have diagonalized the mass matrix in flavor space, i.e. the rescaled quark fields represent the mass eigenstates.

It is then interesting to see how the charged current changes under the rescaling of the quark fields,

$$J^{\mu\dagger} = \frac{1}{\sqrt{2}} \bar{u}_L^i \gamma^\mu d_L^i \to \frac{1}{\sqrt{2}} \bar{u}_L^i \gamma^\mu V_{CKM}^{ij} d_L^j, \tag{1.7}$$

where V_{CKM} is the *Cabibbo-Kobayashi-Maskawa* (CKM) [4, 5] flavor mixing matrix, defined as

$$V_{CKM} = U_u^\dagger U_d. \tag{1.8}$$

This matrix connects the interaction eigenstates (d', s', b') with the mass eigenstates (d, s, b):

$$\begin{pmatrix} d' \\ s' \\ b' \end{pmatrix} = \begin{pmatrix} V_{ud} & V_{us} & V_{ub} \\ V_{cd} & V_{cs} & V_{cb} \\ V_{td} & V_{ts} & V_{tb} \end{pmatrix} \begin{pmatrix} d \\ s \\ b \end{pmatrix} \tag{1.9}$$

Therefore, the mass eigenstates are different from the interaction ones and the charged current interaction mixes different flavors with weight V_{ij} in the mass eigenstates basis. It is worthwhile to underline that within the Standard Model the only flavor changing mechanism is represented by this matrix and that the V_{CKM} unitarity guarantees that there are no flavor changing neutral currents (FCNC) to first order in the weak interactions. The suppression of FCNC at higher orders, the so called GIM mechanism [6], is also a consequence of the unitarity of V_{CKM} and well represents what has been experimentally observed in nature.

In the case of 3 quark generations the CKM matrix is a 3×3 complex-valued matrix. Unitarity constraints and the possibility of arbitrarily choosing the quark fields phases allow us to remove many degrees of fredoom. Thus, we only need four real numbers, three angles and one phase, to describe the matrix. Once the number of independent physical parameters is known, one can introduce different equivalent parametrizations for that matrix. Each one of these parametrizations can be written as a product of three matrices. The most standard choice is the one which writes the matrix as follows:

$$V_{CKM} = \begin{pmatrix} 1 & 0 & 0 \\ 0 & c_{23} & s_{23} \\ 0 & -s_{23} & c_{23} \end{pmatrix} \begin{pmatrix} c_{13} & 0 & s_{13}e^{-i\delta} \\ 0 & 1 & 0 \\ -s_{13}e^{i\delta} & 0 & c_{13} \end{pmatrix} \begin{pmatrix} c_{12} & s_{12} & 0 \\ -s_{12} & c_{12} & 0 \\ 0 & 0 & 1 \end{pmatrix}, \tag{1.10}$$

which leads to

$$V_{CKM} = \begin{pmatrix} c_{12}c_{13} & s_{12}c_{13} & s_{13}e^{-i\delta} \\ -s_{12}c_{23} - c_{12}c_{23}s_{13}e^{i\delta} & c_{12}c_{23} - s_{12}s_{23}s_{13}e^{i\delta} & s_{23}c_{13} \\ s_{12}s_{23} - c_{12}c_{23}s_{13}e^{i\delta} & -c_{12}s_{23} - s_{12}c_{23}s_{13}e^{i\delta} & c_{13}c_{23} \end{pmatrix}, \tag{1.11}$$

where $s_{ij} = sin\theta_{ij}$, $c_{ij} = cos\theta_{ij}$ (θ_{12} being the Cabibbo angle) and δ is the phase. It's important to emphasize that if $\delta = 0$ the matrix becomes real and there is no CP violation in the quark sector (besides the possible tiny strong CP violation). Another interesting feature to notice is that CP violation is possible only in the case of three or more generations of quarks. In the old Cabibbo version of the theory, which involved only the first two generations of quarks, the mixing was a real rotation in flavor space and no CP violation was allowed. Moreover in order for CP violation to occur it is necessary that up-like and down-like quark masses are different because if this is not the case, by means of suitable unitary transformation, one could redefine the

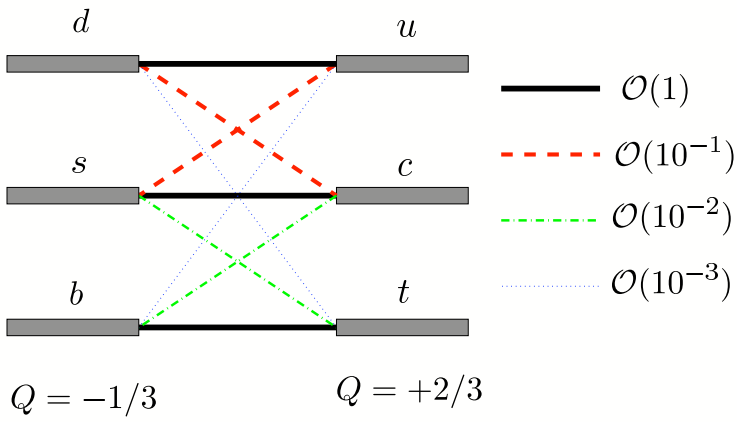

Figure 1.1: In this figure we show the hierarchy of charged currents flavor mixing transitions

quark fields in order to simplify the CP violating phase. It can be shown, in fact, that the necessary condition for having CP violation is

$$(m_t^2 - m_c^2)(m_t^2 - m_u^2)(m_u^2 - m_c^2)(m_b^2 - m_s^2)(m_b^2 - m_d^2)(m_d^2 - m_s^2) \times J_{CP} \neq 0, \tag{1.12}$$

where J_{CP} is the Jarlskog parameter [7, 8]

$$J_{CP} = |Im(V_{ij} V_{kl} V_{il}^* V_{jk}^*)|, \quad (i \neq k, j \neq l), \tag{1.13}$$

which provides a quantitative measurement of the amount of violation. As one can clearly see the amount of CP violation can be traced back to the quark mass hierarchy problem: fermion masses are in fact free parameters in the Standard Model.

The weak interaction mixes flavors according to a specific hierarchy: the diagonal elements of the CKM matrix describe transitions within the same generation and are bigger ($\sim \mathcal{O}(1)$) than off diagonal elements (from $\sim \mathcal{O}(10^{-3})$ to $\sim \mathcal{O}(10^{-1})$), which represent transitions between generations. This can be visually represented as in fig. (1.1) where transitions within the same generation are represented with bold black lines, while transitions between different generations are represented with dashed and dotted lines of different colors. This hierarchy in the CKM matrix can be seen more clearly in the Wolfenstein parametrization [9], which can be obtained by making the

substitutions

$$s_{12} = \lambda, \quad s_{23} = A\lambda^2, \quad s_{13}e^{-i\delta} = A\lambda^3(\rho - i\eta), \tag{1.14}$$

and expanding in povers of λ, thus obtaining

$$V_{\text{CKM}} = \begin{pmatrix} 1 - \frac{1}{2}\lambda^2 & \lambda & A\lambda^3(\rho - i\eta) \\ -\lambda & 1 - \frac{1}{2}\lambda^2 & A\lambda^2 \\ A\lambda^3(1 - \rho - i\eta) & -A\lambda^2 & 1 \end{pmatrix} + \mathcal{O}(\lambda^4). \tag{1.15}$$

As we already noted, the CKM matrix is unitary, i.e. it satisfies the relation

$$V_{CKM}^{\dagger} V_{CKM} = V_{CKM} V_{CKM}^{\dagger} = 1. \tag{1.16}$$

If expressed in terms of matrix elements, eq. (1.16) consists of nine relations, six of orthogonality and three of normalization. The former can be represented as six triangles in a complex plane, all having the same area $A_\Delta = J_{CP}/2$; using Wolfenstein parametrization for the CKM elements, it can be realized that only the triangles coming from the orthogonality of the first and third row and first and third column have sides of the same order of magnitude, $\mathcal{O}(\lambda^3)$; the two relations are

$$\begin{aligned} V_{ud}V_{ub}^* + V_{cd}V_{cb}^* + V_{td}V_{tb}^* &= 0 \\ V_{ud}V_{td}^* + V_{us}V_{ts}^* + V_{ub}V_{tb}^* &= 0. \end{aligned} \tag{1.17}$$

Actually, eqs. (1.17) are equivalent at order $\mathcal{O}(\lambda^3)$, which can be easily verified by substituting the expressions of the matrix elements in the Wolfenstein parametrization. Therefore at this order one has only one independent triangle and we will choose in the following the first one from the relations in eq. (1.17), which is known as the *unitary triangle* of CKM matrix. It is also possible to define the barred parameters $(\bar{\rho}, \bar{\eta})$ [**?**] in the following way

$$\rho + i\eta = \sqrt{\frac{1 - A^2\lambda^4}{1 - \lambda^2}} \frac{\bar{\rho} + i\bar{\eta}}{1 - A^2\lambda^4(\bar{\rho} + i\bar{\eta})}, \tag{1.18}$$

which represent the coordinates in the complex plane of the triangle apex. The associated triangle is shown in fig. (1.2), where sides and angles are defined as

$$\alpha = \phi_2 = arg\left(-\frac{V_{td}V_{tb}^*}{V_{ud}V_{ub}^*}\right) \tag{1.19}$$

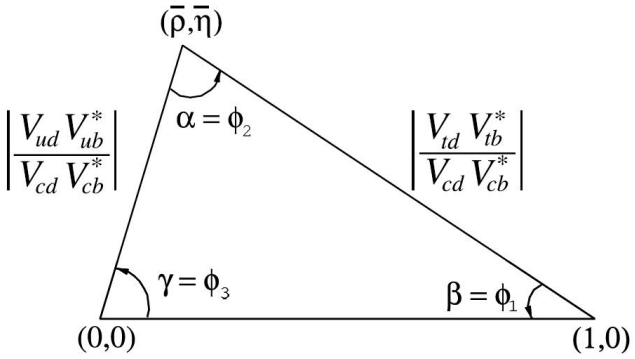

Figure 1.2: The unitary triangle

$$\beta = \phi_1 = arg\left(-\frac{V_{cd}V_{cb}^*}{V_{td}V_{tb}^*}\right) \tag{1.20}$$

$$\gamma = \phi_3 = arg\left(-\frac{V_{ud}V_{ub}^*}{V_{cd}V_{cb}^*}\right) \tag{1.21}$$

$$R_b = \frac{|V_{ud}V_{ub}^*|}{|V_{cd}V_{cb}^*|} \simeq \left(1-\frac{\lambda^2}{2}\right)\frac{1}{\lambda}\left|\frac{V_{ub}}{V_{cb}}\right| \tag{1.22}$$

$$R_t = \frac{|V_{td}V_{tb}^*|}{|V_{cd}V_{cb}^*|} \simeq \frac{1}{\lambda}\left|\frac{V_{td}}{V_{cb}}\right| \tag{1.23}$$

Leptonic decays of pseudoscalar mesons

Charged mesons can decay leptonically, i.e. into a charged lepton (anti-lepton) and the corresponding anti-neutrino (neutrino). In fig. (1.3) we show the Feynman diagram describing the process in which a generic pseudoscalar meson P decays into a lepton ℓ^+ and a neutrino ν_ℓ. Experiments can measure the decay rate, which is related to the product of the relevant CKM matrix element and a strong interaction parameter related to the overlap of the quark and antiquark wave-functions in the meson, called the decay constant. Let us consider the leptonic decay of a meson P; to lowest order in the electroweak interactions, we can write the decay rate as

$$\Gamma(P\to\ell\nu) = \frac{G_F^2}{8\pi}f_P^2 m_\ell^2 M_P\left(1-\frac{m_\ell^2}{M_P^2}\right)|V_{q_1q_2}|^2 \tag{1.24}$$

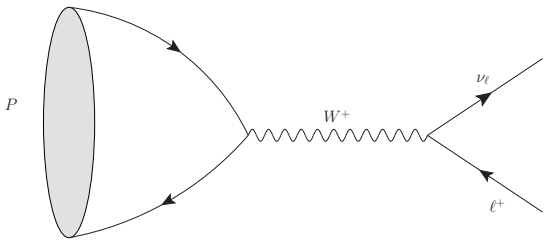

Figure 1.3: An example of a typical leptonic decay $P \to \ell^+ \nu_\ell$ in the Standard Model

Here M_P is the P mesons mass, m_ℓ is the lepton mass, $V_{q_1 q_2}$ is the CKM matrix element between the valence quarks q_1 and q_2 in the P meson, and G_F is the Fermi coupling constant. The parameter f_P is the decay constant, proportional to the matrix element of the axial current between the one-P-meson state and the vacuum,

$$i f_P q_\mu = \langle 0 | A_\mu(0) | P(q) \rangle \, . \tag{1.25}$$

The decay $P \to \ell\nu$ starts with a spin-0 meson, and ends up with a left-handed neutrino or right-handed antineutrino. By angular momentum conservation, the $\ell^+(\ell^-)$ must then also be left-handed (right-handed) if we neglect the small neutrino mass. In the $m_\ell = 0$ limit, the decay is forbidden, and can only occur as a result of the finite ℓ mass. This helicity suppression is the origin of the m_ℓ^2 dependence of the decay width.

Measurements of purely leptonic decay branching fractions and lifetimes allow an experimental determination of the product $|V_{q_1 q_2}| f_P$. If the CKM element is known from other measurements, then f_P can be measured. If, on the other hand, the CKM element is not known, a theoretical input for f_P allows a determination of the CKM element. As V_{ud} is quite accurately measured in super allowed β decays [10], measuremets of $\Gamma(\pi^+ \to \mu^+ \nu_\mu)$ yeld a determination of f_π, which has been used to set the scale in the lattice calculation presented in this thesis.

Semileptonic decays of pseudoscalar mesons

Semileptonic decays are processes in which the final state is composed by leptons and hadrons. A tipical semileptonic process involving a pseudoscalar meson P is the one in which it decays into a lighter meson P', a lepton (anti-

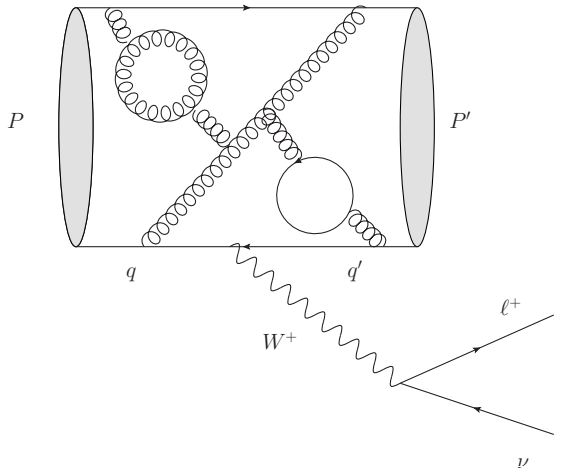

Figure 1.4: An example of semileptonic decay of a pseudoscalar meson $P \to P'\ell^+\nu_\ell$

lepton) and an anti-neutrino (neutrino). In fig. (1.4) we show the Feynman diagram of the process $P \to P'\ell^+\nu_\ell$. In this case the situation is more complicated with respect to the leptonic case, because of the composition of the final state. The Feynman amplitude for the process at lowest order in the weak interactions can be written as

$$A(P \to P'\ell^-\bar{\nu}_\ell) = -\frac{G_F}{\sqrt{2}} V^*_{q'q} \left\langle \ell^-\bar{\nu}_\ell | \bar{\nu}_\ell \gamma_\mu (1-\gamma^5)\ell | 0 \right\rangle \left\langle P' | \bar{q}\gamma^\mu (1-\gamma^5) q' | P \right\rangle \tag{1.26}$$

where $V_{q'q}$ represents the CKM matrix element corresponding to the two quarks involved in the transition. Limiting our attention to the case in which the J^P of the initial state is the same of the final state, i.e. a $0^- \to 0^-$ decay, the hadronic matrix element receives only the vector contribution and we obtain

$$A(P \to P'\ell^-\bar{\nu}_\ell) = -\frac{G_F}{\sqrt{2}} V^*_{q'q} V^\mu L_\mu, \tag{1.27}$$

where

$$V^\mu = \left\langle P'(k) | \bar{q}\gamma^\mu q' | P(p) \right\rangle, \tag{1.28}$$

$$L^\mu = \left\langle \ell\bar{\nu}_\ell | \bar{\ell}\gamma^\mu (1-\gamma^5)\nu_\ell | 0 \right\rangle. \tag{1.29}$$

The current describing the transition between the two mesons is a 4-vector. Thus it can be parametrized in terms of the only two independent 4-vectors

we have, i.e. the 4-momenta of the two mesons:

$$\left\langle P'(k)\left|V_\mu\right|P(p)\right\rangle = (k_\mu + p_\mu)f_+(q^2) + (p_\mu - k_\mu)f_-(q^2), \tag{1.30}$$

where f_+ is the vector form factor. It's also possible to define a scalar form factor as

$$f_0(q^2) = f_+(q^2) + \frac{q^2}{M_P^2 - M_{P'}^2} f_-(q^2), \tag{1.31}$$

and $q^\mu = k_\mu - p_\mu$ is the 4-momentum transfer.

The exclusive semileptonic decay rate of a process $P \to P'\ell\nu_\ell$ can be written as

$$\Gamma(P \to P'\ell\nu_\ell) = \frac{G_F^2 M_P^5}{192\pi^3} C_K^2 |V_{qq'}|^2 f_+(0)^2 I_{P\ell}, \tag{1.32}$$

where C_K is a Clebsch-Gordan coefficient, $f_+(0)$ is the vector form factor calculated at zero 4-momentum transfer and $I_{P\ell}$ is a phase-space integral that is sensitive to the momentum dependence of the form factors. If this integral is measured in the experiment, the knowledge of $f_+(0)$ allows us to determine the corresponding CKM matrix element.

Chapter 2

Lattice QCD

2.1 Lattice regularization

In 1974 Kenneth Wilson proposed a formulation of QCD on a lattice [11]. This intuition paved the way for non perturbative numerical calculation in particle physics. The QCD formulation that is useful to regularize on the lattice is based on path integrals, which allow us to identify correlation functions and physical observables with infinite-dimensional integrals. In lattice QCD space-time is discretized so that path integrals become finite-dimensional, and thus computable numerically. The presence of a lattice represents a regularization of QCD, i.e. it automatically gets rid of the divergencies which are so rampant in QFT. Moreover, performing a rotation from a Minkowskian space-time to a Euclidean one transforms Feynman integrals into something that looks exactly like a partition function of a statistical mechanics system.

Lattice QCD simulations are performed at finite values of the lattice spacing a and of the Volume V. Thus any quantity calculated on the lattice must be studied in the limits $a \to 0$ and $V \to \infty$ so that it represents the corresponding physical quantity in a continuum space-time. Practically speaking, simulations are performed at *several* values of a and V in order to extrapolate to the continuum limit and to evaluate *finite size effects* through the use of Chiral Perturbation Theory.

2.1.1 Gauge action

In order to discretize the gauge action it's necessary to introduce an object called *Link*:

$$U_\mu(n) = U_{n,n+\mu} = e^{ig_0 a A_\mu(n)}, \tag{2.1}$$

where n represents the lattice point considered, μ is the direction of the link and g_0 is the bare coupling of our theory. The quantity $A_\mu(n)$ can be written as

$$A_\mu(n) = \sum_c A_\mu^c T_c, \tag{2.2}$$

where c is the color index and T_c are the SU(3) generators in the adjoint representation. Links can then be used to define the gauge field action in a theory with a SU(N) simmetry:

$$S_G^{(SU(N))} = \beta \sum_P \left[1 - \frac{1}{2N} Tr(U_P + U_P^\dagger) \right], \tag{2.3}$$

where N is the number of colors considered, $\beta = \frac{2N}{g_0^2}$ and P is the index corresponding to a specific *plaquette*, which is defined as

$$U_{\mu\nu}(n) = U_\mu(n) U_\nu(n+\hat{\mu}) U_\mu^\dagger(n+\hat{\nu}) U_\nu^\dagger(n) = e^{ig_0 a^2 F_{\mu\nu}(n)} + \mathcal{O}(a^3), \tag{2.4}$$

with $\mu < \nu$ and

$$\begin{aligned} F_{\mu\nu}(n) = \frac{1}{a} \left[(A_\nu(n\ +\hat{\mu}) - A_\nu(n)) - (A_\mu(n+\hat{\nu}) - A_\mu(n)) \right] \\ + ig_0(a)[A(n+\mu), A(n+\nu)]. \end{aligned} \tag{2.5}$$

It's very easy to verify that eq. (2.3) reduces to the usual continuum gauge action in the limit $a \to 0$

$$\begin{aligned} U_P + U_P^\dagger = e^{ig_0 a^2 F_{\mu\nu}(n)} + e^{-ig_0 a^2 F_{\mu\nu}(n)} \simeq 1 + ig_0 a^2 F_{\mu\nu}(n) \\ - \frac{1}{2} g_0^2 a^4 (F_{\mu\nu}(n))^2 + 1 - ig_0 a^2 F_{\mu\nu}(n) - \frac{1}{2} g_0^2 a^4 (F_{\mu\nu}(n))^2 \end{aligned} \tag{2.6}$$

Eq. (2.3) then becomes

$$\begin{aligned} S_G^{(SU(N))} = \frac{2N}{g_0^2} \sum_P \left[1 - \frac{1}{2N} Tr(2 - g_0^2 a^4 (F_{\mu\nu}(n))^2) \right] = \\ a^4 \sum_P Tr((F_{\mu\nu}(n))^2), \end{aligned} \tag{2.7}$$

and if we substitute the sum with an integral sign we obtain

$$S_G^{(SU(N))} = \int d^4x \frac{1}{2} Tr(F_{\mu\nu}(x) F_{\mu\nu}(x)) + \mathcal{O}(a^2), \tag{2.8}$$

where we have a factor 1/2 by summing on all the values μ and ν.

2.1.2 Fermionic action

For a massive fermionic field of spin 1/2 the naive discretization of the action is of the form

$$a^4 \sum_{n,m,\alpha,\beta} \bar{\psi}_\alpha(n) K_{\alpha\beta} \psi_\beta(m), \tag{2.9}$$

where the n, m indices represent the lattice points, α, β are the spinorial indices of the fields and a represents the lattice spacing. The quantity $K_{\alpha\beta}$ is defined as

$$K_{\alpha\beta}(n,m) = \sum_\mu \frac{1}{2a} (\gamma_\mu)_{\alpha\beta} \left[\delta_{m,n+\hat{\mu}} - \delta_{m,n-\hat{\mu}}\right] + m_0 \delta_{mn} \delta_{\alpha\beta}, \tag{2.10}$$

where m_0 is the bare fermion mass and the Euclidean γ_μ matrix has the form

$$\gamma_0 = \gamma_0^m \qquad \gamma_i = -i\gamma_i^m, \tag{2.11}$$

where the apex ^{m} indicates the γ matrices of a Minkowskian space. This action allows us to calculate the fermionic two-point correlation function

$$\left\langle \psi_\alpha(n) \bar{\psi}_\beta(m) \right\rangle = K^{-1}_{\alpha\beta}(n,m). \tag{2.12}$$

This expression, although it reduces to the usual fermionic action in the continuum limit, has a problem. In fact, the discretized expression of the inverse of the fermionic propagator in the momentum space has the form

$$S^{-1}(p) = m_0 + \frac{i}{a} \gamma_\mu sin(p_\mu a), \tag{2.13}$$

which suffers of what is usually called the *doubling problem*: in eq. (2.13) there are 16 regions in which $\frac{1}{a} sin(p_\mu a)$ remains finite when $a \to 0$. Of all these regions, 15 exist only because of the lattice, and have no corresponding physical particle in the continuum. Wilson proposed a way to solve the doubling problem [11], which consists in adding a term to expression (2.13)

$$S_F^W = a^4 \sum_{n,m,\alpha,\beta} \bar{\psi}_\alpha(n) K^W_{\alpha\beta} \psi_\beta(m), \tag{2.14}$$

where

$$K^{(W)}_{\alpha\beta}(n,m) = \left(m_0 + \frac{4r}{a}\right)\delta_{nm}\delta_{\alpha\beta} - \frac{1}{2a}\sum_{\mu}\left[(r-\gamma_\mu)_{\alpha\beta}\delta_{m,n+\hat{\mu}} + (r+\gamma_\mu)_{\alpha\beta}\delta_{m,n-\hat{\mu}}\right], \tag{2.15}$$

the quantity r is called *Wilson parameter*. It can be easily verified that in the case $r = 0$ we obtain eq. (2.9). This action solves the doubling problem because if we write the inverse of the fermionic propagator in the momentum space we obtain

$$S^{-1}(p) = M_P + \frac{i}{a}\gamma_\mu sin(p_\mu a), \tag{2.16}$$

where

$$M_P = m_0 + \frac{2r}{a}sin(\frac{p_\mu a}{2}). \tag{2.17}$$

What happens now is that for any finite value of r the mass of the 15 additional particles, i.e. the doublers, gets larger and larger with the decreasing of the lattice spacing, and eventually decouples from the system in the continuum. In particular, setting $r = 1$, in a typical lattice simulation with an inverse lattice spacing of roughly 2GeV the 15 doublers have a mass of at least 4GeV, so their presence can be safely ignored in the computation.

Even though eq. (2.14) solves the doubling problem, it explicitly breaks chiral simmetry that is restored once $r = 0$ and $m_0 = 0$. This behavior is actually not specific of the Wilson action, but comes from a general property of QCD, expressed by the No-Go Nielsen and Ninomiya theorem [12], which states that it is impossible to define a discretization of QCD simultaneously free from the fermion doubling problem which reproduces the correct chiral limit when the mass parameter m is set to zero.

Because of the chiral simmetry breaking, the quark field renormalization is not only multiplicative, but it has the form

$$m_R = m_q Z_m, \tag{2.18}$$

where m_R is the renormalized quark mass and

$$m_q = m_0 - m_{cr}, \tag{2.19}$$

where m_{cr} represents the parameter called *critical mass*.

Just like in continuum QFT, to make the fermionic action gauge invariant it's necessary to include in the action the interaction between fermions and gauge bosons. Gauge transformations on the lattice are defined in the

following way

$$\psi(n) \to G(n)\psi(n), \tag{2.20}$$

$$\bar{\psi}(n) \to \bar{\psi}(n)G^{-1}(n), \tag{2.21}$$

$$U_\mu(n) \to G(n)U_\mu(n)G^{-1}(n+\hat{\mu}). \tag{2.22}$$

Once gauge fields are included in the fermionic action, eq. (2.14) becomes

$$S_F^{(W)} = a^4\left(m_0 + \frac{4r}{a}\right)\sum_n \bar{\psi}(n)\psi(n) - \frac{a^3}{2}\sum_{n,\mu}[\bar{\psi}(n)(r-\gamma_\mu)U_{n,n+\mu}\psi(n+\mu) + \bar{\psi}(n+\mu)(r+\gamma_\mu)U^\dagger_{n,n+\mu}\psi(n)]. \tag{2.23}$$

Through some manipulations this expression can be written as

$$S_F^W = \frac{a^3}{2\kappa}\sum_{n,m}\bar{\psi}(n)\tilde{K}_{nm}[U]\psi(m), \tag{2.24}$$

where κ is called the *hopping parameter*

$$\kappa = \frac{1}{8r + 2m_0 a}, \tag{2.25}$$

and $\tilde{K}_{nm}$ is

$$\tilde{K}_{nm} = \delta_{nm} - \kappa\sum_\mu\left[(r-\gamma_\mu)U_\mu(n)\delta_{m,n+\hat{\mu}} + (r+\gamma_\mu)U^\dagger_\mu(n-\hat{\mu})\delta_{m,n-\hat{\mu}}\right]. \tag{2.26}$$

2.1.3 Quenched approximation and dynamical fermions

Let us consider a gauge theory with Wilson fermions. We can compute the expectation value of a physical observable as

$$\langle F\rangle = \frac{\int dU d\psi d\bar{\psi} e^{-S_{QCD}}F[U,\psi,\bar{\psi}]}{\int dU d\psi d\bar{\psi} e^{-S_{QCD}}} = Z^{-1}\int dU d\psi d\bar{\psi} e^{-S_{QCD}}F[U,\psi,\bar{\psi}], \tag{2.27}$$

where S_{QCD} is the total action:

$$S_{QCD} = S_F^W + S_G^{(SU(3))} =$$
$$= a^4 \sum_{n,m,\alpha,\beta} \bar{\psi}_\alpha(n) K^W_{\alpha\beta} \psi_\beta(m) + \beta \sum_P \left[1 - \frac{1}{2N} Tr(U_P + U_P^\dagger) \right]. \tag{2.28}$$

By integrating over the fermionic Grassmann variables we obtain

$$\int d\psi d\bar{\psi} e^{-S_F^W} = det(K^W) = det(K), \tag{2.29}$$

$$\int d\psi d\bar{\psi} \psi(x_1) \bar{\psi}(x_2) e^{-S_F^W} = det(K^W)(K^W)^{-1}_{x_1 x_2} = det(K) S_{x_1 x_2}, \tag{2.30}$$

where $S_{x_1 x_2}$ represents the fermionic propagator between the points x_1 and x_2.

Let us then assume that the quantity F is of the form

$$F = \psi_{x_1} \bar{\psi}_{y_1} \psi_{x_2} \bar{\psi}_{y_2} ... \psi_{x_n} \bar{\psi}_{y_n} A[U]. \tag{2.31}$$

We can then use the properties (2.29) and (2.30) of fermionic integrals to write eq. (2.27) as

$$\langle F \rangle = Z^{-1} \int dU e^{-S_{eff}} A[U] \epsilon^{z_1 z_2 ... z_n}_{y_1 y_2 ... y_n} S_{z_1 x_1} S_{z_2 x_2} ... S_{z_n x_n}, \tag{2.32}$$

where $\epsilon^{z_1 z_2 ... z_n}_{y_1 y_2 ... y_n} S_{z_1 x_1} ... S_{z_n x_n}$ represents the sum over all possible combinations of fermionic propagators (with the proper sign due to the anticommuting properties of the fermionic fields) and S_{eff} is the effective action

$$S_{eff} = S_F^W - log(det(K)). \tag{2.33}$$

It's possible to demonstrate that the term $det(K)$ is the one generating fermionic loops. Specifically it's the exponential of the sum over n of the diagrams representing a fermionic loop with n gauge propagators connected to it. Up to a decade ago the available computing power didn't allow us to compute the fermionic determinant in the simulations, therefore old calculations were performed in the *quenched approximation*, i.e. by approximating

$$det(K) = \text{constant}, \tag{2.34}$$

which corresponds physically to neglect vacuum polarization effects. Today

it has become possible to consider the contribution of the fermionic determinant. A simulation performed with a given number N_f of dynamical fermions is called *unquenched*.

2.1.4 Monte Carlo Simulations

As said before, space-time discretization makes path integrals finite-dimensional and thus numerically computable. The problem with this idea is that the number of integrations that one should perform is simply enormous. Let us consider the expectation value of the operator $O[U]$:

$$\langle O \rangle = \frac{\int dU O[U] e^{-S[U]}}{\int dU e^{-S[U]}}. \tag{2.35}$$

Using a 10^4 space-time lattice, the number of link variables is approximately 4×10^4. For the case of $SU(3)$, each of these link variables is a function of 8 real parameters; hence there are 320000 integrations to be done. If we wanted a rough estimate and use, for example, only ten points for evaluating each integral, the multiple integral would be approximated by a sum of 10^{320000} terms.

It is thus clear the necessity to use the so called *importance sampling* procedure, i.e. a method that samples the *gauge configurations* with the proper weight in the integral. The choice of these configurations is done by Monte Carlo simulations: given the initial state of a system, pseudo-random modifications to the link variables are performed so that the probability of obtaining a configuration C is

$$p(C) \propto e^{-S(C)}, \tag{2.36}$$

as required by eq. (2.35). The most simple algorithm to do so is called *Heat bath*, which consists in substituting the value of every link variable with a pseudo-random one, thus obtaining a new configuration. The probability for a link to have a value x is proportional to the Boltzmann factor containing $S(x)$, i.e. the action calculated in the configuration in which only the given link changed its value to x and all the others didn't change.

The Heat Bath algorithm is an example of *Markov Chain*, i.e. a chain of events in which the probability of obtaining configuration C only depends on the previous configuration C' and doesn't depend on the history of the

system. This allows us to write the relation

$$e^{-S(C)} = \sum_{C'} P(C' \to C) e^{-S(C')}, \tag{2.37}$$

where $P(C' \to C)$ is the probability of getting to configuration C from configuration C'. Moreover, if a chain of events satisfies the relation of *detailed balance*

$$p(C)P(C' \to C) = p(C')P(C \to C'), \tag{2.38}$$

then it's a Markov Chain. When an algorithm generating a Markov Chain is applied to an ensemble, the result is always closer to the equilibrium state. The important feature of Markov Chains is that for N enough large, where N is the number of the elements of the chain, it is possible to approximate eq. (2.35) with a finite sum

$$\langle O \rangle = \frac{1}{N} \sum_{n=1}^{N} O[U_n], \tag{2.39}$$

with an uncertainty $\mathcal{O}(1/\sqrt{N})$, where U_n represents the gauge configuration of the $n-$th element of the Markov chain.

2.1.5 Hybrid Monte Carlo

The Hybrid Monte Carlo algorithm is used to compute the fermionic determinant. The main idea of this algorithm is the following

- We pass from a configuration C to a new one, C', with a certain probability $P(C \to C')$, through a procedure that satisfies the detailed balance condition.
- We accept the new configuration, or reject it, going back to the previous configuration, according to an acceptance probability

$$P_A(C \to C') = min\{1, p(C')P(C' \to C)/p(C)P(C \to C')\}. \tag{2.40}$$

The passage from a configuration to another one is performed by introducing conjugate momenta of U fields, called π, which follow a gaussian distribution. The next step is to make the system evolve in a deterministic way through the hamiltonian

$$H(\phi, \pi) = \frac{1}{2}\pi^2 + S_G, \tag{2.41}$$

for a certain amount of time, and the resulting configuration is accepted or rejected according to eq. (2.40).

If we perform an unquenched simulation with N_f dynamical flavors the fermionic determinant is of the form

$$[det(K)]^{N_f}. \tag{2.42}$$

It's easy to demonstrate that $det(K) = det(K^\dagger) > 0$, and that K satisfies the relation

$$det(K) = \sqrt{det(Q)} \qquad Q = K^\dagger K. \tag{2.43}$$

It is thus possible to write the determinant as an integral on scalar variables

$$[det(Q)]^{N_f/2} = [det(Q^{-1})]^{-N_f/2} = \int d\phi d\phi^* e^{-N_f \sum_{n,m} \phi_n^* Q^{-1}_{n,m} \phi_m}, \tag{2.44}$$

where n, m are the lattice points we're considering. The ϕ fields are called *pseudofermions*, they follow Bose-Einstein statistics but they have color and Dirac indexes. In eq. (2.44) enters the quantity $Q^{-1} = [K^\dagger K]^{-1}$, so it's necessary to calculate the inverse of the Dirac matrix. This makes unquenched simulations computationally more expensive compared to quenched ones.

2.2 Improvement

In lattice QCD any physical observable has a dependence on the lattice spacing a, i.e. if we consider the expectation value of an operator $\langle O \rangle$ we can write it as

$$\langle O \rangle_{Latt} = \langle O \rangle_{continuum} + \mathcal{O}(a) + ... \tag{2.45}$$

where $\langle O \rangle_{Latt}$ represents the expectation value calculated on the lattice, $\langle O \rangle_{continuum}$ is its continuum counterpart and the last term on the r.h.s. of eq. (2.45) are discretization effects. The latter, depending on the quantity and on the action, can be as high as $20-30\%$. In order to decrease discretization effects it's possible to use a procedure called *improvement* proposed by Symanzik [13], which consists in adding to the action and to the operators *counterterms*, aimed to cancel discretization effects up to some power of the lattice spacing. The coefficients of these counterterms are not known *a priori*, but have to be calculated either in perturbation theory or with some non-perturbative approach. Under specific conditions it's possible to obtain *automatic improvement*, which gives automatically $\mathcal{O}(a^2)$ discretization effects without the need of additional counterterms in the action or in the

fields.

As far as regards the work treated in this thesis, in order to obtain automatic improvement in a theory with massive fermions we used the action called Twisted Mass (with only one tuned parameter) [14], which consists in adding to the lagrangian a mass term of the form

$$i\mu_q \bar{\chi}\gamma_5\tau^3\chi, \tag{2.46}$$

where τ^3 is the third Pauli matrix, μ_q is the quantity called *Twisted Mass* and χ and $\bar{\chi}$ are fermionic fields in a basis which is commonly called twisted basis.

2.2.1 Symanzik procedure

For small enough values of the lattice spacing it's possible to write the lattice action as in an effective theory:

$$S_{eff} = S_0 + aS_1 + a^2S_2 + ... \tag{2.47}$$

where every term in the expansion satisfies the theory simmetries on the lattice. The term S_0 represents the continuum action, while the other terms are written as

$$S_k = \int d^4y \mathcal{L}_k(y), \tag{2.48}$$

where $\mathcal{L}_k(y)$ is a linear combination of operators of dimension $4 + k$. The dependence on the lattice spacing is not only explicit in eq. (2.47), but there is a dependence also in the local operators entering the correlation functions of interest. Let us consider a gauge invariant field $\phi(x)$, which comprises both fermion and gluon fields; we can write the renormalized n-points correlation function as

$$G(x_1, ...x_n) = Z_\phi^n \left\langle \phi(x_1).....\phi(x_n) \right\rangle, \tag{2.49}$$

which has a finite continuum limit once the renormalization constant is choosen correctly and if

$$x_1 \neq x_2 \neq ... \neq x_n. \tag{2.50}$$

The renormalized field $Z_\phi\phi = \Phi$ can be also represented in terms of the expression

$$\Phi_{eff}(x) = \Phi_0 + a\Phi_1(x) + a^2\Phi_2(x) + ... \tag{2.51}$$

where, if Φ_0 has dimension d, the generic term Φ_k is an operator of dimension $d+k$. We can thus write eq. (2.49) at $\mathcal{O}(a)$ in the following way:

$$G(x_1,...x_n) = \langle \Phi_0(x_1)...\Phi_0(x_n)\rangle_0 - a\int d^4y\, \langle \Phi_0(x_1)...\Phi_0(x_n)\mathcal{L}_1(y)\rangle_0 + \\ +a\sum_{k=1}^{n}\langle \Phi_0\ (x_1)...\Phi_1(x_k)...\Phi_0(x_n)\rangle_0\,, \tag{2.52}$$

where the index $_0$ indicates the expectation value computed using the action S_0 of the continuum limit. The second term in the r.h.s. comes from the corrections to the action, is of $\mathcal{O}(a)$ and can generate divergent contact terms when $y = x_k$. It's thus necessary to define a subtraction prescription. The way in which this subtraction is implemented is not important because different choices correpond to different redefinitions of the field Φ. Other dependences on a can arise from the field $\Phi_1(x)$, which is a linear combination of basis fields. While the other fields are not a dependent, the coefficients can depend on the lattice spacing. In perturbation theory these coefficiencies are polynomials function of $\ln a$.

2.2.2 Twisted Mass

The twisted mass action in the continuum is of the form

$$S_F[\chi,\bar\chi,G] = \int d^4x\bar\chi(\gamma_\mu D_\mu + m_q + i\mu_q\gamma_5\tau^3)\chi, \tag{2.53}$$

where D_μ is the covariant derivative relative to a specific gauge field G and χ is a degenerate quark doublet in the twisted basis. We can define the polar mass M and write the mass term of the action as

$$m_q + i\mu_q\gamma_5\tau^3 = Me^{i\alpha\gamma_5\tau^3}, \tag{2.54}$$

$$M = \sqrt{m_q^2+\mu_q^2}. \tag{2.55}$$

In the continuum case, it's easy to go from the twisted mass action to the canonical one through the transformation

$$\psi = e^{i\omega\gamma_5\tau^3/2}\chi, \tag{2.56}$$

$$\bar\psi = \bar\chi e^{i\omega\gamma_5\tau^3/2}, \tag{2.57}$$

where ψ and $\bar{\psi}$ represent the fields in the standard physical basis. By making this substitution in eq. (2.53) the mass term becomes

$$Me^{i(\alpha-\omega)\gamma_5\tau^3}. \tag{2.58}$$

Moreover, if we impose the condition $\omega = \alpha$, which is equivalent to

$$tan\omega = \mu_q/m_q, \tag{2.59}$$

we obtain the usual continuum fermionic action

$$S_F[\psi, \bar{\psi}, G] = \int d^4x \bar{\psi}(\gamma_\mu D_\mu + M)\psi. \tag{2.60}$$

The possibility of passing from eq. (2.53) to (2.60) with a chiral transformation indicates that physically the two actions are the same. This is made possible by the fact that the action has a chiral simmetry when the mass goes to zero; if we decide to use some kind of regularization that breaks chiral simmetry, like Wilson fermions, the twisted mass term can't be reabsorbed and the ω angle parametrizes a family of inequivalent regularizations. We will show that on the lattice, for a specific choice of the angle ω, it's possible to eliminate discretization effects up to $\mathcal{O}(a)$.

If we discretize eq. (2.53) we have *Wilson twisted mass action* of the form

$$S_F^{(Wtm)} = a^4 \sum_n \bar{\chi}(n) \left(m_0 + i\mu_q\gamma_5\tau^3 + \frac{4r}{a} \right) \chi(n) - \frac{a^3}{2} \sum_{n,\mu} [\bar{\chi}(n)(r - \gamma_\mu)U_{n,n+\mu}\chi(n+\mu) + \bar{\chi}(n+\mu)(r+\gamma_\mu)U^\dagger_{n,n+\mu}\chi(n)]. \tag{2.61}$$

2.2.3 Automatic improvement

In this section we'll discuss a fundamental property of the wilson twisted mass action in the case of *maximal twist*, i.e. when $\omega = \frac{\pi}{2}$. From eq. (2.59) we see that the maximal twist condition is equivalent to $m_q = 0$. It can be demonstrated that correlation functions of positive parity fields and renormalizable in a multiplicative way don't have any $\mathcal{O}(a)$ discretization effects when calculated at $m_q = 0$. Thus there is no need of any improvement coefficient [15]. For this demonstration we can use a massless theory, i.e. with $m_0 = m_{cr}$ and $\mu_q = 0$, in a finite volume, but it can be easily generalized for the massive case in infinite volume. As in the Symanzik procedure, eq.

(2.47) is true, where S_0 is the continuum action

$$S_0 = \int d^4x \bar{\chi}(x) \left[\gamma_\mu D_\mu\right] \chi(x). \tag{2.62}$$

In applying the Symanzik procedure, it's necessary to specify the $\mathcal{O}(a)$ correction to the effective action. Tipically, there is only one operator needed

$$\mathcal{L}_1 = c_1 \mathcal{O}_1, \tag{2.63}$$

where

$$\mathcal{O}_1 = i\bar{\chi}\sigma_{\mu\nu}F_{\mu\nu}\chi, \tag{2.64}$$

If we consider a generic renormalizable field that can be expanded as in eq. (2.51), eq. (2.52) is valid.

For an operator expectation value to be different from zero it's necessary that the operator has the same simmetries of the action. The action (2.62) has a simmetry with respect to the chiral transformation

$$\mathcal{R}_5^{1,2} : \begin{cases} \chi(x_0, \mathbf{x}) \to i\gamma_5 \tau^{1,2} \chi(x_0, \mathbf{x}) \\ \bar{\chi}(x_0, \mathbf{x}) \to \bar{\chi}(x_0, \mathbf{x}) i\gamma_5 \tau^{1,2} \end{cases} , \tag{2.65}$$

while the $\mathcal{O}_1$ operator is odd with respect to this transformation. For this reason the second term in the r.h.s. of eq. (2.52) is zero. To demonstrate that also the last term of eq. (2.52) is zero we notice that the dimension of Φ_1 is one more of the one of operator Φ_0. We can thus use the property stating that if an operator like Φ_1 has the same simmetries of Φ_0 then it must have opposite chirality. To show this we can then define the transformation

$$\mathcal{D} : \begin{cases} U_\mu(x) \to U_\mu^\dagger(-x - a\hat{\mu}) \\ \chi(x) \to e^{3i\pi/2} \chi(-x) \\ \bar{\chi}(x) \to \bar{\chi}(-x) e^{3i\pi/2} \end{cases} \tag{2.66}$$

so that the lattice action is invariant under $\mathcal{R}_5^{1,2} \times \mathcal{D}$. Φ_0 is simmetric under $\mathcal{R}_5^{1,2}$ so it must be simmetric under $\mathcal{D}$ too. When $\mathcal{D}$ acts on Φ_1 the field acquires an extra $e^{i\pi} = -1$ factor, so to have a non-zero expectation value it must be odd under $\mathcal{R}_5^{1,2}$. In other words Φ_0 and Φ_1 have opposite chirality under $\mathcal{R}_5^{1,2}$, which is a simmetry of the continuum action used to calculate the expectation value. This implies that in eq. (2.51) there can't be the Φ_1 term. Thus we have demonstrated the presence of automatic improvement in the case of maximal twist.

2.2.4 Non-degenerate quarks

The Wilson twisted mass action can be extended to the case of non-degenerate quarks, which is useful in the case of unquenched simulations in which not only the $u-d$ quarks are included in the sea (which can be reasonably considered to be degenerate) but also the strange and charm quarks, as in the case of the work presented in this dissertation. For non degenerate quarks the action can be written as

$$S^h_{(Wtm)} = \sum_n \bar{\chi}_h(n) a^4 \left(m_{0,h} + i\mu_\sigma \gamma_5 \tau^1 + \mu_\delta \tau^3 + \frac{4r}{a} \right) \chi_h(n)$$
$$-\frac{a^3}{2} \sum_{n,\mu} [\bar{\chi}_h(n)(r-\gamma_\mu) U_{n,n+\mu} \chi_h(n+\mu) + \bar{\chi}_h(n+\mu)(r+\gamma_\mu) U^\dagger_{n,n+\mu} \chi_h(n)], \tag{2.67}$$

where

$$\chi_h = \begin{pmatrix} \chi_s \\ \chi_c \end{pmatrix}, \tag{2.68}$$

$m_{0,h}$ is the bare Wilson mass of the doublet, μ_σ is the twisted mass, this time twisted in the τ^1 direction, and μ_δ is a splitting term along the τ^3 direction. To get to the physical base from the twisted one we can use a transformation similar to the one used in the degenerate case:

$$\psi_h = e^{i\omega_h \gamma_5 \tau^1/2} \chi_h, \tag{2.69}$$

$$\bar{\psi}_h = \bar{\chi}_h e^{i\omega_h \gamma_5 \tau^1/2}. \tag{2.70}$$

Once again, the maximal twist condition corresponds to $\omega = \frac{\pi}{2}$.

2.3 What to compute in Lattice QCD

The basic idea of Lattice QCD is to calculate correlation functions numerically and to extract useful information from the behavior of these correlators at large values of the euclidean time t. In this section we will shortly describe how it's possible to extract data from two-point and three-point correlation functions.

2.3.1 Two-point correlation functions

The euclidean two-point correlation function, for two generic operators O_1 and O_2 can be written as

$$G(x) = G(\vec{x}, t) = \langle 0 | \, T\{O_1(x) O_2^\dagger(0)\} \, | 0 \rangle \,, \tag{2.71}$$

where T represents the time-ordered product. By choosing $t > 0$ and performing the Fourier transform with respect to spatial coordinates we obtain

$$C(\vec{p}, t) = \frac{1}{L^3} \sum_{\vec{x}} G(x) e^{i\vec{p}\cdot\vec{x}} = \frac{1}{L^3} \sum_{\vec{x}} \langle 0 | \, O_1(x) O_2^\dagger(0) \, | 0 \rangle \, e^{i\vec{p}\cdot\vec{x}}, \tag{2.72}$$

where we have a sum instead of an integral because of space-time discretization. Let us then insert between O_1 and O_2 a complete set of covariantly normalized energy eigenstates with definite momentum $|n, \vec{p}_n\rangle$

$$\langle n, \vec{p}_n | m, \vec{p}_m \rangle = 2E_n \delta_{n,m}, \tag{2.73}$$

$$\sum_{n,\vec{p}_n} |n, \vec{p}_n\rangle \, \frac{1}{2E_n} \, \langle n, \vec{p}_n| = 1. \tag{2.74}$$

Eq. 2.72 thus becomes

$$C(\vec{p}, t) = \frac{1}{L^3} \sum_{\vec{x}} \sum_{n,\vec{p}_n} \frac{1}{2E_n} \, \langle 0 | \, O_1(x) \, | n, \vec{p}_n \rangle \, \langle n, \vec{p}_n | \, O_2^\dagger(0) \, | 0 \rangle \, e^{i\vec{p}\cdot\vec{x}}. \tag{2.75}$$

Thanks to translation properties of operators we can write

$$O_1(x) = e^{Ht + i\vec{p}\cdot\vec{x}} O_1(0) e^{-Ht - i\vec{p}\cdot\vec{x}}, \tag{2.76}$$

so that eq. 2.75 becomes

$$C(t) = \frac{1}{L^3} \sum_{\vec{x}} \sum_{n,\vec{p}_n} \frac{1}{2E_n} \, \langle 0 | \, O_1(0) \, | n, \vec{p}_n \rangle \, \langle n, \vec{p}_n | \, O_2^\dagger(0) \, | 0 \rangle \, e^{-E_n t - i(\vec{p}_n - \vec{p})\cdot\vec{x}}. \tag{2.77}$$

Moreover, given the identity $\sum_{\vec{x}} e^{-i(\vec{p}_n - \vec{p})\cdot\vec{x}} = L^3 \delta_{n,m}$ we obtain

$$C(t) = \sum_n \frac{\langle 0 | \, O_1(0) \, | n, \vec{p} \rangle \, \langle n, \vec{p} | \, O_2^\dagger(0) \, | 0 \rangle}{2E_n} e^{-E_n t}. \tag{2.78}$$

In the case of single particle states E_n can be written as

$$E_n = \sqrt{m_n^2 + |\vec{p}|^2}. \tag{2.79}$$

For large enough t values only the ground state contributes significally to expression (2.78). Thus we obtain

$$C(t) \simeq \frac{\langle 0| O_1(0) |m_0, \vec{p}\rangle \langle m_0, \vec{p}| O_2^\dagger(0) |0\rangle}{2E_0} e^{-E_0 t}. \tag{2.80}$$

Moreover, if T is the finite temporal size of the lattice eq. 2.80 should be corrected consequently. By assuming periodic boundary conditions and using the notation $\sqrt{\mathcal{Z}_{O_1}} = \langle 0| O_1(0) |m_0, \vec{p}\rangle$ and $\sqrt{\mathcal{Z}_{O_2}} = \langle m_0, \vec{p}| O_2^\dagger(0) |0\rangle$ the previous relation becomes

$$C(t) \simeq \frac{\sqrt{\mathcal{Z}_{O_1}\mathcal{Z}_{O_2}}}{2E_0} \left(e^{-E_0 t} + \eta e^{-E_0(T-t)}\right), \tag{2.81}$$

where η is the eigenvalue of the two-point green function with respect to the transformation $t \to T - t$. In the specific case in which $O_1 = O_2 = O$ eq. (2.81) can be written as

$$C(t) \simeq \frac{\mathcal{Z}_O}{E_0} e^{-E_0 T/2} cosh\left[E_0\left(t - \frac{T}{2}\right)\right]. \tag{2.82}$$

The simplest bilinear operators in the quark fields are of the form

$$O_\Gamma(x) = \bar{q}_1^a(x)\Gamma q_2^a(x), \tag{2.83}$$

where $\bar{q}_1^a$ and q_2^a represent fermionic quark fields, a is a color index which is summed over, Γ is one of the 16 Dirac matrices and Dirac indices have been omitted for the sake of simplicity. The choice of Γ determines the eigenvalues of the mesonic operator with respect to spin J, parity P and charge conjugation C (see table 2.1). Specifically, in this work we studied pseudoscalar mesons, i.e. states corresponding to the Dirac matrices $i\gamma_5$ or $\gamma_5\gamma_0$.

An important quantity constructed in terms of the two-point function is the so called *effective mass*.

$$m_{eff}(t) = ln\left[\frac{C(t)}{C(t+1)}\right], \tag{2.84}$$

Matrix Γ	J^{PC}
1	0^{++}
γ_0	0^{+-}
$\gamma_5\gamma_0$	0^{-+}
$i\gamma_5$	0^{-+}
σ_{oi}	1^{--}
γ_k	1^{--}
$\gamma_5\gamma_k$	1^{++}
σ_{ik}	1^{+-}

Table 2.1: We show the J^{PC} quantum numbers of the physical state corresponding to the choice of Γ matrix in a bilinear quark operator.

This quantity, if studied for large values of time, reaches a plateaux in correspondence of the mass of the ground state of the operator present in the two-point function.

2.3.2 Three-point correlation functions

Another basic ingredient of Lattice QCD calculations are three-point correlation functions. Studying the behavior of these function for large values of the time t allows us to extract the matrix elements of currents connecting two external states. Let us consider a three-point function in the Fouries space

$$C_\Gamma^{BA}(t,t_s;\vec{p},\vec{p'}) = \frac{1}{L^3}\sum_{\vec{x},\vec{x_s}} \langle 0|\, B(x_s)O_\Gamma(x)A(0)\,|0\rangle\, e^{i\vec{p}\vec{x}_s + i\vec{p'}\vec{x}} \tag{2.85}$$

where A and B are operators interpolating two hadrons A and B, and O_Γ is a generic operator. Following the same manipulation steps used for the two-point function case we can insert the completeness relation twice

$$C_\Gamma^{BA}(t,t_s;\vec{p},\vec{p'}) = \frac{1}{L^3}\sum_{\vec{x},\vec{x_s}}\sum_{n,\vec{p}_n}\sum_{n',\vec{p}'_n} \langle 0|B(x_s)|n',\vec{p}'_n\rangle \frac{1}{2E_{n'}} \langle n',\vec{p}'_n|O_\Gamma(x)|n,\vec{p}_n\rangle$$
$$\frac{1}{2E_{n'}} \langle n,\vec{p}_n|A(0)|0\rangle\, e^{i\vec{p}\vec{x}_s + i\vec{p'}\vec{x}} \tag{2.86}$$

Using again the translation law to shift the operators in the origin and the Kronecker delta to eliminate the spatial volume integration we obtain

$$C_{\Gamma}^{BA}(t,t_s;\vec{p},\vec{p'}) = \sum_{n,n'} \frac{\sqrt{Z^A}\sqrt{Z^B}}{4E_nE_{n'}} e^{-E_{n'}(t_s-t)} e^{-E_n t} \left\langle B_{n'},\vec{p}|O_{\Gamma}(0)|A_n,\vec{p}+\vec{p'}\right\rangle, \tag{2.87}$$

where the $A_n(B_{n'})$ states belong to the subset of the states $n(n')$ which have the right quantum numbers to interpolate the $A(B)$ operator and $Z^{A(B)}$ indicates the square modulus of the matrix elements

$$\begin{aligned} Z^A &= |\langle 0|A(0)|A_n,\vec{p}_n\rangle|^2 \\ Z^B &= |\langle 0|A(0)|B_{n'},\vec{p}_{n'}\rangle|^2. \end{aligned} \tag{2.88}$$

If we consider a time interval in which both t and $t_s - t$ are large enough only the ground states of A and B will contribute to the sum. Thus we can write the correlation function as

$$C_{\Gamma}^{BA}(t,t_s;\vec{p},\vec{p'}) \xrightarrow{t\to\infty \;\; (t_s-t)\to\infty} \frac{\sqrt{Z_A}\sqrt{Z_B}e^{-E_B(t_s-t)}e^{-E_A t}}{4E_AE_B} \left\langle B,\vec{p}|O_{\Gamma}(0)|A,\vec{p}+\vec{p'}\right\rangle. \tag{2.89}$$

It should be now clear that the general strategy is based on extracting, from the corresponding two-point functions, the energies and the matrix elements Z_A and Z_B and then, from the large time behavior of the three-point correlator the relevant matrix element of the operator O_{Γ}.

2.4 The non-perturbative renormalization method RI-MOM

Lattice simulations makes it possible to use non-perturbative renormalization procedures, which have the advantage of not having the uncertainty induced by the truncation of the perturbative series. In this section we will describe the RI-MOM renormalization method [16], the one used in this work for the bilinear quark operators. This method consists in studying Green functions of a given operator and in imposing that for a fixed value of the external momenta $p^2 = \mu^2$ and in a fixed (Landau) gauge, the renormalized green function is equal to its tree level value. By choosing the renormalization scale μ^2 so that it lies in the perturbative regime , $\mu^2 \gg \Lambda^2_{QCD}$, it's possible to connect the renormalization scheme imposed on the lattice with other perturbative schemes such as $\overline{\text{MS}}$. Moreover, in order to simultaneously

avoid large cutoff effects the condition on the scale μ becomes

$$\frac{1}{a} \gg \mu \gg \Lambda_{QCD}. \tag{2.90}$$

Let us consider an operator of the form (2.83) and define the following Green function in the continuum

$$G_\Gamma(p) = \int d^4x d^4y e^{-ip(x-y)} \left\langle \hat{q}(x) O_\Gamma(0) \hat{\bar{q}}(y) \right\rangle, \tag{2.91}$$

where $\hat{q}(x)$ and $\hat{\bar{q}}(y)$ represent renormalized fields. The corresponding amputated green function is defined as

$$\Lambda_\Gamma(p) = \hat{S}(p)^{-1} G_\Gamma(p) \hat{S}(p)^{-1}, \tag{2.92}$$

where $\hat{S}(p)$ is the renormalized fermionic propagator. The function $\Lambda_\Gamma(p)$ is a matrix in Dirac and color spaces. To impose the renormalization condition it's useful to project it in the following way

$$\Omega_\Gamma(p) = \frac{1}{12} Tr \left[P_\Gamma \Lambda_\Gamma(p) \right], \tag{2.93}$$

where the trace is taken over Dirac and color indices and P_Γ is a projector chosen so that $\Omega_\Gamma(p) = 1$ at the tree level. The RI-MOM renormalization scheme consists in imposing the condition

$$\left[\Omega_\Gamma(p)_R \right]_{p^2=\mu^2} = \frac{1}{Z_q^{-1}} Z_\Gamma \Omega_\Gamma(\mu) = 1, \tag{2.94}$$

which allows us to determine the renormalization constant Z_Γ once the fermionic field renormalization constant Z_q is known. A possible way to calculate Z_q uses the quark propagator. The RI-MOM renormalization condition on the propagator reads:

$$\frac{i}{12} Tr \left[\frac{\not{p} \hat{S}(p)^{-1}}{p^2} \right]_{p^2=\mu^2} = Z_q^{-1} \frac{i}{12} Tr \left[\frac{\not{p} S(p)^{-1}}{p^2} \right]_{p^2=\mu^2} = 1, \tag{2.95}$$

An alternative approach to compute non-perturbatively (some of) the lattice renormalization constants is based on Ward identities

2.5 Twisted boundary conditions

Tipically when one studies quantum field theory on a finite volume chooses periodic boundary conditions in the spatial directions, i.e. the fermionic field satisfies the relation

$$\psi(x_i + L) = \psi(x_i) \quad i = 1, 2, 3... \tag{2.96}$$

In this case, the allowed momenta of the field ψ are of the form

$$k_i = \frac{2\pi}{L} n_i, \qquad n_i = 1, 2, 3... \tag{2.97}$$

where L is the lattice size. For a lattice spacing $a^{-1} = 2.3\,\mathrm{GeV}$, as the smallest one introduced in our simulation, and a lattice size $L/a = 24$ this results in $2\pi/L = 0.6\,\mathrm{GeV}$ which is very restrictive, considering that we are interested in simulating particles with momenta much smaller than that. In particular, for physical observables that need to be studied as functions of momenta, having the possibility of simulating an arbitrary value of momentum is of crucial importance.

To cope with this problem one has to notice that physically there is no reason for having single value fields. The only quantities that should be single valued are the physical observables, and thus the action of our theory. For this reason, we can define a quark field $\tilde{\psi}$ that satisfies boundary conditions in the space directions like

$$\tilde{\psi}(x_i + L) = U_i \tilde{\psi}(x_i) \tag{2.98}$$

where U_i is a generic global transformation which is a simmetry of the action. The most generic U_i is a diagonal transformation in the flavor space of the form

$$U_i = e^{2\pi i \Theta_i} \tag{2.99}$$

Thus the quark field satisfies *twisted boundary conditions*, i.e.

$$\tilde{\psi}(x_i + L) = \exp(2\pi i \theta_i) \tilde{\psi}(x_i), \tag{2.100}$$

which in Fourier space is equivalent to impose

$$exp\left[i \left(k_i - \frac{2\pi\theta_i^f}{L} \right) L \right] = 1 \iff k_i = \frac{2\pi}{L}(\theta_i^f + n_i) \quad i = 1, 2, 3, n_i \in Z \tag{2.101}$$

When the quark field satisfies the twisted BCs (2.100), the corresponding quark propagator $\widetilde{S}(x,0) \equiv \langle \widetilde{\psi}(x)\ \overline{\widetilde{\psi}}(0)\rangle$ satisfies the standard Dirac equation but with different BCs. From a computational point of view it might be convenient to work always with periodic BCs on the fields. Therefore, following Refs. [17, 18], one can define a new quark field as $\psi_{\vec{\theta}}(x) = e^{-2\pi i\vec{\theta}\cdot\vec{x}/L}\widetilde{\psi}(x)$, which obviously satisfies periodic boundary conditions. In such a way the new quark propagator $S^{\vec{\theta}}(x,0) \equiv \langle \psi_{\vec{\theta}}(x)\ \overline{\psi}_{\vec{\theta}}(0)\rangle$ satisfies the following equation

$$\sum_y D^{\vec{\theta}}(x,y)\ S^{\vec{\theta}}(y,0) = \delta_{x,0} \tag{2.102}$$

with a modified Dirac operator $D^{\vec{\theta}}(x,y)$ but periodic BCs. The new Dirac operator is related to the untwisted one by simply rephasing the gauge links

$$U_\mu(x) \to U^{\vec{\theta}}_\mu(x) \equiv e^{2\pi i a\theta_\mu/L}\ U_\mu(x) \tag{2.103}$$

with the four-vector θ given by $(0,\vec{\theta})$. Note that the plaquette $P_{\mu\nu}(x)$ is left invariant by the rephasing of the gauge links. In terms of $S^{\vec{\theta}}(x,y)$, related to the quark fields $\psi_{\vec{\theta}}(x)$ with periodic BCs, the quark propagator $\widetilde{S}(x,y)$, corresponding to the quark fields $\widetilde{\psi}(x)$ with twisted BCs, is simply given by

$$\widetilde{S}(x,y) = e^{2\pi i\vec{\theta}\cdot(\vec{x}-\vec{y})/L}\ S^{\vec{\theta}}(x,y)\ . \tag{2.104}$$

2.6 Simulation details

In this section the simulation details will be discussed. We will start presenting the action used in the simulation and then give some details on the gauge ensembles considered in this analysis.

The work presented in this dissertation is based on the $N_f = 2+1+1$ gauge configurations generated by the ETM Collaboration [19] with the action

$$S = S_g + S^l_{tm} + S^h_{tm}. \tag{2.105}$$

The terms in the r.h.s. of eq. (2.105) represent respectively the Iwasaki gluonic action [20], the Wilson twisted mass action at maximal twist for the degenerate u,d doublet [14] and for the heavy doublet s,c [21]. The fermionic

terms read

$$S^l_{tm} = a^4 \sum_x \bar{\psi}(x) \left\{ \frac{1}{2} \sum_\mu \gamma_\mu (\nabla_\mu + \nabla^*_\mu) - i\gamma_5 \tau^3 \left[M_0 - \frac{a}{2} \sum_\mu \nabla_\mu \nabla^*_\mu \right] + \mu_l \right\} \psi(x) \tag{2.106}$$

$$S^h_{tm} = a^4 \sum_x \bar{\psi}(x) \left\{ \frac{1}{2} \sum_\mu \gamma_\mu (\nabla_\mu + \nabla^*_\mu) - i\gamma_5 \tau^1 \left[M_0 - \frac{a}{2} \sum_\mu \nabla_\mu \nabla^*_\mu \right] + \mu_\sigma + \mu_\delta \tau^3 \right\} \psi(x) \tag{2.107}$$

where ∇_μ and ∇^*_μ are nearest-neighbor forward and backward covariant derivative, μ_l is the bare light quark mass and M_0 is the untwisted bare mass tuned to its critical value M_{cr} as discussed in [19] in order to guarantee the automatic $\mathcal{O}(a)$ improvement at maximal twist [15, 22]. The parameters μ_σ and μ_δ are related to the renormalized strange and charm sea quark masses [22] via the relation

$$m_{c,s} = \frac{1}{Z_P} \left(\mu_\sigma \pm \frac{Z_P}{Z_S} \mu_\delta \right) \tag{2.108}$$

where Z_P and Z_S are respectively the pseudo-scalar and the scalar renormalization constants. The twisted-mass action (2.105) is known to lead to a mixing in the strange and charm sectors [23]. In order to avoid the mixing of K and D meson states in the correlation functions we adopted a non unitary setup in which the valence quarks are simulated as Osterwalder-Seiler (OS) fermions [24]. The action for each valence quark flavor q_f ($f = ll', ss', cc'$) reads as

$$S^f_{OS} = a^4 \sum_x \bar{q}_f(x) \left\{ \frac{1}{2} \sum_\mu \gamma_\mu (\nabla_\mu + \nabla^*_\mu) - i\gamma_5 r_f \left[M_0 - \frac{a}{2} \sum_\mu \nabla_\mu \nabla^*_\mu \right] + \mu_f \right\} q_f(x). \tag{2.109}$$

Each valence doublet is mass-degenerate ($\mu_l = \mu_{l'}, \mu_s = \mu_{s'}$ and $\mu_c = \mu_{c'}$), and their Wilson parameters r_f are always chosen such that the two valence quarks in a PS meson have opposite $r-$ values. This choice guarantees that the squared PS meson mass, M^2_{PS}, differs from its continuum counterpart only by terms $\mathcal{O}(a^2\mu)$ [15].

2.7 Lattice setup used in this analysis

The details of our simulation are collected in Table 2.2, where the number of gauge configurations correspond to a separation of 20 trajectories. At

ensemble	β	V/a^4	$a\mu_{sea} = a\mu_\ell$	$a\mu_\sigma$	$a\mu_\delta$	N_{cfg}	$a\mu_s^{(\mathrm{local})}$	$a\mu_c^{(\mathrm{local})}$	$a\mu_s^{(\mathrm{smeared})}$	$a\mu_c^{(\mathrm{smeared})}$
$A30.32$	1.90	$32^3 \times 64$	0.0030	0.15	0.19	150	0.0145,	0.1800,0.2200,	0.0180,	0.21256, 0.25000,
$A40.32$			0.0040			90	0.0185,	0.2600,0.3000	0.0220,	0.29404, 0.34583
$A50.32$			0.0050			150	0.0225	0.3600,0.4400	0.0260	
$A40.24$	1.90	$24^3 \times 48$	0.0040	0.15	0.19	150				
$A60.24$			0.0060			150				
$A80.24$			0.0080			150				
$A100.24$			0.0100			150				
$B25.32$	1.95	$32^3 \times 64$	0.0025	0.135	0.170	150	0.0141	0.1750,0.2140	0.0155,	0.18705, 0.22000,
$B35.32$			0.0035			150	0.0180	0.2530,0.2920	0.0190,	0.25875, 0.30433
$B55.32$			0.0055			150	0.219	0.3510,0.4290	0.0225	
$B75.32$			0.0075			75				
$B85.24$	1.95	$24^3 \times 48$	0.0085	0.135	0.170	150				
$D15.48$	2.10	$48^3 \times 96$	0.0015	0.12	0.1385	60	0.0118	0.1470,0.1795	0.0123,	0.14454, 0.17000,
$D20.48$			0.0020			90	0.0151	0.2120,0.2450	0.0150,	0.19995, 0.23517
$D30.48$			0.0030			90	0.0184	0.2945,0.3595	0.0177	

Table 2.2: *Values of the simulated sea and valence quark bare masses for each ensemble used in this work. The apex* ^{local} *or* ^{smeared} *indicates the valence strange and charm masses used respectively in the calculation of local and smeared operators.*

each lattice spacing different values of the light sea quark masses have been simulated. In the light sector the valence quark mass and the sea quark one are always equal. On the contrary the masses of the strange and charm sea quarks are fixed at each β to a value chosen to be close to its physical one [19]. Effects on observables induced by a possible mistuning of the sea strange and charm quark masses will be estimated in sec. 3.1.1. To be able to analyse mesons in the strange and charm sectors we have simulated three values of the valence strange quark mass (which are reasonably close to the physical value) and six values (4 values in the case of smeared operators) of the valence heavy quark mass, which are needed for the interpolation in the physical charm regime as well as to possibly extrapolate to the b-quark sector. In particular, in the light sector the masses were simulated in a range $0.1m_s^{phys} \leq \mu_l \leq 0.5m_s^{phys}$, in the strange sector $0.7m_s^{phys} \leq \mu_s \leq 1.2m_s^{phys}$, while for the charm sector in $0.7m_c^{phys} \leq \mu_c \leq 1.2m_c^{phys}$. Quark propagators with different valence masses are computed using the so-called multiple mass solver method [25, 26], which allows to invert the Dirac operator for several quark masses at a relatively low computational cost. The values of the lattice spacing were calculated in [27] and are

$$a|_{\beta=1.90,1.95,2.10} = \{0.0885(36), 0.0815(30), 0.0619(18)\} fm. \qquad (2.110)$$

ensemble	β	$L(fm)$	M_π(MeV)	$M_\pi L$
A30.32	1.90	2.84	245	3.53
A40.32			282	4.06
A50.32			314	4.53
A40.24	1.90	2.13	282	3.05
A60.24			344	3.71
A80.24			396	4.27
A100.24			443	4.78
B25.32	1.95	2.61	239	3.16
B35.32			281	3.72
B55.32			350	4.64
B75.32			408	5.41
B85.24	1.95	1.96	435	4.32
D15.48	2.10	2.97	211	3.19
D20.48			243	3.66
D30.48			296	4.46

Table 2.3: *Values of the pion mass and of the quantity $M_\pi L$ for the various gauge ensembles used in this work. The values of M_π are already extrapolated to the continuum and infinite volume limits.*

Lattice volumes go from $\simeq 2$ to $\simeq 3$ fm. In table 2.3 we show the values of the pion masses M_π and of the quantity $M_\pi L$, where the values of M_π are already extrapolated to the continuum and infinite volume limits.

The statistical accuracy of the correlators is significantly improved by using the so-called "one-end" stochastic method, implemented in [28], which includes spatial stochastic sources at single time slice chosen randomly. Statistical errors on the quantities directly extracted from the correlators are evaluated using the jackknife procedure, while statistical errors on data obtained from independent ensembles of gauge configurations, like the errors of the fitting procedures, are evaluated using a bootstrap sampling in order to take properly into account cross-correlations.The sampling structure will be described in details in each section covering a specific analysis.

Once correctly sampled, the uncertainty on an observable was calculated considering the results coming from a number of different analyses.

We assign to all these analyses the same weight and therefore we assume that the observable x has a distribution $f(x)$ given by $f(x) = (1/N)\sum_{i=1}^{N} f_i(x)$, where N is the number of different analyses, $f_i(x)$ is the distribution pro-

vided by the bootstrap sample of the i-th analysis characterized by central value x_i and standard deviation σ_i. Thus we estimate the central value and the error for the observable x through the mean value and the standard deviation of the distribution $f(x)$, which are given by

$$\begin{aligned} \overline{x} &= \frac{1}{N}\sum_{i=1}^{N} x_i \ , \\ \sigma^2 &= \frac{1}{N}\sum_{i=1}^{N} \sigma_i^2 + \frac{1}{N}\sum_{i=1}^{N} (x_i - \overline{x})^2 \ . \end{aligned} \tag{2.111}$$

The second term in the r.h.s. of Eq. (2.111), accounting for the spread among the results of the different analyses, is one of the sources of systematic error in the calculation.

Chapter 3

Leptonic decay constants

In this chapter we present our determination of the decay constants f_{K^+}, f_{D_s}, f_D and the ratios f_{K^+}/f_{π^+} and f_{D_s}/f_D. This quantities are useful because when combined with experimental data concerning the leptonic decay rates of the K and D mesons they allows us to determine with good accuracy the CKM matrix elements $|V_{us}|, |V_{cd}|$ and $|V_{cs}|$. This analysis has already been published in [29] .

3.1 Calculation of the kaon decay constant

The first step in the dermination of the kaon decay constant is the extraction of the pseudoscalar meson mass M_K and the matrix element $Z_K = |\langle K|\overline{u}\gamma_5 s|0\rangle|^2$ from the two-point correlation function. At large time distances the two point correlation function of the operator interpolating the Kaon has the form

$$C_K(t) \xrightarrow[t\gg a,\ (T-t)\gg a]{} \frac{Z_K}{2M_K}\left(e^{-M_K t} + e^{-M_K(T-t)}\right) , \tag{3.1}$$

so that the kaon mass and the matrix element Z_K can be extracted from the exponential fit given in the r.h.s. of Eq. (3.1). The time intervals $[t_{min}, t_{max}]$ adopted for the fit are the same used in our paper on the quark masses [27]. These intervals were determined by requiring that the changes in the meson masses and decay constants due to a modification in the value of t_{min} by one or two lattice units are well below the statistical uncertainty.

For maximally twisted fermions, the non-singlet axial Ward Identity allows a determination of the kaon decay constant f_K from the matrix element

Z_K without the need of any renormalization constant [15, 14], namely

$$af_K = a(\mu_\ell + \mu_s)\frac{\sqrt{a^4 Z_K}}{aM_K \sinh(aM_K)} \ . \tag{3.2}$$

The statistical uncertainty of the decay constant has been calculated using a jackknife procedure with 15 samples. In order to properly take into account the correlation with our results for the quark masses and the lattice spacing we formed a bootstrap sampling of 100 measurements and then associated it with each of the 8 analyses performed for the quark masses following the same structure used in [27].

Specifically we have used the values of the RCs Z_P corresponding to the methods M1 and M2 and considered 4 different approaches in the analysis, so that we end up with 8 analyses, which are referred to as analyses A1, B1, C1, D1 and A2, B2, C2, D2, respectively. The 4 analyses for each determination of RCs differ because of the use of either a chiral fit or a polynomial one, and for the use of r_0 or M_{ss} (the mass of a pseudoscalar meson with two strange valence quarks) as scaling variable.

The next step consisted in performing a small interpolation of lattice data to the value of the strange quark mass, m_s, given in ref. [27] for each analysis and corresponding to the average value $m_s = 99.6(4.3)\,\mathrm{MeV}$. Then, we analyzed the dependence of the kaon decay constant on the (renormalized) light quark mass $m_\ell \equiv (a\mu_\ell)/(aZ_P)$ and on the lattice spacing, using fitting procedures based either on ChPT or on a polynomial expansion as in the corresponding analysis of [27].

The first fit ansatz we used is the next-to-leading order (NLO) SU(2) ChPT prediction for f_K, including discretization and finite size effects. The formula reads

$$f_K = P_1 \left(1 - \frac{3}{4}\xi_\ell \log \xi_\ell + P_2 \xi_\ell + P_4 a^2\right) \cdot K_f^{FSE} \ , \tag{3.3}$$

where $\xi_\ell = 2Bm_\ell/16\pi^2 f^2$, with B and f being the SU(2) low-energy constants (LECs) entering the LO chiral Lagrangian, whose values have been determined in [27]. The term proportional to a^2 in Eq. (3.3) takes into account discretization effects. The factor K_f^{FSE} represents the correction for finite size effects (FSE) in the kaon decay constant, which are at most at the level of 3%, and are well computed according to the formula by Colangelo, Durr and Haefeli [30].

The second fit ansatz we used for the combined chiral and continuum

extrapolation is based on a polynomial expression of the form

$$f_K = P'_1 \left(1 + P'_2 \xi_\ell + P'_3 \xi_\ell^2 + P'_4 a^2\right) \cdot K_f^{FSE} \ . \tag{3.4}$$

The (combined) chiral and continuum extrapolation of f_K is shown in Figs. 3.1-3.2 in units of either r_0 or the mass $M_{s's'}$ of the fictitious PS meson made of two strange-like valence quarks with mass fixed at $r_0 m_{s'} = 0.22$. The impact of discretization effects using r_0 as scaling variable is at the level of $\simeq 3\%$[1], while the use of $M_{s's'}$, which is affected by cutoff effects similar to the ones of the K-meson mass (without having however any significant dependence on the light quark mass), reduces the lattice artefacts down to $\simeq -1.5\%$.

We followed the same strategy adopted in [27] to identify the various contributions to the systematic error. The sources are the choice of using either r_0 or $M_{s's'}$ as scaling variable (labelled as Disc in the error budget), the use of a chiral or polynomial fit to extrapolate to the physical light quark mass $m_{u/d}$ (labelled as Chiral) and the difference between the two methods M1 and M2 for computing the RCs Z_P (labelled as Z_P). As for the FSE we compared the results obtained by applying the correction with those obtained without correcting for FSE. Finally, the error on our determination of the strange quark mass, as well as of the other input parameters in the fit, has been included in the (stat+fit) error, which includes also the statistical uncertainty and the error associated with the fitting procedure (i.e. the amplification of the pure statistical error due to the chiral and continuum extrapolation).

Notice in Figs. 3.1-3.2 that after taking the continuum limit the kaon decay constant has been extrapolated to two different values of the light quark mass, namely the isospin symmetric, average up/down quark mass $m_{ud} = 3.70(17)\,\text{MeV}$ and the up quark mass $m_u = 2.36(24)\,\text{MeV}$ [27]. These two values of f_K have been used to evaluate the isospin breaking effect, induced by the difference $m_u \neq m_d$. This effect will be described and evaluated in sec. 3.1.2.

In the isospin symmetric limit we get for f_K the value

$$\begin{aligned} f_K &= 155.0\ (1.4)_{stat+fit}(0.4)_{Chiral}(1.1)_{Disc}(0.1)_{Z_P}(0.4)_{FSE}\,\text{MeV} \\ &= 155.0\ (1.9)\,\text{MeV} \ , \end{aligned} \tag{3.5}$$

which can be compared with the FLAG averages [31]: $f_K = 158.1(2.5)\,\text{MeV}$

[1]The impact of discretization effects is quantified here by the distance between the data at the finest lattice spacing and the continuum limit curve.

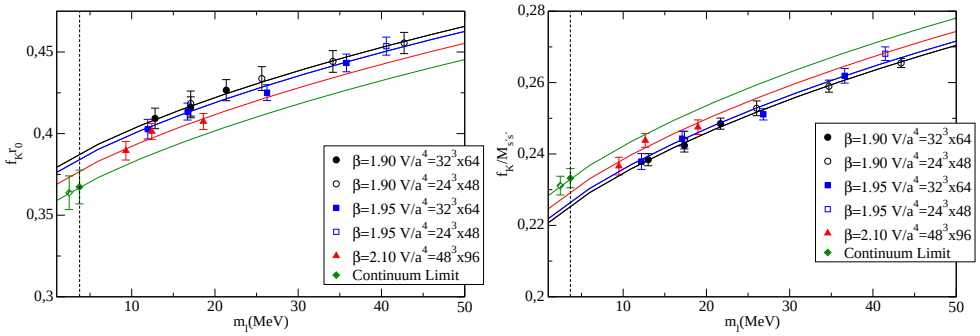

Figure 3.1: *Chiral and continuum extrapolation of $f_K r_0$ (left) and $f_K/M_{s's'}$ (right) based on the NLO ChPT fit of Eq. (3.3). Lattice data have been corrected for FSE following Ref. [30]. The green diamond represents the continuum limit evaluated at the average up/down quark mass $m_{ud} = 3.70(17)\,\mathrm{MeV}$, while the open diamond corresponds to the up-quark mass $m_u = 2.36(24)\,\mathrm{MeV}$ [27].*

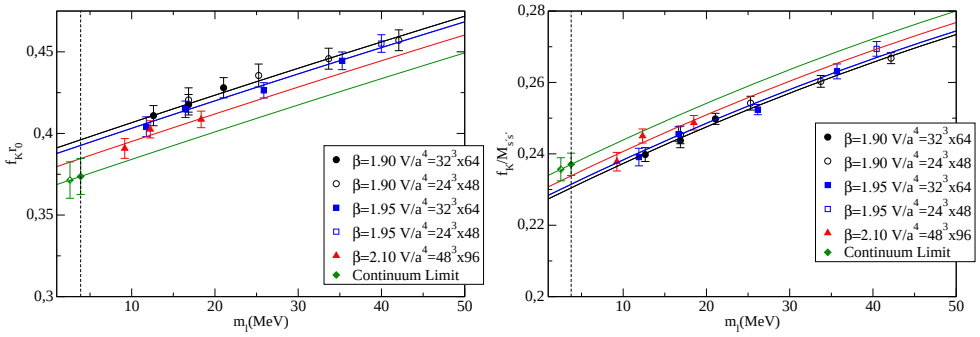

Figure 3.2: *The same as in Fig. 3.1, but using for the chiral and continuum extrapolation the polynomial fit of Eq. (3.4).*

at $N_f = 2$ from Ref. [32] and $f_K = 156.3(0.9)\,\mathrm{MeV}$ at $N_f = 2+1$ from Refs. [33, 34, 35]. Dividing the result (3.5) by the experimental value of the pion decay constant, $f_{\pi^+} = 130.41(20)\,\mathrm{MeV}$ [36], which has been used as input to set the lattice scale [27], we get for the ratio f_K/f_π the value

$$\begin{aligned} f_K/f_\pi &= 1.188\ (11)_{stat+fit}(4)_{Chiral}(9)_{Disc}(1)_{Z_P}(4)_{FSE}(2)_{f_{\pi^+}} \\ &= 1.188\ (15)\ . \end{aligned} \tag{3.6}$$

3.1.1 Mistuning of the strange and charm sea quark masses

In Ref. [27] we calculated the strange and charm sea quark masses corresponding to the bare masses adopted for generating the ETM gauge ensembles at the three values of the lattice spacing. This was done by comparing data obtained using the OS and the unitary setups for the valence quarks. For the strange sea quark mass m_s^{sea} we got the values $m_s^{sea} = \{99.2\ (3.5),\ 88.3\ (3.8),\ 106.4\ (4.6)\}$ MeV at $\beta = \{1.90,\ 1.95,\ 2.10\}$ respectively, which differ from the determination of the physical strange quark mass, $m_s = 99.6(4.3)$ MeV, by $\approx 10\%$ at most, with the largest difference occurring at $\beta = 1.95$.

The mistuning between the m_s^{sea} and m_s is a source of systematic effect in possibly any observable. To estimate the effect of the mistuning of the strange sea quark mass on f_K we used the partially quenched SU(3) ChPT predictions at NLO developed in Refs. [37]-[38] for arbitrary values of sea and valence quark masses. In this way one obtains

$$\begin{aligned} \Delta f_K &\equiv f_K(m_\ell, m_s; m_s^{sea}) - f_K(m_\ell, m_s; m_s) \\ &= \frac{2}{f_0}\left\{ 4L_4^r(\mu)\,(\chi_s^{sea} - \chi_s) - \frac{1}{12}\overline{A}(\chi_\eta^{sea})\frac{(\chi_s-\chi_\ell)^2(\chi_\eta^{sea}-\chi_s^{sea})}{(\chi_\eta^{sea}-\chi_s)^2(\chi_\eta^{sea}-\chi_\ell)} - \frac{3}{8}\overline{A}(\chi_\eta) \right. \\ &- \frac{1}{12}\overline{A}(\chi_s)\frac{(\chi_s^{sea}-\chi_\ell)(\chi_s-\chi_\eta^{sea}) - (\chi_s-\chi_\ell)(\chi_s-\chi_s^{sea})}{(\chi_s-\chi_\eta^{sea})^2} + \frac{1}{4}\overline{A}(\chi_s) \\ &+ \frac{1}{4}\left[\overline{A}\left(\frac{\chi_\ell+\chi_s^{sea}}{2}\right) - \overline{A}\left(\frac{\chi_\ell+\chi_s}{2}\right) + \overline{A}\left(\frac{\chi_s+\chi_s^{sea}}{2}\right) - \overline{A}(\chi_s)\right] \\ &\left. - \frac{1}{12}\frac{\partial\overline{A}(\chi_s)}{\partial\chi_s}\frac{(\chi_s-\chi_\ell)(\chi_s-\chi_s^{sea})}{\chi_s-\chi_\eta^{sea}} \right\}\ , \end{aligned} \tag{3.7}$$

where

$$\begin{aligned}
\chi_\ell &\equiv 2B_0 m_\ell \ , \qquad \chi_s \equiv 2B_0 m_s \ , \qquad \chi_\eta \equiv \frac{1}{3}\left(\chi_\ell + 2\chi_s\right) \ , \\
\chi_s^{sea} &\equiv 2B_0 m_s^{sea} \ , \qquad \chi_\eta^{sea} \equiv \frac{1}{3}\left(\chi_\ell + 2\chi_s^{sea}\right) \ , \\
\overline{A}(\chi) &\equiv -\frac{\chi}{16\pi^2}\log\left(\frac{\chi}{\mu^2}\right)
\end{aligned} \tag{3.8}$$

and B_0 and f_0 are the SU(3) LECs at LO, while $L_4^r(\mu)$ is a NLO LEC evaluated at the renormalization scale μ. Taking the values $B_0/f_0 = 19\ (2)$ and $L_4^r(\mu) = 0.04\ (14)\cdot 10^{-3}$ at $\mu = M_\rho = 0.770$ GeV from Ref. [31], the correction (3.7) is found to be below the 0.4% level at our simulated light-quark masses and decreases toward the physical point. We checked that by applying the correction (3.7) to the lattice data the changes observed in the predictions for f_K at the physical point are smaller than 0.3 MeV.

In a similar way the charm sea quark mass m_c^{sea} has been determined in Ref. [27], obtaining the values $m_c^{sea} = \{1.21(5),\ 1.21(5),\ 1.38(4)\}$ GeV at $\beta = \{1.90,\ 1.95,\ 2.10\}$. These values should be compared with the determination of the physical charm quark mass $m_c = 1.176\ (39)$ GeV. It follows that, while there is a good agreement at $\beta = 1.90$ and 1.95, a $\approx 18\%$ mistuning is present at $\beta = 2.10$. Since scaling distortions are not visible in our data, we expect that in the continuum limit the mistuning of the charm sea quark mass has a negligible effect compared to the one of the strange sea quark and, therefore, it does not affect our determination of decay constants in a significant way.

3.1.2 Isospin breaking effect on the kaon decay constant

In this Section we discuss the estimate of the isospin breaking (IB) effects on the charged kaon decay constant f_{K^+}. As is known, IB effects are generated by the up and down quark electric charges and by the up and down quark mass difference. While in the case of hadron masses both QED and QCD IB effects have been determined using a variety of approaches on the lattice, the situation for the decay constant is different. Indeed it is not even possible to give a physical definition of the decay constant in the presence of QED interactions [39]. The corresponding matrix element is both infrared divergent and (QED) gauge dependent. QED effects on the decay rate of a charged pseudoscalar meson have been only evaluated so far relying on ChPT and model-dependent approximations. A promising approach for a lattice determination of QED corrections to generic hadronic processes has recently proposed in Ref. [40].

In what follows we limit ourselves to the IB effect on f_{K^+} due to the up and down quark mass difference in pure QCD, i.e. switching off the QED interactions.

Let us consider the dependence of the decay constant f_{K^+} on the sea u- and d-quark masses, m_u^{sea} and m_d^{sea}, and on the valence u-quark mass, m_u^{val}. For the sake of simplicity we will not indicate the dependence on the strange and charm quark masses. At leading order in the mass differences $(m_u^{sea} - m_{ud})$, $(m_d^{sea} - m_{ud})$ and $(m_u^{val} - m_{ud})$, where m_{ud} is the isospin symmetric, average up/down quark mass, one has

$$\begin{aligned} f_{K^+} &= f_K(m_u^{sea}, m_d^{sea}; m_u^{val}) = f_K(m_{ud}, m_{ud}; m_{ud}) + \left[\frac{\partial f_K}{\partial m_u^{sea}}\right]_{m_{ud}} (m_u^{sea} - m_{ud}) \\ &+ \left[\frac{\partial f_K}{\partial m_d^{sea}}\right]_{m_{ud}} (m_d^{sea} - m_{ud}) + \left[\frac{\partial f_K}{\partial m_u^{val}}\right]_{m_{ud}} (m_u^{val} - m_{ud}) + \dots , \end{aligned} \tag{3.9}$$

where all derivatives are evaluated at the isospin symmetric point $m_u^{sea} = m_d^{sea} = m_u^{val} = m_{ud}$ and the ellipsis represents terms of higher order. Since $m_u^{sea} + m_d^{sea} = 2m_{ud}$ and $[\partial f_K/\partial m_u^{sea}]_{m_{ud}} = [\partial f_K/\partial m_d^{sea}]_{m_{ud}}$, it follows

$$f_{K^+} - f_K = \left[\frac{\partial f_K}{\partial m_u^{val}}\right]_{m_{ud}} (m_u^{val} - m_{ud}) + \dots , \tag{3.10}$$

which means that the leading IB correction to f_K is obtained from the partial derivative of the decay constant with respect to the valence light-quark mass.

The IB slope $\left[\partial f_K/\partial m_u^{val}\right]_{m_{ud}}$ can be determined with high precision using the method of Refs. [41, 42], which is based on the insertion of the isovector scalar density in the correlators of the isospin symmetric theory. This calculation is in progress and will be presented in a future publication.

For the time being we derive an estimate of the partial derivative (3.10) following two methods:

- using partially quenched SU(3) ChPT developed in Refs. [37]-[38]

- by studying numerically in the lattice simulation the dependence of the decay constant f_K on the light-quark mass.

The first method relies on partially quenched SU(3) ChPT, which predicts

at NLO [37]-[38]

$$\left[\frac{\partial f_K}{\partial m_u^{val}}\right]_{m_{ud}} = \frac{4B_0}{f_0}\left\{2L_5^r(\mu) - \frac{1}{128\pi^2}\left[1 + 2\log\left(2B_0\frac{m_{ud}}{\mu^2}\right) + \right.\right. \\ \left.\left. + \log\left(B_0\frac{m_s + m_{ud}}{\mu^2}\right) + \log\left(\frac{2m_s + m_{ud}}{3m_{ud}}\right)\right]\right\} \quad (3.11)$$

Using the values $B_0/f_0 = 19\ (2)$ and $L_5^r(\mu) = 0.84\ (38)\cdot 10^{-3}$ at $\mu = M_\rho = 0.770$ GeV from Ref. [31], as well as the values of m_{ud} and m_s determined in Ref. [27], the partial derivative of f_K with respect to the valence light-quark mass is estimated to be equal to 0.37(7) in the $\overline{\rm MS}(2\,{\rm GeV})$ scheme. Combined with the determination of $m_u - m_{ud}$ from [27]. This leads to

$$f_{K^+} - f_K = -0.49\ (13)\,{\rm MeV}\ , \quad (3.12)$$

where the error does not include any estimate of the impact of ChPT orders higher than the NLO one.

In the second method we use our non-perturbative results for f_K at $m_\ell = m_u$ and at $m_\ell = m_{ud}$, presented in Figs. 3.1-3.2. In our simulations, however, the sea and valence light-quark masses are taken to be degenerate and therefore the difference between the two results for f_K at $m_\ell = m_u$ and at $m_\ell = m_{ud}$ does not provide directly an estimate for $(f_{K^+} - f_K)$. Rather we have

$$f_{K^+} - f_K = f_K(m_u, m_u; m_u) - f_K(m_{ud}, m_{ud}; m_{ud}) + \Delta_{f_K}(m_u - m_{ud}) + \ldots\ , \quad (3.13)$$

where the ellipsis stands for higher order terms and the correction Δ_{f_K} is given by

$$\Delta_{f_K} = \left[\frac{\partial f_K(m_\ell^{sea}, m_\ell^{sea}; m_\ell^{val})}{\partial m_\ell^{val}} - \frac{df_K(m_\ell, m_\ell; m_\ell)}{dm_\ell}\right]_{m_\ell^{val}=m_\ell^{sea}=m_\ell=m_{ud}} \\ = -\left[\frac{\partial f_K(m_\ell^{sea}, m_\ell^{sea}; m_\ell^{val})}{\partial m_\ell^{sea}}\right]_{m_\ell^{val}=m_\ell^{sea}=m_{ud}}\ . \quad (3.14)$$

We estimate the derivative of the decay constant with respect to the sea light-quark mass using again the prediction of partially quenched SU(3) ChPT at

NLO [37]-[38], which gives

$$\begin{aligned}\Delta_{f_K} &= \frac{4B_0}{f_0}\left\{-8L_4^r(\mu)+\frac{1}{64\pi^2}\left[3+\log\left(2B_0\frac{m_{ud}}{\mu^2}\right)+\log\left(B_0\frac{m_s+m_{ud}}{\mu^2}\right)\right.\right.\\ &- \left.\left.\frac{1}{2}\frac{m_s+2m_{ud}}{m_s-m_{ud}}\log\left(\frac{2m_s+m_{ud}}{3m_{ud}}\right)\right]\right\} \qquad (3.15)\end{aligned}$$

Using the values $B_0/f_0 = 19\ (2)$ and $L_4^r(\mu) = 0.04\ (14)\cdot 10^{-3}$ at $\mu = M_\rho = 0.770$ GeV, the derivative Δ_{f_K} in the $\overline{\rm MS}(2\,{\rm GeV})$ scheme is estimated to be equal to $\Delta_{f_K} = -0.38(10)$, which leads to $\Delta_{f_K}(m_u - m_{ud}) = 0.51(17)\,{\rm MeV}$.

From the lattice data (see Figs. 3.1-3.2) we find $f_K(m_u, m_u; m_u) - f_K(m_{ud}, m_{ud}; m_{ud}) = -1.25(31)$ MeV. Therefore, using Eq. (3.13) we get the estimate

$$f_{K^+} - f_K = -0.74\ (35)\,{\rm MeV}\ , \qquad (3.16)$$

which is consistent with the estimate of the direct method (3.12) within the errors.

Finally we average the two determinations (3.12) and (3.16) obtaining our final result

$$f_{K^+} - f_K = -0.62\ (29)\,{\rm MeV}\ . \qquad (3.17)$$

Using Eq. (3.5) we also get

$$\frac{f_{K^+} - f_K}{f_K} = -0.0040\ (19)\ , \qquad (3.18)$$

which is quite close to the more precise determination $(f_{K^+} - f_K)/f_K = -0.0040(4)$ obtained with $N_f = 2$ in Ref. [42] using a dedicated approach.

In conclusion for the charged kaon decay constant f_{K^+} we quote the value

$$\begin{aligned}f_{K^+} &= 154.4\ (1.5)_{stat+fit}(0.4)_{Chiral}(1.1)_{Disc}(0.1)_{Z_P}(0.4)_{FSE}(0.3)_{(f_{K^+}-f_K)}\,{\rm MeV}\\ &= 154.4\ (2.0)\,{\rm MeV} \qquad (3.19)\end{aligned}$$

and, after dividing by the experimental value of the pion decay constant, we get

$$\begin{aligned}f_{K^+}/f_{\pi^+} &= 1.184\ (12)_{stat+fit}(3)_{Chiral}(9)_{Disc}(1)_{Z_P}(3)_{FSE}(2)_{f_{\pi^+}}(3)_{(f_{K^+}-f_K)}\\ &= 1.184\ (16)\ . \qquad (3.20)\end{aligned}$$

The result (3.20) can be compared with the FLAG averages [31]: $f_{K^+}/f_{\pi^+} = 1.205(18)$ at $N_f = 2$ from Refs. [32, 41], $f_{K^+}/f_{\pi^+} = 1.192(5)$ at $N_f = 2+1$ from Refs. [33, 34, 35, 43] and $f_{K^+}/f_{\pi^+} = 1.194(5)$ at $N_f = 2+1+1$ from

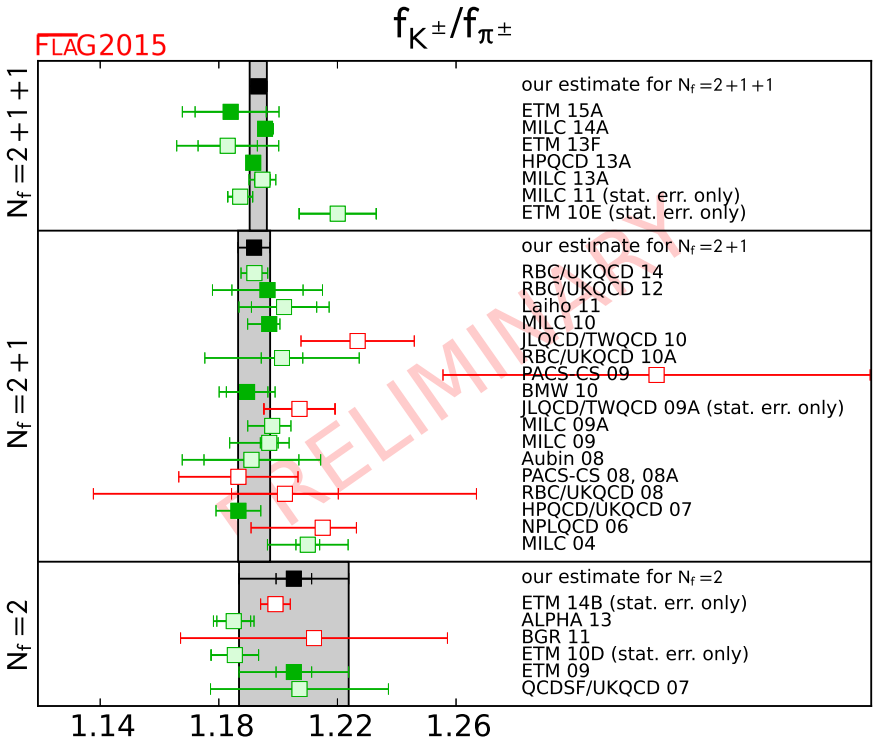

Figure 3.3: Comparison of the values of f_{K^+}/f_{π^+} found by several collaborations as reported in [31] classified by the number of dynamical flavors considered in the simulations. The solid green points represent the values that are considered in the computation of the FLAG average

Refs. [44, 45]. In fig. 3.3, which is taken from the 2015 update of FLAG, our result is indicated by a green solid point, meaning that it has been considered for the computation of the FLAG average value for f_{K^+}/f_{π^+}. The FLAG group follows very strict criteria that collaborations need to satisfy for their results to be included in the averages [31]. Specifically, the results indicated by green solid points are the ones whose systematic uncertainties (induced by chiral and continuum extrapolations, FSEs, renormalization and running of scaling variables) are well evaluated and under control.

3.1.3 Determination of $|V_{us}|$

The next step in our analysis consisted in combining the result of eq. (3.20) with the experimental data on $|V_{us}/V_{ud}|$ $f_{K^+}/f_{\pi^+} = 0.2760(4)$ [46] and $|V_{ud}| = 0.97417(21)$ from superallowed nuclear β decay [10] in order to obtain a determination of the CKM matrix element $|V_{us}|$. We find

$$|V_{us}| = 0.2271\ (4)_{\rm exp}(29)_{f_{K^+}/f_{\pi^+}} = 0.2271\ (31)\ , \tag{3.21}$$

where the first error comes from the experimental uncertainties, while the second is due to the uncertainty on f_{K^+}/f_{π^+}.

Since the CKM matrix is unitary in the Standard Model, the elements of the first row should obey the constraint

$$|V_{ud}|^2 + |V_{us}|^2 + |V_{ub}|^2 = 1\ . \tag{3.22}$$

The contribution from $|V_{ub}|$ is very tiny, being $|V_{ub}| = 4.13(49) \cdot 10^{-3}$ [36], and can be neglected. Using our result (3.21) we obtain

$$|V_{ud}|^2 + |V_{us}|^2 + |V_{ub}|^2 = 1.0007\ (5)_{\rm exp}(13)_{f_{K^+}/f_{\pi^+}} = 1.0007\ (14)\ , \tag{3.23}$$

which confirms the first-row CKM unitarity at the permille level.

3.2 Calculation of f_D, f_{D_s} and f_{D_s}/f_D

In this Section we present our determinations of the decay constants f_D and f_{D_s}, as well as of the ratio f_{D_s}/f_D. Our analysis is based on the study of the quark mass dependence of two dimensionless ratios, namely f_{D_s}/M_{D_s} and $(f_{D_s}/f_D)/(f_K/f_\pi)$. This choice is motivated by the following observations:

- the ratio f_{D_s}/M_{D_s} is affected by smaller discretization effects with re-

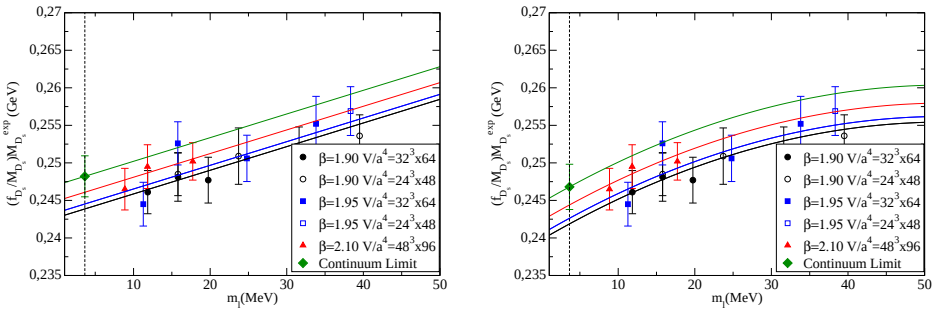

Figure 3.4: *Chiral and continuum extrapolation of* $(f_{D_s}/M_{D_s})M_{D_s}^{exp}$ *based on Eq. (3.24), assuming* $P_3 = 0$ *(left) and* $P_3 \neq 0$ *(right). The diamond represents the continuum limit evaluated at the average up/down quark mass* $m_{ud} = 3.70(17)\,\mathrm{MeV}$ *[27].*

spect to other quantities like $f_{D_s} r_0$ or $f_{D_s}\sqrt{M_{D_s}} r_0^{3/2}$ (see also Ref. [47]);

- the double ratio $(f_{D_s}/f_D)/(f_K/f_\pi)$ exhibits a very mild dependence on the light quark mass [48] at variance with the ratio f_{D_s}/f_D.

As in the case of f_K, at first we performed a jackknife sampling and then a bootstrap sampling of 100 events. We then associated our data with each one of the 8 analyses performed in ref. [27] following the same structure used for the charm sector. For each bootstrap event we performed a small interpolation of the lattice data for f_{D_s}/M_{D_s} and $(f_{D_s}/f_D)/(f_K/f_\pi)$ to the strange and charm quark masses determined in [27]. The dependences of f_{D_s}/M_{D_s} on the light-quark mass m_ℓ and on the lattice spacing turn out to be well described by the simple polynomial expression. As is known, the Heavy Meson ChPT (HMChPT) predicts the absence of chiral logarithms at NLO for both f_{D_s} and M_{D_s}. Therefore we have adopted for f_{D_S}/M_{D_s} either a linear ($P_3 = 0$) or a quadratic ($P_3 \neq 0$) extrapolation in m_ℓ, supplemented with a linear term in a^2,

$$f_{D_s}/M_{D_s} = P_1(1 + P_2 m_\ell + P_3 m_\ell^2 + P_4 a^2)\ . \tag{3.24}$$

The chiral and continuum extrapolations of $(f_{D_s}/M_{D_s})M_{D_s}^{exp}$, obtained according to Eq. (3.24) and using the experimental value $M_{D_s}^{exp} = 1.969\,\mathrm{GeV}$, are shown in Fig. 3.4, where it can be seen that a simple a^2-scaling behavior fits nicely our data on f_{D_s}/M_{D_s}.

The systematic uncertainty associated with the chiral extrapolation has been estimated by comparing the results obtained using a linear ($P_3 = 0$) or a quadratic ($P_3 \neq 0$) fit in m_ℓ, while the one related to discretization effects has been taken from the difference of the results corresponding to the continuum limit and to the finest lattice spacing. Lattice data corresponding to the same β and light quark mass, but different lattice volumes show that FSE are well within the statistical uncertainty. Finally, in the (stat+fit) error (quoted below) we have included the errors induced by the uncertainties on the light, strange and charm quark masses as well as on the input parameters related to the scale setting and to the chiral extrapolation.

Our final result for f_{D_s} reads

$$\begin{aligned} f_{D_s} &= 247.2\ (3.9)_{stat+fit}(0.7)_{Chiral}(1.2)_{Disc}(0.3)_{Z_P}\,\text{MeV} \\ &= 247.2\ (4.1)\,\text{MeV} \end{aligned} \tag{3.25}$$

This value can be compared with the FLAG averages [31]: $f_{D_s} = 250(7)\,\text{MeV}$ at $N_f = 2$ from Ref. [49] and $f_{D_s} = 248.6(2.7)\,\text{MeV}$ at $N_f = 2+1$ from Refs. [50, 51]. Moreover, our result (3.25) agrees very well with the recent determination $f_{D_s} = 249.0(0.3)(^{+1.1}_{-1.5})\,\text{MeV}$ obtained by the FNAL/MILC Collaboration [52] with $N_f = 2+1+1$.

We fit the double ratio $(f_{D_s}/f_D)/(f_K/f_\pi)$ by combining the ChPT predictions for f_π and f_K with the HMChPT prediction for f_{D_s}/f_D, obtaining

$$\frac{f_{D_s}/f_D}{f_K/f_\pi} = P'_1\left[1 + P'_2 m_\ell + \left(\frac{9}{4}\hat{g}^2 - \frac{1}{2}\right)\xi_\ell \log \xi_\ell\right]\frac{K^{FSE}_{f_\pi}}{K^{FSE}_{f_K}}\,, \tag{3.26}$$

where for the HMChPT coupling constant $\hat{g}$ we adopt the value $\hat{g} = 0.61(7)$ [36]. The latter, among the presently available determinations of $\hat{g}$, maximizes the impact of the chiral log in Eq. (3.26). Notice that discretization effects have not been included in Eq. (3.26), since within the statistical errors no cutoff dependence is visible in the lattice data, see Fig. 3.5. As a further check of the impact of discretization effects we perform the fit (3.26) without including the data at the coarsest lattice spacing (this corresponds roughly to keep half of the data), obtaining for the double ratio the same final result.

In Eq. (3.26) we have included the FSE corrections for both f_π and f_K taken from Ref. [53] and Ref. [30], respectively. The former accounts also for the effects of the $\pi^0 - \pi^+$ mass splitting. In this way the FSE observed in the data at the same light quark mass and lattice spacing but different lattice volumes are accurately reproduced [27].

An alternative fit without no chiral logs has been performed in order to evaluate the systematic error associated to chiral extrapolation, namely

$$\frac{f_{D_s}/f_D}{f_K/f_\pi} = \overline{P}_1 \left(1 + \overline{P}_2 m_\ell\right) \frac{K_{f_\pi}^{FSE}}{K_{f_K}^{FSE}} \ . \tag{3.27}$$

The chiral extrapolations for the double ratio $(f_{D_s}/f_D)/(f_K/f_\pi)$, using either the ChPT (3.26) or the linear (3.27) fit, are shown in Fig. 3.5, where it can be seen that the two fits provide compatible results for all pion masses within the statistical uncertainties.

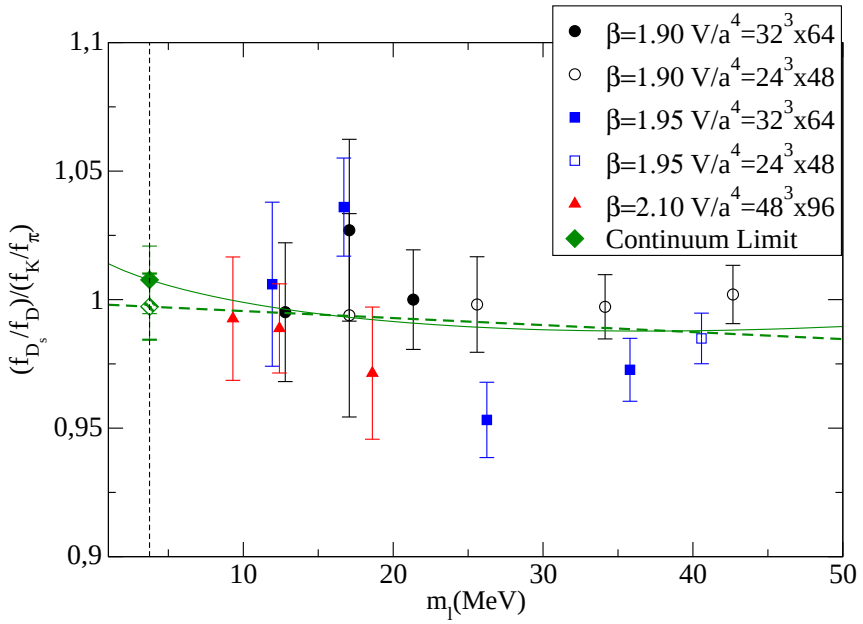

Figure 3.5: *Chiral and continuum extrapolation of the double ratio* $(f_{D_s}/f_D)/(f_K/f_\pi)$ *using both the ChPT fit (3.26) (solid line) and the polynomial expansion (3.27) (dashed line) in the light quark mass* m_ℓ*. The full and open diamonds represent the corresponding continuum limit evaluated at the average up/down quark mass* m_{ud}*, respectively. Lattice data have been corrected for FSE using Ref. [30] for* f_K *and Ref. [53] for* f_π*.*

The result for the double ratio $(f_{D_s}/f_D)/(f_K/f_\pi)$ can be finally used to get a determination of f_{D_s}/f_D. The most relevant source of systematic errors

for the double ratio $(f_{D_s}/f_D)/(f_K/f_\pi)$ is the chiral extrapolation, while for f_{D_s}/f_D also the discretization error coming from f_K/f_π is important. On the other hand, the errors on the strange and charm quark masses, as well as the uncertainty on the RC Z_P, contribute negligibly.

Our final results for $(f_{D_s}/f_D)/(f_K/f_\pi)$ and f_{D_s}/f_D are

$$\begin{aligned} \frac{f_{D_s}/f_D}{f_K/f_\pi} &= 1.003\ (13)_{stat+fit}(5)_{Chiral}(3)_{FSE} \\ &= 1.003\ (14)\ , \end{aligned} \tag{3.28}$$

$$\begin{aligned} f_{D_s}/f_D &= 1.192\ (19)_{stat+fit}(8)_{Chiral}(8)_{Disc}(1)_{Z_P} \\ &= 1.192\ (22)\ . \end{aligned} \tag{3.29}$$

The latter one can be compared with the FLAG averages [31]: $f_{D_s}/f_D = 1.20(2)$ at $N_f = 2$ from Ref. [49] and $f_{D_s}/f_D = 1.187(12)$ at $N_f = 2+1$ from Refs. [51, 54]. Notice the remarkable precision for the double ratio (3.28), which also indicates that SU(3) breaking effects in the ratio of PS meson decay constants are the same in the light and charm sectors within a percent accuracy.

Finally we combine our results for f_{D_s} and f_{D_s}/f_D to obtain for f_D the value

$$\begin{aligned} f_D &= 207.4\ (3.7)_{stat+fit}(0.6)_{Chiral}(0.7)_{Disc}(0.1)_{Z_P}\,\text{MeV} \\ &= 207.4\ (3.8)\,\text{MeV}\ . \end{aligned} \tag{3.30}$$

The FLAG averages [31] are: $f_D = 212(8)\,\text{MeV}$ at $N_f = 2$ from Ref. [49] and $f_D = 209.2(3.3)\,\text{MeV}$ at $N_f = 2+1$ from Refs. [51, 54].

Our data have been extrapolated to the average up/down quark mass m_{ud} and therefore our results for f_D, f_{D_s}, f_{D_s}/f_D and $(f_{D_s}/f_D)/(f_K/f_\pi)$ correspond to the isospin symmetric limit of QCD.

In the case of the D-meson decay constant an estimate of the leading IB effects due to the up- and down-quark mass difference may be obtained in a way similar to the one adopted for the kaon decay constant in Section 3.1.2. Using the results of the partially quenched Heavy Meson ChPT (HMChPT) of Refs. [55, 56] to correct for the derivative of the D-meson decay constant with respect to the sea light-quark mass, we obtain from our lattice data the rough estimate $f_{D^+} - f_D = -0.4 \pm 0.8\,\text{MeV}$, which is not inconsistent with the more precise result $f_{D^+} - f_D = 0.47^{+25}_{-06}\,\text{MeV}$ obtained recently in Ref. [52]. However, because of the large error of the above numerical result and of the uncertainty related to the use of an effective field theory valid

only in the static limit, we do not provide in this dissertation any estimate for f_{D^+}, which is left to a future work, where the method of Refs. [41, 42] will be applied.

For the leptonic decay rates of D- and D_s-mesons we use the latest experimental results $f_D|V_{cd}| = 46.06(1.11)\,\text{MeV}$ and $f_{D_s}|V_{cs}| = 250.66(4.48)\,\text{MeV}$, obtained in Ref. [57] by averaging the electron and muon channels and by including an estimate of structure-dependent Bremsstrahlung effects. Neglecting other electroweak corrections (see Ref. [52] for a first estimate), our results for f_D and f_{D_s} provide the following determinations of the second-row CKM matrix elements:

$$\begin{aligned} |V_{cd}| &= 0.2221\ (53)_{exp}(41)_{f_D} = 0.2221\ (67)\ , \\ |V_{cs}| &= 1.014\ (18)_{exp}(16)_{f_{D_s}} = 1.014\ (24)\ . \end{aligned} \tag{3.31}$$

Using $|V_{cb}| = 0.0413(49)$ [36], the sum of the squares of the second-row CKM elements turns out to be equal to

$$|V_{cd}|^2 + |V_{cs}|^2 + |V_{cb}|^2 = 1.08\ (5)\ , \tag{3.32}$$

showing good agreement with unitarity.

Chapter 4

Vector and scalar form factors of K and D semileptonic decays

In this chapter we present our determination of the CKM matrix elements $|V_{us}|, |V_{cd}|$ and $|V_{cs}|$ by means of the vector and scalar form factors of the K and D semileptonic decays combined with experimental data on the $K_{\ell 3}$, $D \to \pi \ell \nu$ and $D \to K \ell \nu$ decay rates.

The main novelty of the present analysis is the fact that we didn't limit ourselves to study the vector form factor at zero 4-transfer momentum, i.e. $f_+(0)$, instead we managed to study the whole dependence on q^2 of both f_+ and f_0 and then we compared our result with those obtained by several experimental collaborations.

4.1 Vector and scalar form factors of $K_{\ell 3}$ decay

4.1.1 Preliminary analysis

The matrix element of the vector current between two pseudoscalar mesons decomposes into two Lorentz invariant form factors, f_+ and f_0:

$$\langle \pi(p') | V_\mu | K(p) \rangle = (p'_\mu + p_\mu) f_+(q^2) + (p_\mu - p'_\mu) f_-(q^2), \tag{4.1}$$

where with $\langle \pi(p') | V_\mu | K(p) \rangle$ we represent the renormalized vector current, which depends on the 4-momentum transfer $q_\mu = p_\mu - p'_\mu$. The scalar form factor f_0 is defined as

$$f_0(q^2) = f_+(q^2) + \frac{q^2}{M_K^2 - M_\pi^2} f_-(q^2), \tag{4.2}$$

and therefore satisfies the relation $f_+(0) = f_0(0)$. The matrix element in eq. (4.1) can be derived from the time dependence of a convenient combination of Euclidean three-point correlation functions in lattice QCD. As it is well known at large time distances the renormalized three-point function can be written as

$$C_\mu^{K\pi}(t_x, t_y, \vec{p}, \vec{p}') \xrightarrow{tx \gg a \quad (t_y - t_x) \gg a} Z_V \frac{\sqrt{Z_K Z_\pi}}{4 E_K E_\pi} \left\langle \pi(p') \left| V_\mu \right| K(p) \right\rangle_0 e^{-E t_x - E'(t_y - t_x)} \tag{4.3}$$

where with $\langle \pi(p') |V_\mu| K(p)\rangle_0$ we represent the *bare* vector current. Three point correlation functions can then be combined calculating the ratios R_μ

$$R_\mu(t, \vec{p}, \vec{p}') = \frac{C_\mu^{K\pi}(t, T/2, \vec{p}, \vec{p}') C_\mu^{\pi K}(t, T/2, \vec{p}', \vec{p})}{C_\mu^{\pi\pi}(t, T/2, \vec{p}', \vec{p}') C_\mu^{KK}(t, T/2, \vec{p}, \vec{p})} \tag{4.4}$$

which is independent of the vector renormalization constant Z_V and on the matrix elements Z_π and Z_K. In our simulation setup we used the same momentum in all three spatial directions for a specific quark, so the identity $\langle R_1 \rangle = \langle R_2 \rangle = \langle R_3 \rangle$ is valid up to statistical uncertainties. With $\langle R_i \rangle$ we thus denote the numerical average of the spatial components of R_μ.

The matrix elements $\langle V_0 \rangle$ and $\langle V_i \rangle$ can then be extracted with a constant fit of the $R_\mu(t, \vec{p}, \vec{p}')$ plateaux around $T/4$ through the relations

$$\begin{aligned} \langle V_0 \rangle &= \left\langle \pi(p') \left| V_0 \right| K(p) \right\rangle = 2\sqrt{R_0}\sqrt{E E'} \\ \langle V_i \rangle &= \left\langle \pi(p') \left| V_i \right| K(p) \right\rangle = 2\sqrt{R_i}\sqrt{p p'}. \end{aligned} \tag{4.5}$$

We can then use the matrix elements to extract the form factors through the relations

$$\begin{aligned} f_+(q^2) &= \frac{(E - E') \langle V_i \rangle - (p_i - p_i') \langle V_0 \rangle}{2E p_i' - 2E' p_i} \\ f_-(q^2) &= \frac{(p_i + p_i') \langle V_0 \rangle - (E + E') \langle V_i \rangle}{2E p_i' - 2E' p_i} \end{aligned} \tag{4.6}$$

The energies appearing in eq. (4.6) are calculated through the dispersion relation $E = \sqrt{p^2 + M^2}$ with the masses obtained fitting the same two-points correlation functions of pseudoscalar mesons at zero momentum that we used in the previous chapters to study the decay constants of K and D mesons. The scalar form factor f_0 can then be extracted from eq. (4.2).

In order to decrease statistical errors we decided to calculate f_0 also from the three point correlation functions of the scalar current S. This method is

based on the Ward identity relating the matrix element of a vector current to that of the corresponding scalar current

$$q^\mu \left\langle \pi(p') \left| V_\mu \right| K(p) \right\rangle = (m_s - m_l) \left\langle \pi(p') \left| S \right| K(p) \right\rangle , \tag{4.7}$$

where $\langle \pi(p') |S| K(p)\rangle$ represents the renormalized scalar current and m_s and m_l are the renormalized strange and light quark masses . Once obtained $\langle \pi(p') |S| K(p)\rangle$ we can easily calculate the scalar form factor as

$$f_{0(s)}(q^2) = \frac{m_s - m_l}{M_K^2 - M_\pi^2} \left\langle \pi(p') \left| S \right| K(p) \right\rangle , \tag{4.8}$$

where M_K and M_π are respectively the kaon and the pion meson masses. With the Twisted mass actions it's possible to demonstrate that the RC of the quark mass is the inverse of the one of the scalar density (with the chosen values of the Wilson parameters) so that the r.h.s. of eq. (4.8) doesn't depend on any renormalization constant and it can be written as

$$f_{0(s)}(q^2) = \frac{\mu_s - \mu_l}{M_K^2 - M_\pi^2} \left\langle \pi(p') \left| S \right| K(p) \right\rangle_0 , \tag{4.9}$$

where $\langle \pi(p') |S| K(p)\rangle_0$ represents the bare matrix element of the scalar current. Similarly to the vector current, we can obtain the matrix element $\langle S \rangle_0$ by studying the large time behaviour of the three-point correlation function $C_S^{K\pi}(t_x, t_y, \vec{p}, \vec{p}')$, thus obtaining $f_{0(s)}(q^2)$ from the ratio

$$f_{0(s)}(q^2) = \frac{\mu_s - \mu_l}{M_K^2 - M_\pi^2} \left(\frac{4EE'}{Z_K Z_\pi} \right) \sqrt{\frac{C_S^{K\pi}(t_x, t_y, \vec{p}, \vec{p}') C_S^{\pi K}(t_x, t_y, \vec{p}', \vec{p})}{e^{-(E+E')T/2}}}, \tag{4.10}$$

where the pseudoscalar meson matrix elements Z_K and Z_π were extracted, as in the case of the masses, from the time behavior of the two-point correlators. The time interval chosen for the fit of the matrix elements $\langle V_0 \rangle$, $\langle V_i \rangle$ and $f_{0(s)}$ was $[T/2 - 2, T/2 + 2]$, and it was determined by requiring that the changes in the matrix elements due to a modification of the interval by one or two lattice units were well below the statistical uncertainty. By having numerical data of the quantities $\langle V_0 \rangle$, $\langle V_i \rangle$ and $f_{0(s)}$, i.e. the scalar form factor obtained by analysing the scalar three-point correlation function, we can perform an overconstrained fit according to eqs. (4.6) and (4.8) in order to obtain both the vector and the scalar form factors as function of q^2 with greater accuracy compared to the one we would have obtained by using only the vector current. In fig. 4.1 an example of the extraction of $\langle V_0 \rangle$, $\langle V_i \rangle$ and

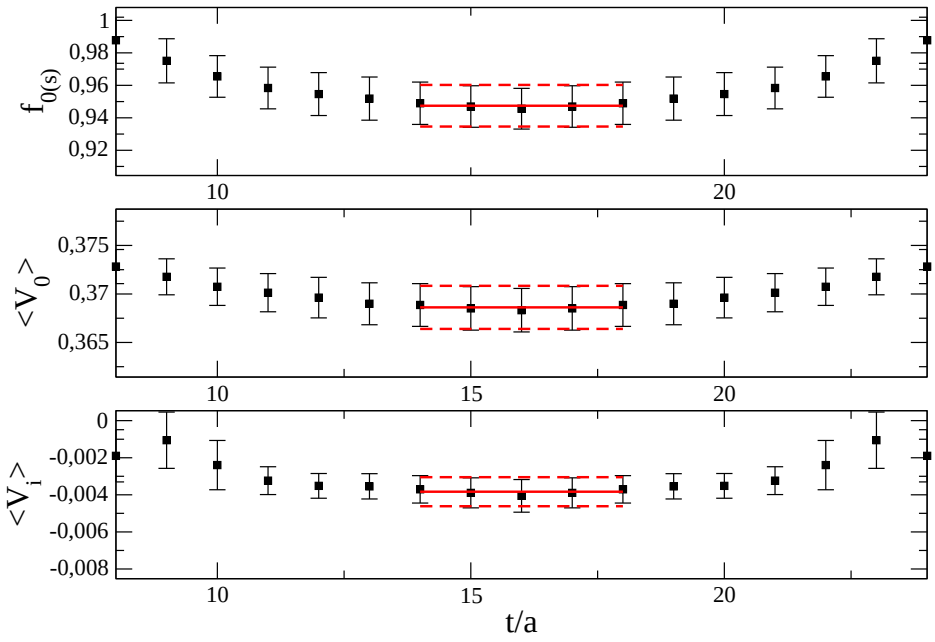

Figure 4.1: Example of the extraction of the matrix elements $\langle V_0 \rangle$, $\langle V_i \rangle$ and of the scalar form factor $f_{0(s)}$ obtained from the three-point correlation functions in the interval $[T/2-2, T/2+2]$. The data corresponds to $\beta = 1.90$, $a\mu_l = 0.0040$, $L/a = 32$, $a\mu_s = 0.0185$ and $p' = -p \simeq 151$MeV

$f_{0(s)}$ is shown.

The next step was a selection of good quality data, i.e. we excluded data points that were too noisy or had a very big statistical error, i.e. they were irrelevant in the fits. The excluded data points are those with at least one meson having the largest momentum simulated. This allowed us to use the exact same criteria of exclusion for all the ensembles of our simulation. In fig. 4.2 an example of data selection is presented. It should be noted in fig. 4.2 that the selected data includes both points belonging to the physical range, i.e. from $q^2 = 0$ to $q^2 = (M_K - M_\pi)^2$, and points with $q^2 < 0$. This allowed us to determine the q^2 dependence of our data with good accuracy.

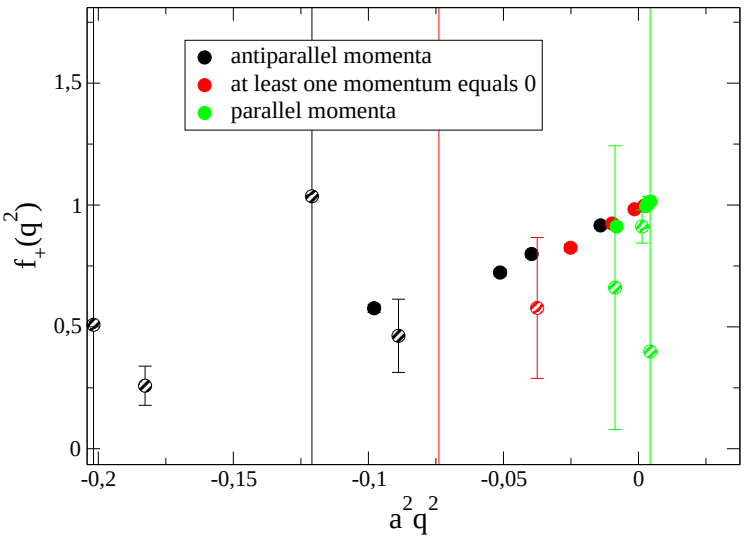

Figure 4.2: An example of the selection performed on our data of the form factors. In the figure we show data of $f_+(q^2)$ corresponding to the ensemble A32.40 where the different color correspond to different kinematical conditions. The dashed data points correspond to the excluded data. The selected data, plotted with solid, shows a very smooth dependence on q^2.

Selected data was sampled using the jackknifing procedure with 15 samples. We then performed a bootstrap sampling of 800 events, which were associated with the 800 events corresponding to our determinations of lattice input parameters, namely the light quark mass, the strange quark mass and the lattice spacing. The gauge ensembles used for the present analysis are the same used for the determination of the quark masses and the values of the lattice spacing. After the selection, every data point corresponding to a specific value of the lattice spacing, q^2 and μ_l was analysed as a function of the strange quark mass in order to perform the interpolation to the physical strange quark mass, which was obtained in ref. [27].

4.1.2 Global fits

The next step consisted in performing a global fit of both the vector and the scalar form factors analysing simultaneously their dependences on a^2,μ_l and q^2 in order to determine the form factors at the physical point as functions of q^2.

Different functional forms have been considered to this purpose. The first ansatz that we used was based on SU(2) ChPT, and was obtained by expanding in $x = M_\pi^2/M_K^2$ the SU(3) NLO expressions for the form factors obtained by Gasser and Leutwyler [58, 59]. As shown in ref. [60] the result of the expansion is

$$\begin{aligned} f_+(s) &= F_+(s)\left\{1 + C_+(s)x + \frac{M_K^2}{(4\pi f)^2}\left[-\frac{3}{4}x\log x - xT_1^+(s) - T_2^+(s)\right]\right\}, \\ f_0(s) &= F_0(s)\left\{1 + C_0(s)x + \frac{M_K^2}{(4\pi f)^2}\left[-\frac{3}{4}x\log x + xT_1^0(s) - T_2^0(s)\right]\right\}, \end{aligned} \tag{4.11}$$

where $s = q^2/M_K^2$. The terms in the brackets of eq. (4.11) are obtained from the kaon and pion loop contributions expanded in x, keeping only the $\mathcal{O}(x), \mathcal{O}(x\log x)$ and $\mathcal{O}(\log(1-s))$ terms. The functions $T_{1,2}^{0,+}(s)$ are then given by

$$\begin{aligned} T_1^+(s) &= [(1-s)\log(1-s) + s(1-s/2)]3(1+s)/4s^2 \\ T_2^+(s) &= [(1-s)\log(1-s) + s(1-s/2)](1-s)^2/4s^2 \\ T_1^0(s) &= [\log(1-s) + s(1+s/2)](9+7s^2)/4s^2 \\ T_2^0(s) &= [(1-s)\log(1-s) + s(1-s/2)](1-s)(3+5s)/4s^2 \end{aligned} \tag{4.12}$$

.

It can be seen that the coefficients of the pion chiral log in eq. (4.11) are in agreement with those predicted by SU(2) ChPT, both at $q^2 = 0$ and $q^2 = q^2_{max}$ [61]. At $q^2 = 0$ the leading chiral log has the coefficient $-3/4$, while close to $q^2 = q^2_{max}$, i.e. for $s \simeq (1 - \sqrt{x})^2$, the functions $T^0_{1,2}(s)$ also contribute to the chiral log leading, for $f_0(s)$, to an overall coefficient equal to $-11/4$.

The functions $F_{+,0}$ and $C_{+,0}$ are not predicted by Chiral Perturbation Theory, therefore we used some phenomenological arguments to estabilish their behavior. Inspired by the vector-meson dominance we considered a pole behavior corrected by a polynomial formula in q^2 and a^2 for $F_{+,0}(s)$ and a simple quadratic formula in q^2 for $C_{0,+}(s)$, namely

$$\begin{aligned} F_{0,+}(s) &= \frac{F(1 + A_{0,+}q^2 + B_{0,+}a^2)}{1 - q^2(1 + P_{0,+}M^2_\pi)/M^2_{S,V}}, \\ C_{0,+}(s) &= C + C^{(1)}_{0,+}(s) + C^{(2)}_{0,+}s^2, \end{aligned} \tag{4.13}$$

where $M_{S,V}$ represent the mass of the scalar ($K^*_0(1430)$) and the vector resonance ($K^*(892)$) respectively. These two masses were expressed as

$$M_{S,V} = M_K + \Delta_{S,V} \tag{4.14}$$

where M_K is the kaon mass calculated on the lattice and $\Delta_{S,V}$ is the difference between the experimental value of the scalar (vector) resonance mass, taken from the PDG, and the isospin symmetric kaon mass. In this way we avoided the use in our analysis of lattice data of M_V and M_S, which are tipically very noisy, still maintaining a dependence on the light quark mass in the pole sector of our formulas. It should be noticed that while for the vector form factor a pole parametrization with the dominance of the $K^*(892)$ is in good agreement with the data, for the scalar form factor such dominance is less clear. For this reason, we also tried a global fit in which we removed the pole parametrization for f_0 replacing it with a polynomial dependence in q^2.

Further constraints used in the analysis are the equality $f_+(0) = f_0(0)$, which holds for any value of the light quark mass and the lattice spacing, and the Callan-Treiman theorem (ref. [62]), which relates in the chiral limit the scalar form factor calculated at the unphysical $q^2_{CT} = M^2_K - M^2_\pi$ to the ratio of the decay constants f_K/f_π. Specifically, we imposed the relation

$$F(s = 1) = \frac{f^0_K}{f}, \tag{4.15}$$

where f_K^0 and f are respectively the kaon and the pion decay constants in the SU(2) chiral limit.

The second fit ansatz that we considered is a modified version of the z-expansion, in the formulation proposed by Bourrely, Caprini and Lellouch [63]. The modification of the original formula consists in considering the coefficients of the z-expansion and of the slope in q^2 as functions of μ_l and a^2. Specifically, by truncating the expansion at $\mathcal{O}(z)$ we considered the ansatz

$$\begin{aligned} f_+(q^2) &= \frac{a_0(M_\pi^2, a^2) + a_1(M_\pi^2, a^2)\left[z + \frac{1}{2}z^2\right]}{1 - q^2(1 + P_+ M_\pi^2)/M_V^2} \\ f_0(q^2) &= \frac{b_0(M_\pi^2, a^2) + b_1(M_\pi^2, a^2)\left[z + \frac{1}{2}z^2\right]}{1 - q^2(1 + P_0 M_\pi^2)/M_S^2} \\ z &= \frac{\sqrt{t_+ - q^2} - \sqrt{t_+ - t_0}}{\sqrt{t_+ - q^2} + \sqrt{t_+ - t_0}} \end{aligned} \tag{4.16}$$

where $t_+ = (M_K + M_\pi)^2$ and $t_0 = (M_K + M_\pi)(\sqrt{M_K} - \sqrt{M_\pi})^2$. We adopted linear dependences on μ_l and a^2 for all the coefficients, i.e.

$$\begin{aligned} a_i &= A_i + B_i M_\pi^2 + C_i a^2, \\ b_i &= D_i + E_i M_\pi^2 + F_i a^2, \end{aligned} \tag{4.17}$$

where $i = 0, 1$. Resonance masses M_V and M_S were calculated in the same way as in the SU(2) ChPT fit ansatz. In the case of the modified z-expansion an additional term to the χ^2 was added in order to implement the constraint $f_+(0) = f_0(0)$.

As discussed, in this analysis we have studied the dependences of the form factors data. Judging the goodness of the fit just by the final result can be misleading. Rather it's useful to plot the data by keeping everything fixed except for one variable. We fixed the light quark mass and the lattice spacing in ordert to check how the q^2 dependence of our data was fitted. As can be seen from fig. 4.3 the agreement between the data and fit result as a function of q^2 is good. Moreover, in fig. 4.6 we check the dependence of our data on a^2.

Once reassured that the data are in agreement with the fit results we extrapolated to the physical point, obtaining the curves shown in fig. 4.4.

4.1.3 FSE evaluation

An investigation of ensembles A40.24 and A40.32, which share the same pion mass at different volumes, shows the presence of non negligible FSE in

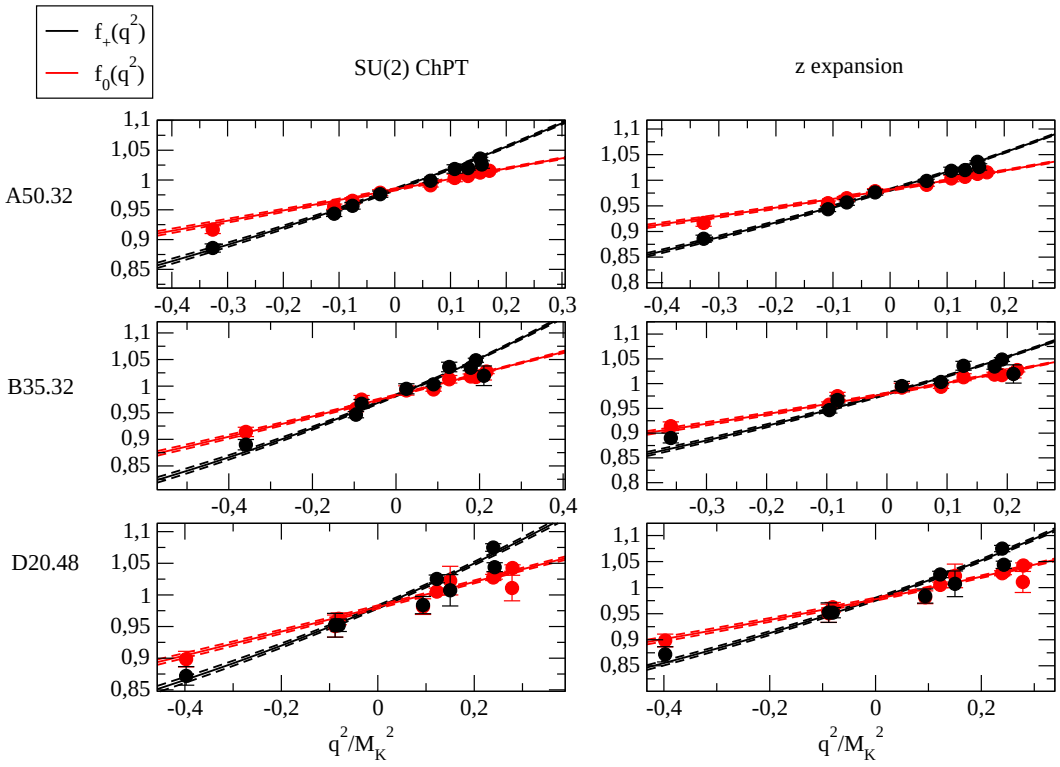

Figure 4.3: Data points of $f_+(q^2)$ and $f_0(q^2)$ corresponding to several lattice ensembles. The solid curves represent the results of the SU(2) χPT global fit (left panel) and of the modified z expansion (right panel), together with their uncertainties (indicated by dashed curves). It can be seen that there is good agreement between data and the results of the fit

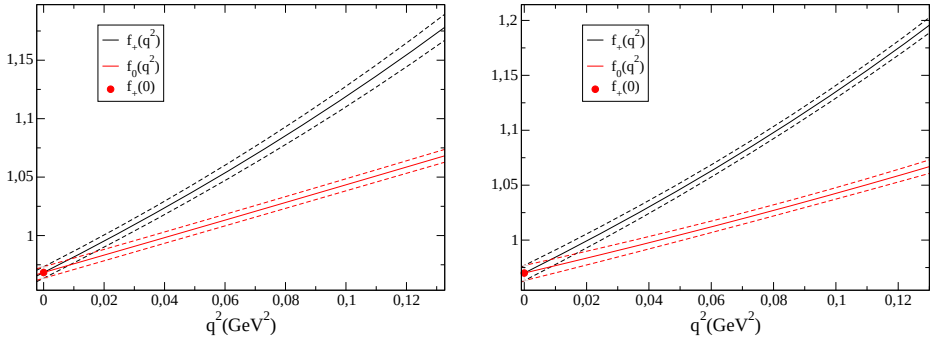

Figure 4.4: Final results of $f_+(q^2)$ and $f_0(q^2)$ at the physical point obtained by the global fit using SU(2) χPT (left panel) and the modified z-expansion (right panel)

the slope of the form factors. This is illustrated in fig. 4.5. Following the strategy used in ref. [64] for FSE corrections in the pion electromagnetic form factor we adopted the following phenomenological ansatz for the slope:

$$\left(\frac{q^2}{M_{S,V}^2}\right)_{V_{inf}} = \left(\frac{q^2}{M_{S,V}^2}\right)_{V_{fin}} \left(1 + PM_\pi^2 \frac{e^{-M_\pi L}}{(M_\pi L)^{\alpha_{eff}}}\right) \tag{4.18}$$

where P is a free parameter determined in the global fit and α_{eff} is an effective fractional power. Typically it's possible to calculate the parameters of FSE expressions in ChPT, but so far there has been no computation of the finite size effects for the form factors with out lattice setup.

For this reason, as a phenomenological approach, we decided to test different values of α_{eff} and noticed that a good estimate of the systematic uncertainty associated to the FSE is given by the spread on the final results found with $\alpha_{eff} = 0$ (which is considered for the central value of our determination of the form factors) and $\alpha_{eff} = 3/2$, which is the exponent that can be found in other physical observables affected by FSE, e.g. the decay constant f_K.

4.1.4 Discretization effects evaluation

Another important systematic uncertainty to take into account is the one induced by discretization effects. In order to evaluate this effect we interpolated our lattice data of f_+ and f_0 for different values of q^2/M_K^2, at

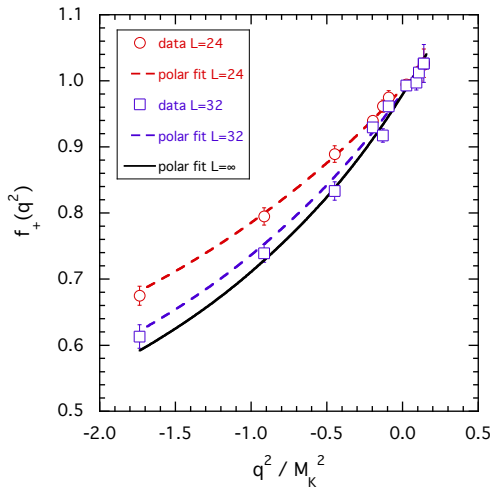

Figure 4.5: Lattice data points of $f_+(q^2)$ corresponding to the ensembles A40.24 and A40.32, which share the same pion mass but different volumes, specifically $L = 24$ and $L = 32$

the physical strange quark mass and at a reference value of the light quark mass. We then plotted the results of these interpolations, together with the result of the SU(2) ChPT fit, as a function of a^2 as shown in fig. 4.6. It can be seen from fig. 4.6 that the behavior of the data in a^2 is very mild and thus we can reasonably assume a linear dependence on the square of the lattice spacing. Judging from the slope of the SU(2) ChPT fit we can estimate discretization effects to be at the permille level.

4.1.5 Dispersive parametrization and experimental results

By having obtained results for the form factors at the physical point, we compare them with those obtained by the experimental collaborations. Experiments tipically measure the ratio between the differential and the total semileptonic decay rate, and perform a fit of the normalized form factors through what is called a dispersive parametrization, in the formulation proposed in ref. [65]. This parametrization is basically a polynomial formula, for both $\bar{f}_+(q^2) = f_+(q^2)/f_+(0)$ and $\bar{f}_0(q^2) = f_0(q^2)/f_+(0)$, in which specific relations among the coefficients of the expansion are imposed by unitarity.

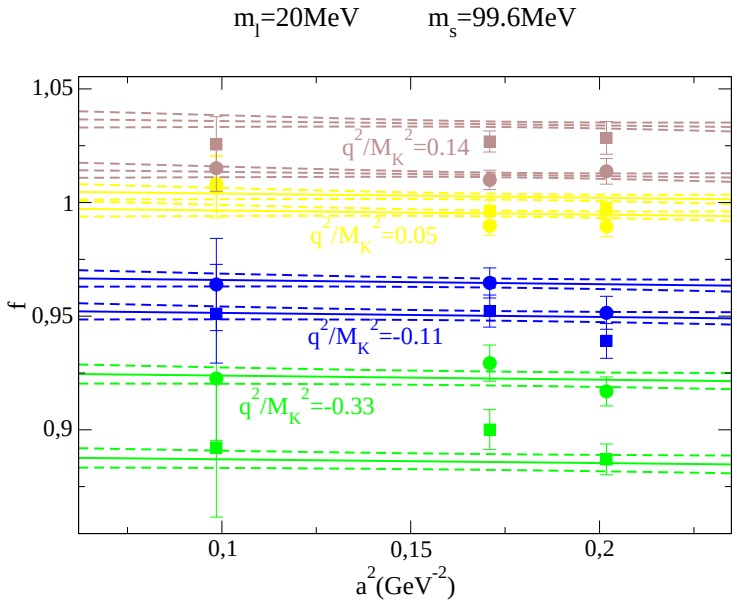

Figure 4.6: A plot showing the dependence on a^2 of lattice data. Results for f_+ (square data points) and f_0 (circle data points) have been interpolated at different values of q^2/M_K^2, represented by different colors, at the physical strange quark mass and at a reference light quark mass of 20 MeV. We also show the result of the SU(2) ChPT fit as a function of a^2.

This parametrization can be written as follows:

$$f_{+,0}(q^2) = f_+(0)\left[1 + \lambda'_{+,0}\frac{q^2}{M_\pi^2} + \frac{1}{2}\lambda''_{+,0}\left(\frac{q^2}{M_\pi^2}\right)^2 + \frac{1}{6}\lambda'''_{+,0}\left(\frac{q^2}{M_\pi^2}\right)^3\right] \quad (4.19)$$

where the expansion parameters are related by

$$\begin{aligned}
\lambda'_0 &= \frac{M_\pi^2}{q_{CT}^2}[\ln C - G(0)],\\
\lambda''_0 &= (\lambda'_0)^2 - 2\frac{M_\pi^4}{q_{CT}^2}G'(0),\\
\lambda'''_0 &= (\lambda'_0)^3 - 6\frac{M_\pi^4}{q_{CT}^2}G'(0)\lambda'_0 - 3\frac{M_\pi^6}{q_{CT}^2}G''(0),\\
\lambda'_+ &= \Lambda_+,\\
\lambda''_+ &= (\lambda'_+)^2 + 2M_\pi^2 H'(0),\\
\lambda'''_+ &= (\lambda'_+)^3 + 6M_\pi^2 H'(0)\lambda'_+ + 3M_\pi^4 H''(0).
\end{aligned} \quad (4.20)$$

The constant C represents the scalar form factor calculated at the Callan-Treiman point $q_{CT}^2 = (M_K - M_\pi)^2$

$$C = \bar{f}_0(q_{CT}^2) = \frac{f_K}{f_\pi}\frac{1}{f_+(0)} + \Delta_{CT} \quad (4.21)$$

where the correction $\Delta_{CT} = \mathcal{O}(m_{ud}/4\pi f_\pi)$ can be evaluated in ChPT. At NLO, in the isospin symmetric limit, $\Delta_{CT} = (-3.5 \pm 8) \times 10^{-3}$.

The functions G and H are defined as

$$\begin{aligned}
G(q^2) &= \frac{q_{CT}^2(q_{CT}^2 - q^2)}{\pi} \times \int_{q_{lim}^2}^{\infty} \frac{ds}{s}\frac{\phi_0(s)}{(s - q_{CT}^2)(s - q^2 - i\epsilon)}\\
H(q^2) &= \frac{M_\pi^2 q^2}{\pi}\int_{q_{lim}^2}^{\infty}\frac{ds}{s^2}\frac{\phi_+(s)}{(s - q^2 - i\epsilon)}
\end{aligned} \quad (4.22)$$

where the phases $\phi_0(s)$ and $\phi_+(s)$ are determined by respectively the S-wave $(K\pi)_{I=1/2}$ scattering and the P-wave $(K\pi)_{I=1/2}$ elastic scattering. Numerical estimates of these functions and its derivatives at $q^2 = 0$ can be found

in literature [66]:

$$\begin{aligned} G(0) &= 0.0398(44) \\ -2\frac{M_\pi^4}{q_{CT}^2}G'(0) &= 4.16(56)\times 10^{-4}, \\ -3\frac{M_\pi^6}{q_{CT}^2}G''(0) &= 2.72(21)\times 10^{-5}, \end{aligned} \tag{4.23}$$

$$\begin{aligned} 2M_\pi^2 H'(0) &= 5.79(97)\times 10^{-4}, \\ 3M_\pi^4 H''(0) &= 2.99(21)\times 10^{-5}. \end{aligned} \tag{4.24}$$

Reading (4.19) and (4.20) it is evident that the only parameters that need to be determined are $\ln C$ and λ_+. This can be done by fitting data coming either from experiments or simulations. In a recent review from M. Moulson [46] experimental results on the kaon semileptonic decay rate from KTeV [67], KLOE [66, 68], NA48/2 [69] and ISTRA+ [70] were combined together in order to perform a global fit and determine average values of $\ln C$ and Λ_+. The results are

$$\begin{aligned} \Lambda_+ &= 25.75(36)\times 10^{-3} \\ \ln C &= 0.1985(70) \end{aligned} \tag{4.25}$$

Combining the experimental results (4.25) and the FLAG average of $f_+(0)$ at $N_f = 2+1$ [31] we can construct the full q^2 dependence of the form factors $f_+(q^2)$ and $f_0(q^2)$ and compare it with our lattice results at the physical point.

This comparison is presented in fig. 4.7. In order to obtain a determination of $f_+(0), \Lambda_+$ and $\ln C$ we generated some "synthetic" data points starting from our global fit results in correspondence of 8 different values of q^2 in the physical range, and to fit them using eq. (4.19).

Our final results are

$$\begin{aligned} f_+(0) &= 0.9684(59)_{stat+fit}(29)_{syst} = 0.9684(66) \\ \ln C &= 0.1937(113)_{stat+fit}(90)_{syst} = 0.1937(138) \\ \Lambda_+ &= 25.2(1.2)_{stat+fit}(1.1)_{syst}\times 10^{-3} = 25.2(1.6)\times 10^{-3} \end{aligned} \tag{4.26}$$

- The $()_{stat+fit}$ error includes the statistical uncertainties, the total error on the light and strange quark masses and the uncertainties due to the fitting procedure.

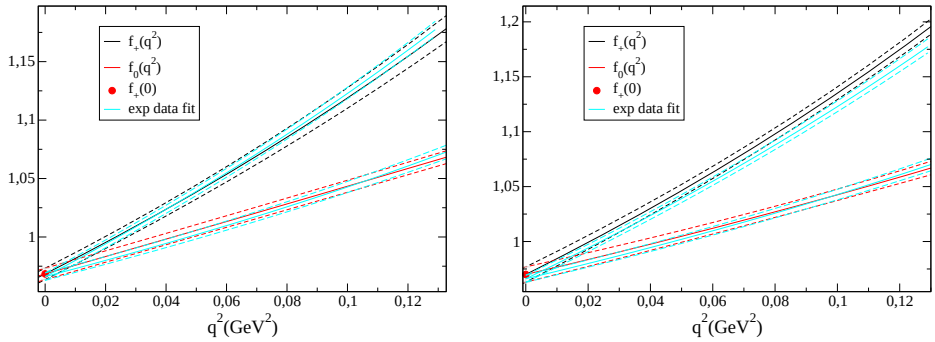

Figure 4.7: Final results for $f_+(q^2)$ and $f_0(q^2)$ at the physical point obtained by the global fit using SU(2) χPT (left panel) and the modified z-expansion (right panel). Results obtained by combining the experimental measurements [46] and the FLAG average of $f_+(0)$ [31] are also shown for comparison.

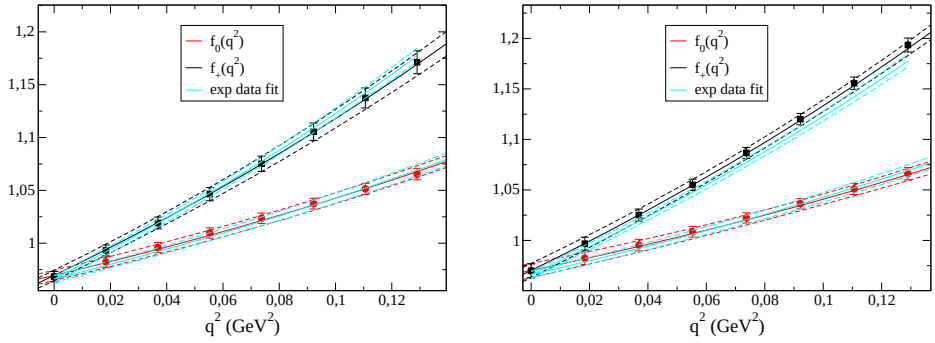

Figure 4.8: Same as fig. (4.7) but with the lattice results represented by the synthetic data points.

- The error denoted as $()_{syst}$ in eq. (4.26) takes into account the systematic errors induced by the chiral extrapolation, evaluated comparing the results obtained with the SU(2) ChPT formula with the ones obtained with the modified z-expansion; the uncertainty induced by FSE, which are mainly relevant for the slope of the form factors; the systematic error induced by discretization effects, which has been evaluated comparing our main fit with a fit in which all the data corresponding to the coarsest lattice spacing were removed.

Using the determinations in eq. (4.26) to construct the full curves for $f_+(q^2)$ and $f_0(q^2)$ gives the result shown in fig. 4.9, which can be seen to be very compatible with the combination of the experimental result and the average value of $f_+(0)$ given by FLAG.

We thus think that a future perspective of this work, and of phenomenological lattice QCD calculations in general, should be to compute this quantities with a greater accuracy, i.e. trying to decrease both the statistical and systematic errors, the most relevant source in our analysis coming from the chiral extrapolation.

Finally, we can combine our result of $f_+(0)$ with experimental data for $f_+(0)|V_{us}|$ [71] in order to obtain the value of the CKM matrix element $|V_{us}|$:

$$|V_{us}| = 0.2234(16). \tag{4.27}$$

As we have already done in the case of the V_{us} determination from $K_{\ell 2}$ we can perform a unitarity test using the $|V_{ud}|$ determination from the superallowed β nuclear decay [10] and neglecting the contribution from $|V_{ub}|$, obtaining

$$|V_{ud}|^2 + |V_{us}|^2 + |V_{ub}|^2 = 0.9991(8), \tag{4.28}$$

in good agreement with the unitarity expectation.

4.2 Smearing with heavy quark masses

As can be seen from ref. [27], the time intervals chosen to fit the two points correlation functions relative to mesons containing a heavy quark are shorter compared to *light-light* and *light-strange* mesons. This has a clear physical reason: the more the valence quarks are heavier, the smaller the gap between the lowest energy state and the first excited state is. Thus, when dealing with heavy quarks, one has to go to larger times to isolate the ground state. For this reason, in some quantities if the signal to noise ratio is too low or if there is too much excited states contamination the evaluation

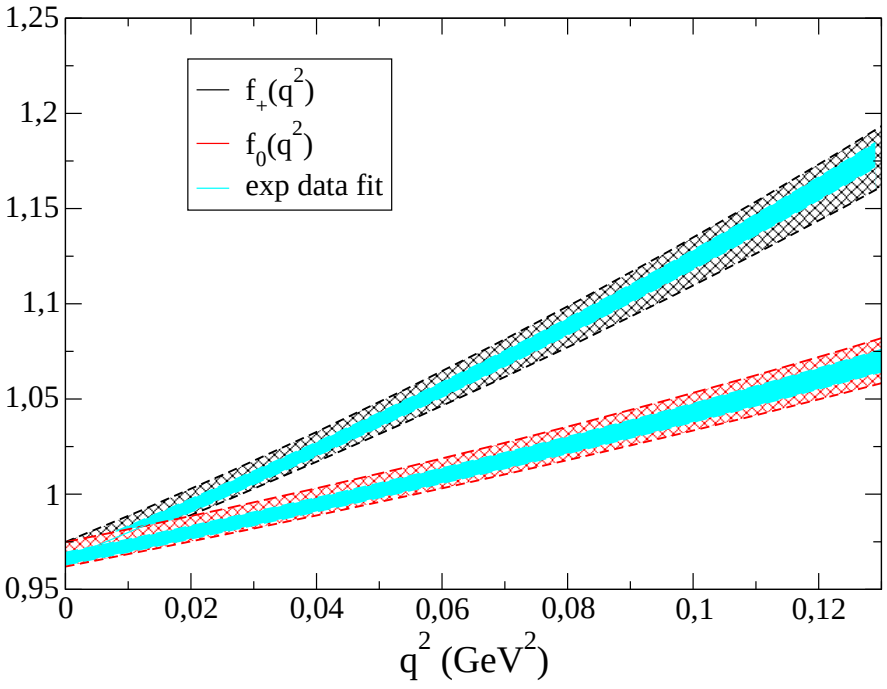

Figure 4.9: Final results for $f_+(q^2)$ (black area) and $f_0(q^2)$ (red area) including all the statistical and systematic uncertainties. We also show the result corresponding to the combination of experimental results and the FLAG average of $f_+(0)$.

of the ground state matrix element might be impossible. When computing correlation functions we basically create out of the vacuum the state we're interested in, $|s\rangle$, (which we assume to be a single particle state), together with all the other state sharing the same quantum numbers, through an operator O:

$$O|0\rangle = |s\rangle + \left|s^{(1)}\right\rangle + \left|s^{(2)}\right\rangle + ... \tag{4.29}$$

Ideally we would like to find a combination of operators O_s built in such a way that when acting on the vacuum it creates *only* the ground state. This must exist, in fact it can be expressed as $O_s = |s\rangle\langle s|O$. The operator O_s generally will be a non-local combination of operators at different lattice points, corresponding to the wave function of the state. Knowing the distribution of such fields, one could build this interpolating operator and compute correlation functions containing just the state s, thus improving the quality of the signal.

In order to build an operator that approximates O_s and have a better overlap with the state $|s\rangle$, one has to make some kind of guess on the shape of the hadron wave function. The general criteria relies on the observation that the wave function of a hadron with mass M extends over a spatial region of dimension $\sim \frac{1}{M}$. Increasing the spatial extent of operators one can achieve better overlap with the lower lying state and thus obtain correlation functions with minor excited states contamination. One can assume the shape of the wave function to be Gaussian-like, and build a creation operator with such form.

4.2.1 Gaussian Smearing

One possibility called *Gaussian smearing* is to substitute the creation operator O with

$$O_s = G^n(k)O, \qquad G(k) = \frac{1+kH}{1+6k}, \tag{4.30}$$

where H is given by

$$H_{x,y} = \sum_{\mu=1,2,3} (U_{x;\mu}\delta_{y,x+\hat{\mu}} + U^{\dagger}_{x-\hat{\mu};\mu}\delta_{y,x-\hat{\mu}}), \tag{4.31}$$

where k is a real number and n an integer number called the *smearing level*.

Let us consider a two points correlation function $C_{\vec{x},t} = \left\langle O^{\dagger}_{s_2}(x)O_{s_1}(0)\right\rangle$

of smeared operators:

$$O_{s_i} = G^{n_i}(k_i)O_i = G^{n_i}(k_i)\bar{\psi}\Gamma_i\psi, \qquad i \in 1,2. \tag{4.32}$$

The correlation function is given by the contraction

$$C_{\vec{x},t} = -\left\langle Tr\left[\Gamma_2(M^{SS})^{-1}_{x,0}\Gamma_1(M^{SS})^{-1}_{0,x}\right]\right\rangle, \tag{4.33}$$

where we have defined the sink and source smeared (SS) propagator $(M^{SS})^{-1}$, which can be expressed in terms of the usual propagator as

$$(M^{SS})^{-1}_{x,0} = G^{n_2}(k_2)_{x,y}(M_{y,z})^{-1}G^{n_1}(k_1)_{z,0}. \tag{4.34}$$

In order to compute the correlator, let us define a vector $\eta_x = \delta_{x,0}$ and apply to it the source smearing operator

$$\phi_y = G^{n_1}(k_1)_{y,z}\eta_x. \tag{4.35}$$

Let us then solve for the vector χ the system

$$M_{x,y}\chi_y = \phi_y \tag{4.36}$$

and apply the sink smearing operator so that

$$(M^{SS})^{-1}_{x,0} = G^{n_2}(k_2)_{x,y}\chi_y. \tag{4.37}$$

The effect of smearing the source operator is to build an extended source ϕ on which to invert the fermionic matrix. If the original source η is a Kronecker delta at the origin, the extended or *smeared* source ϕ is a Gaussian-like source distributed in space:

$$|\phi|^2_x \propto e^{-\left(\frac{|\vec{x}|}{2\sigma}\right)^2}\delta_{t,0}, \tag{4.38}$$

where the parameter σ is a function of k and n which must be tuned in order to obtain the desired Gaussian width. Increasing the number of iteration n and decreasing at the same time the smearing strenght k one can have an approximately constant source width σ. The smearing of the sink operator acts in a very similar way, enhancing the overlap of operator O_2 between the vacuum and the state s. This discussion is also valid when working with stochastic sources with (or without) the one-end trick.

	$\beta = 1.90$	$\beta = 1.95$	$\beta = 2.10$
Z_V	0.5920(4)	0.6095(3)	0.6531(2)

Table 4.1: *Values of the vector renormalization constant Z_V for each lattice spacing of the simulation. These values were used to extract the renormalized vector current matrix element from the smeared-smeared three point correlation functions of the $D \to \pi\ell\nu$ and $D \to K\ell\nu$ decays.*

4.3 Vector and scalar form factors of the D semileptonic decay

In this section we'll describe our preliminary study of the vector and scalar form factors of the semileptonic decay of D meson. The first step of the analysis has been the study of the time dependence of three point smeared-smeared correlators connecting the two mesons (a pion and a D or a kaon and a D) through a local vector current. The latter, similarly to the $K_{\ell 3}$ decay case, has the following time behavior:

$$C_\mu^{DM(SS)}(t_x, t_y, \vec{p}, \vec{p}') \xrightarrow{tx \gg a \;\; (t_y - t_x) \gg a} Z_V \frac{\sqrt{Z_D^{(SS)} Z_M^{(SS)}}}{4 E_D E_M} \left\langle M(p') \left| V_\mu \right| D(p) \right\rangle_0 e^{-E t_x - E'(t_y - t_x)}. \tag{4.39}$$

where M represents either a π or a K meson. At variance with the Kaon case, for the D meson we found that precise results are obtained by extracting the matrix element using only the three point function, i.e. without the need of introducing double ratios:

$$\left\langle M(p') \left| V_\mu \right| D(p) \right\rangle = Z_V \left\langle M(p') \left| V_\mu \right| D(p) \right\rangle_0 = Z_V \frac{lim \xrightarrow{tx \gg a \;\; (t_y - t_x) \gg a} C_\mu^{DM(SS)}(t_x, t_y, \vec{p}, \vec{p}')}{\frac{\sqrt{Z_D^{(SS)} Z_M^{(SS)}}}{4 E_D E_M} e^{-E t_x - E'(t_y - t_x)}} \tag{4.40}$$

It appears from this relation that the vector current renormalization constant Z_V is needed for the calculation of the matrix element. This quantity has been calculated very precisely by the ETMC in ref. [27]. For this work we used the set of Z_V calculated through the Ward-Takahashi Identity method collected in tab. 4.1.

From the matrix elements of the vector current we computed the vector and the scalar form factors according to eqs. (4.6) and (4.2).

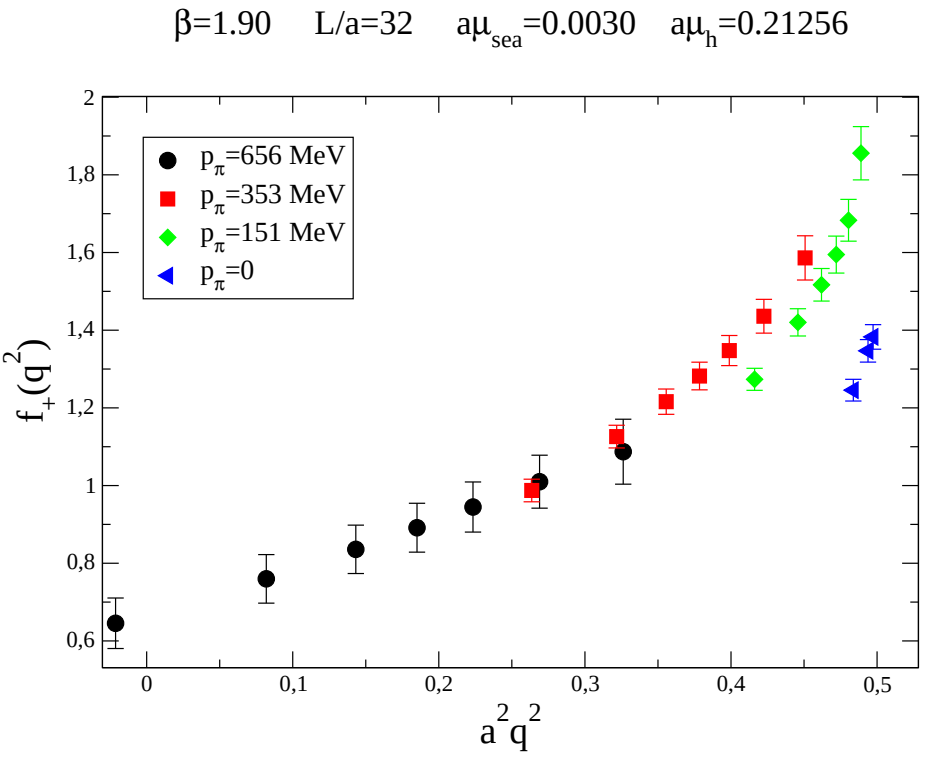

Figure 4.10: q^2 dependence of the vector form factor $f_+(q^2)$ of the $D \to \pi\ell\nu$ decay. The data corresponds to the ensemble A30.32 with $a\mu_h = 0.21256$. Different values of the pion momentum are shown with different colors. The "fishbone" problem (see text) is clearly visible in this plot.

4.3.1 The "fishbone" problem

The next step in the analysis consisted in studying the q^2 dependence of the form factors at fixed quark masses and lattice spaing. We then observed the peculiar behavior shown in fig. 4.10 for the form factor f_+. Namely, there is a clear systematic difference between data corresponding to different values of the momentum of the light meson. This effect proved to be more relevant in the case of the $D \to \pi$ vector form factor than in the $D \to K$ one.

The behavior shown in fig. 4.10 is clearly due to the breaking of Lorentz invariance, and the discretization effects responsible for this behavior should

be described by hypercubic invariants. In terms of the quantities $q_E^2 = \sum_{i=1}^4 q_i^2$ and $\tilde{q}_E^4 = \sum_{i=1}^4 q_i^4$ an example of such hypercubic invariant of $\mathcal{O}(a^2)$ is $\frac{a^4\tilde{q}_E^4}{a^2 q_E^2}$.

By looking at the values of $\frac{a^4\tilde{q}_E^4}{a^2 q_E^2}$ for all the ensembles we noticed that it is very big in some cases. Thus we decided to apply a cut by selecting for further analysis only those data that satisfied the condition $\frac{1}{a^2}\frac{a^4\tilde{q}_E^4}{a^2 q_E^2} < 2.5\,\mathrm{GeV}^2$. In fig. 4.11 we show the effect of this cut for a given ensemble. The full red dots represent the data passing the cut condition. It is clear that the selected data shows a much smoother dependence on q^2.

4.3.2 Global fits

The next step in the analysis consisted in performing global fits of the vector and scalar form factors analysing at the same time their dependences on m_l, a^2 and q^2 in a way similar to what was done in the case of the kaon semileptonic decay. We used a simple polar expression with polynomial corrections in m_l, a^2 and q^2:

$$\begin{aligned} f_+(q^2) &= \frac{f_+(0)}{1-\frac{q^2}{M_V^2}}(1+Aq^2)(1+P_1 m_l + P_2 a^2) \\ f_0(q^2) &= \frac{f_+(0)}{1-\frac{q^2}{M_S^2}}(1+Bq^2)(1+P_1 m_l + P_2 a^2) \end{aligned} \tag{4.41}$$

where M_V and M_S are the vector and scalar resonances that dominate the polar expansion, i.e. the $D^*(2010)$ and $D_0^*(2400)$, and are calculated as

$$M_{S,V} = M_D + \Delta_{S,V} \tag{4.42}$$

where M_D is the D meson mass calculated on the lattice and $\Delta_{S,V}$ is the difference between the experimental value of the scalar (vector) resonance mass, taken from the PDG, and the isospin symmetric D mass.

The comparison between lattice data and the results of the fits, in the case of both $D \to \pi\ell\nu$ and $D \to K\ell\nu$ is shown in fig. 4.12 and we can see that the agreement is good.

In figs. 4.13 and 4.14 we show our results for the form factors extrapolated at the physical point together with experimental data from the Belle [72], Babar [73, 74] and Cleo [75, 76] experiments. Our results for the quantity

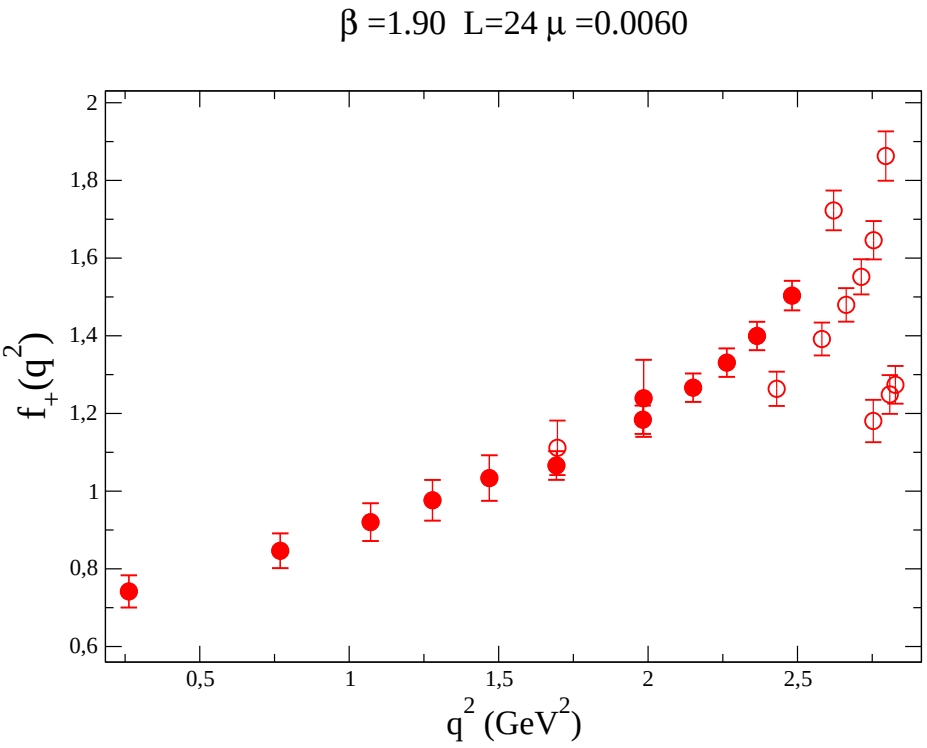

Figure 4.11: q^2 dependence of the vector form factor $f_+(q^2)$ of the $D \to \pi\ell\nu$ decay lattice data points corresponding to the ensemble A60.24 interpolated to the physical charm quark mass. Hollow points represent data excluded basing on the cut on the hypercubic invariant $\frac{a^4\tilde{q}_E^4}{a^2 q_E^2}$ (see text). Selected data (solid points) show a very smooth dependence on q^2.

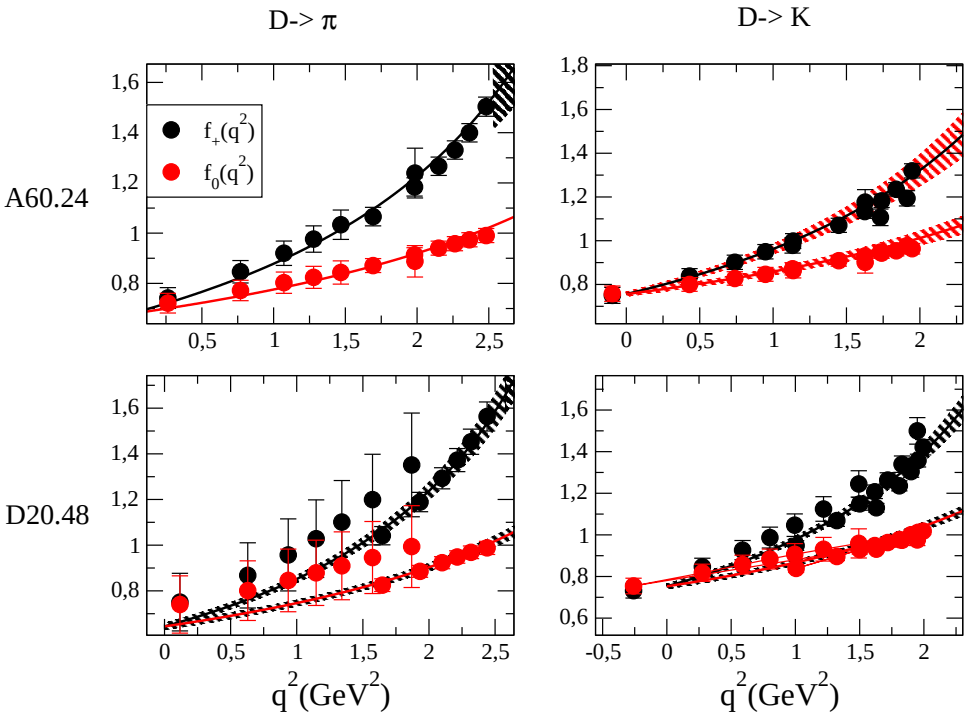

Figure 4.12: Data points of $f_+(q^2)$ and $f_0(q^2)$ for the $D \to \pi\ell\nu$ decay (left panel) and for the $D \to K\ell\nu$ decay (right panel) corresponding to several lattice ensembles. The solid curves represent the results of the fit performed using the ansatz of eq. (4.41), together with their uncertainties (indicated by dashed curves). It can be seen that there is good agreement between data and the results of the fit

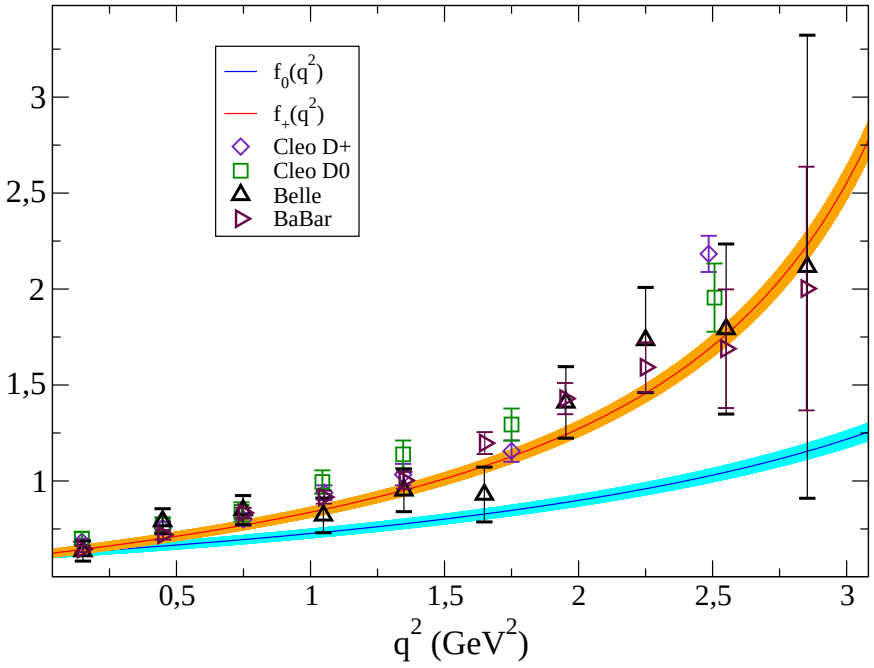

Figure 4.13: Result of the vector and scalar form factors of the $D_\pi \ell\nu$ decay at the physical point as functions of q^2. We also show for comparison the results of the Belle [72], Babar [74] and Cleo [75, 76] experiments.

$f_+(0)$ are

$$\begin{aligned} f_+(0)^{(D\to\pi)} &= 0.610(23), \\ f_+(0)^{(D\to K)} &= 0.747(22), \end{aligned} \tag{4.43}$$

where the uncertainties are only statistical. The estimate of the systematic uncertainty is in progress. These results can be compared with the FLAG averages $f_+(0)^{(D\to\pi)} = 0.666(29)$ and $f_+(0)^{(D\to K)} = 0.747(19)$.

4.3.3 Calculation of V_{cd} and V_{cs}

The results for the form factor at zero 4-momentum transfer can be combined with the experimental averages $f_+(0)|V_{cd}| = 0.146(3)$ and $f_+(0)|V_{cs}| =$

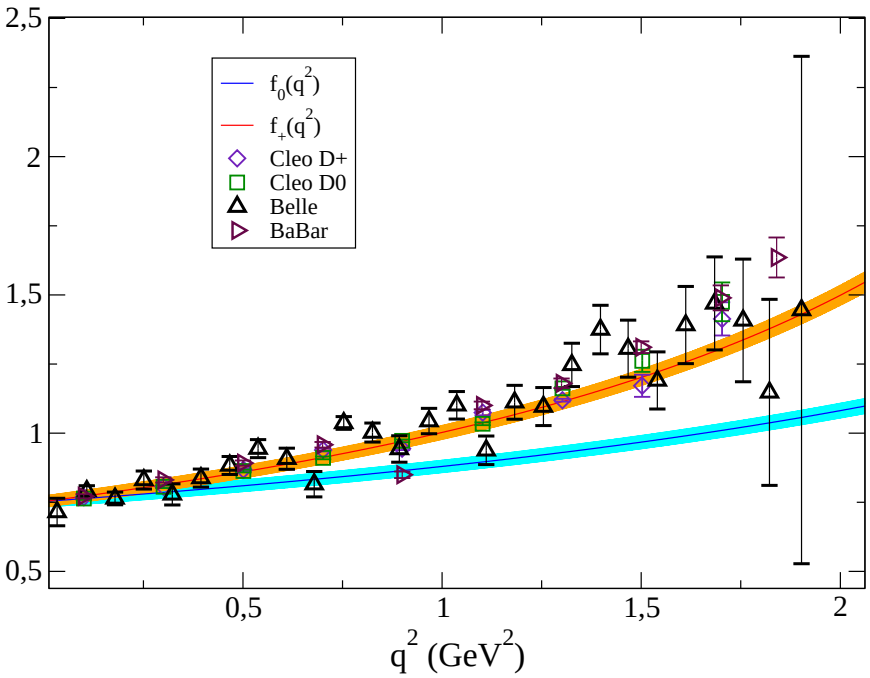

Figure 4.14: Result of the vector and scalar form factors of the $D_K \ell\nu$ decay at the physical point as functions of q^2. We also show for comparison the results of the Belle [72], Babar [73] and Cleo [75, 76] experiments.

0.728(5) [77] in order to calculate the CKM matrix elements. We obtain

$$\begin{aligned} |V_{cd}| &= 0.2336(93), \\ |V_{cs}| &= 0.975(29). \end{aligned} \tag{4.44}$$

These results can then be used to perform a unitarity test of the second row of the CKM matrix, which gives

$$|V_{cd}|^2 + |V_{cs}|^2 + |V_{cb}|^2 = 1.007(57), \tag{4.45}$$

,where $|V_{cb}| = 0.0413(49)$ [36]. This result is in good agreement with the unitarity expectation.

Conclusions

In this work we have presented a lattice QCD calculation of the decay constants of the leptonic decays and of the form factors of the semileptonic decays for K and D mesons. We have used the gauge configurations generated by the European Twisted Mass collaboration with $N_f = 2 + 1 + 1$ dynamical quarks using the Iwasaki gauge action and the Twisted Mass action at maximal twist. We considered three different values of the lattice spacing and pion masses as low as $\simeq 210$MeV. We have extracted the decay constants and the form factors at different values of the quark masses, allowing us to extrapolate to the physical point through either ChPT or a polynomial expansion. We also studied the q^2 dependence of the form factors, by performing a multi-combined fit of its a^2, μ_ℓ and q^2 dependences.

After calculating the decay constant f_K at the phyisical point and evaluating the isospin symmetry breaking effects we combined our result

$$f_{K^+}/f_{\pi^+} = 1.184(16) \tag{4.46}$$

with the experimental result for $|V_{us}/V_{ud}|$ f_{K^+}/f_{π^+} [46] and obtained

$$\frac{|V_{us}|}{|V_{ud}|} = 0.2331(32) \tag{4.47}$$

Then we combined this result with the determination of $|V_{ud}|$ from the superallowed nuclear beta decay, $|V_{ud}| = 0.97417(21)$ [10], to obtain

$$|V_{us}|_{K_{\ell 2}} = 0.2271(31). \tag{4.48}$$

Taken together, the results for $|V_{us}|$ and $|V_{ud}|$ satisfy the unitarity test of the SM at the permille level.

Our analysis of the form factors of the $K_{\ell 3}$ decay gave us the results

$$\begin{aligned} f_+(0) &= 0.9684(59)_{stat+fit}(29)_{syst} = 0.9684(66) \\ \ln C &= 0.1937(113)_{stat+fit}(90)_{syst} = 0.1937(138) \\ \Lambda_+ &= 25.2(1.2)_{stat+fit}(1.1)_{syst} \times 10^{-3} = 25.2(1.6) \times 10^{-3} \end{aligned} \tag{4.49}$$

for the form factor at zero 4-momentum transfer and the slope parameters. Combining our determination of $f_+(0)$ with the experimental average of $f_+(0)|V_{us}|$ [46] gave us

$$|V_{us}|_{K_{\ell 3}} = 0.2234(16), \tag{4.50}$$

which, combined with the determination of $|V_{ud}|$ from the superallowed nuclear beta decay, $|V_{ud}| = 0.97417(21)$ [10], satisfies the unitarity test of the SM at the permille level and is compatible with the result in eq. (4.48) within approximately 1 standard deviation. To check more thorougly the consistency betwen the results obtained in the two analyses, and to compare them with other results in literature, we decided to combine the result of eq. (4.47) with the one of eq. (4.50). This comparison is shown in fig. 4.15. As far as regards the decay constants in the charm sector, we studied the dependences on M_π and a^2 of the quantities f_{D_s}/M_{D_s} and $(f_{D_s}/f_D)/(f_K/f_\pi)$. Combining these quantities determined at the physical point with the experimental value of M_{D_s}, and our determination of f_K/f_π of eq. (3.6), we obtained

$$f_{D_s} = 247.2(4.1)\,\text{MeV} \tag{4.51}$$

$$f_{D_s}/f_D = 1.192(22), \tag{4.52}$$

from which we also obtain

$$f_D = 207.4(3.8)\,\text{MeV}\ . \tag{4.53}$$

Eqs. (4.51) and (4.53) can then be combined with experimental data of $f_{D_s}|V_{cs}|$ and $f_D|V_{cd}|$ in order to get

$$\begin{aligned} |V_{cd}|_{\text{lep}} &= 0.2221(67), \\ |V_{cs}|_{\text{lep}} &= 1.014(24). \end{aligned} \tag{4.54}$$

Using $|V_{cb}| = 0.0413(49)$ [36], the sum of the squares of the second-row CKM elements turns out to be equal to

$$|V_{cd}|^2 + |V_{cs}|^2 + |V_{cb}|^2 = 1.08\ (5)\ , \tag{4.55}$$

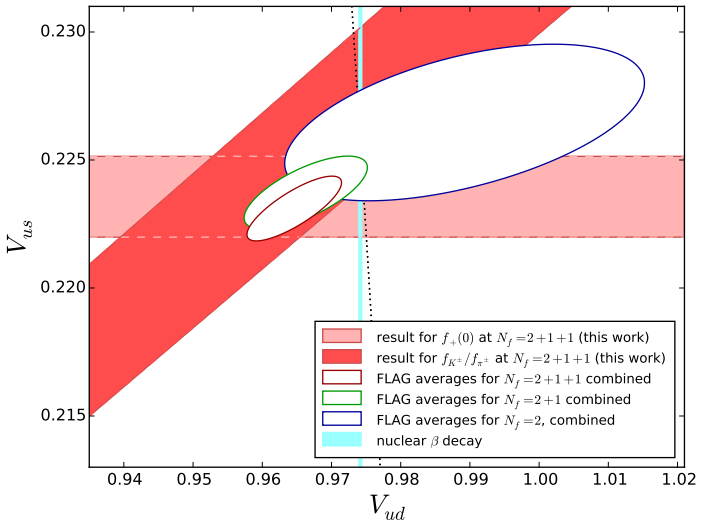

Figure 4.15: The combination of our results of V_{us}/V_{ud} (coming from the analysis of the kaon decay constant), represented by the red area, and V_{us} (coming from the analysis of the kaon form factors), represented by the pink area. We also show the combinations of the FLAG averages for $|V_{us}|/|V_{ud}|$ and V_{us} corresponding to $N_f = 2$ (blue ellipse), $N_f = 2 + 1$ (green ellipse) and $N_f = 2+1+1$ (dark red ellipse). All the areas and the ellipses represent a confidence level of 68%. We also plot the phenomenological constraints given by the unitarity (black dotted line) and the value of V_{ud} as determined in [10] (azure line).

showing good agreement with unitarity.

Our preliminary study of the form factors of the $D \to \pi\ell\nu$ and $D \to K\ell\nu$ decays gave the results

$$\begin{aligned} f_+(0)^{(D\to\pi)} &= 0.610(23), \\ f_+(0)^{(D\to K)} &= 0.747(22), \end{aligned} \tag{4.56}$$

where the uncertainties are only statistical. The estimate of the systematic uncertainty is in progress. The results for the form factor at zero 4-momentum transfer can be combined with the experimental averages $f_+(0)|V_{cd}| = 0.146(3)$ and $f_+(0)|V_{cs}| = 0.728(5)$ [77] in order to calculate the CKM matrix elements. We obtain

$$\begin{aligned} |V_{cd}|_{\text{semilep}} &= 0.2336(93), \\ |V_{cs}|_{\text{semilep}} &= 0.975(29). \end{aligned} \tag{4.57}$$

These results can then be used to perform a unitarity test of the second row of the CKM matrix, which gives

$$|V_{cd}|^2 + |V_{cs}|^2 + |V_{cb}|^2 = 1.007(57), \tag{4.58}$$

where $|V_{cb}| = 0.0413(49)$ [36]. This result is in good agreement with the unitarity expectation.

In conclusion, there are still several issues that will be interesting to address. During the last few years some collaborations published the first results of lattice calculations with pion masses equal (or very close) to the physical one. Simulating at the physical point, and thus decreasing the systematic uncertainty induced by the chiral extrapolation, is one of the priorities in order to improve the present work. Another systematic effect that could be further addressed is the one induced by the continuum extrapolation by simulating at lower values of the lattice spacing.

Other improvements concerning the present analysis of the semileptonic decays form factors are: (i) a more thorough and detailed study of the "fish-bone" problem, described in sec. 4.3.1,(ii) a study of alternative ways to combine the vector and the scalar current matrix elements in order to decrease statistical errors of lattice data, and lastly (iii) the inclusion in the analysis of the tensor current form factor in order to study processes like $K \to \pi\ell^+\ell^-$ and $B \to K\ell^+\ell^-$. These decays, being suppressed by the GIM mechanism, are possible sources of New Physics and thus worth studying.

Bibliography

[1] G. Aad *et al.* [ATLAS Collaboration], Phys. Lett. B **716** (2012) 1 [arXiv:1207.7214 [hep-ex]].

[2] S. Chatrchyan *et al.* [CMS Collaboration], Phys. Lett. B **716** (2012) 30 [arXiv:1207.7235 [hep-ex]].

[3] G. Aad *et al.* [ATLAS and CMS Collaborations], Phys. Rev. Lett. **114** (2015) 191803 [arXiv:1503.07589 [hep-ex]].

[4] N. Cabibbo, Phys. Rev. Lett. **10** (1963) 531.

[5] M. Kobayashi and T. Maskawa, Prog. Theor. Phys. **49** (1973) 652.

[6] S. L. Glashow, J. Iliopoulos and L. Maiani, Phys. Rev. D **2** (1970) 1285.

[7] C. Jarlskog, Phys. Rev. Lett. **55** (1985) 1039.

[8] C. Jarlskog, Z. Phys. C **29** (1985) 491.

[9] L. Wolfenstein, Phys. Rev. Lett. **51** (1983) 1945.

[10] J. C. Hardy and I. S. Towner, Phys. Rev. C **79** (2009) 055502 [arXiv:0812.1202 [nucl-ex]].

[11] K. G. Wilson, Phys. Rev. D **10** (1974) 2445.

[12] H. B. Nielsen and M. Ninomiya, Phys. Lett. B **105** (1981) 219.

[13] K. Symanzik, Nucl. Phys. B **226** (1983) 187.

[14] R. Frezzotti *et al.* [Alpha Collaboration], JHEP **0108** (2001) 058 [hep-lat/0101001].

[15] R. Frezzotti and G. C. Rossi, JHEP **0408** (2004) 007 [hep-lat/0306014].

[16] G. Martinelli, C. Pittori, C. T. Sachrajda, M. Testa and A. Vladikas, Nucl. Phys. B **445** (1995) 81 [hep-lat/9411010].

[17] P. F. Bedaque, Phys. Lett. B **593** (2004) 82 [arXiv:nucl-th/0402051].

[18] G. M. de Divitiis, R. Petronzio and N. Tantalo, Phys. Lett. B **595** (2004) 408 [arXiv:hep-lat/0405002].

[19] R. Baron *et al.*, JHEP **1006** (2010) 111 [arXiv:1004.5284 [hep-lat]].

[20] Y. Iwasaki, Nucl. Phys. B **258** (1985) 141.

[21] R. Frezzotti and G. C. Rossi, Nucl. Phys. Proc. Suppl. **128** (2004) 193 [hep-lat/0311008].

[22] R. Frezzotti and G. C. Rossi, JHEP **0410** (2004) 070 [hep-lat/0407002].

[23] R. Baron *et al.* [European Twisted Mass Collaboration], Comput. Phys. Commun. **182** (2011) 299 [arXiv:1005.2042 [hep-lat]].

[24] K. Osterwalder and E. Seiler, Annals Phys. **110** (1978) 440.

[25] B. Jegerlehner, hep-lat/9612014.

[26] K. Jansen *et al.* [XLF Collaboration], JHEP **0509** (2005) 071 [hep-lat/0507010].

[27] N. Carrasco *et al.* [European Twisted Mass Collaboration], Nucl. Phys. B **887** (2014) 19 [arXiv:1403.4504 [hep-lat]].

[28] C. McNeile *et al.* [UKQCD Collaboration], Phys. Rev. D **73** (2006) 074506 [hep-lat/0603007].

[29] N. Carrasco *et al.*, Phys. Rev. D **91** (2015) 5, 054507 [arXiv:1411.7908 [hep-lat]].

[30] G. Colangelo, S. Durr and C. Haefeli, Nucl. Phys. B **721** (2005) 136 [hep-lat/0503014].

[31] S. Aoki *et al.*, Eur. Phys. J. C **74** (2014) 2890 [arXiv:1310.8555 [hep-lat]].

[32] B. Blossier *et al.* [ETM Collaboration], JHEP **0907** (2009) 043 [arXiv:0904.0954 [hep-lat]].

[33] E. Follana *et al.* [HPQCD and UKQCD Collaborations], Phys. Rev. Lett. **100** (2008) 062002 [arXiv:0706.1726 [hep-lat]].

[34] A. Bazavov *et al.* [MILC Collaboration], PoS LATTICE **2010** (2010) 074 [arXiv:1012.0868 [hep-lat]].

[35] R. Arthur *et al.* [RBC and UKQCD Collaborations], Phys. Rev. D **87** (2013) 094514 [arXiv:1208.4412 [hep-lat]].

[36] K. A. Olive *et al.* [Particle Data Group Collaboration], Chin. Phys. C **38** (2014) 090001.

[37] C.W. Bernard and M.F.L. Golterman, Phys. Rev. D **46** (1992) 853 [hep-lat/9204007].

[38] J. Bijnens, N. Danielsson and T.A. Lahde, Phys. Rev. D **73** (2006) 074509 [hep-lat/0602003].

[39] J. Gasser and G.R.S. Zarnauskas, Phys. Lett. B **693** (2010) 122 [arXiv:1008.3479 [hep-ph]].

[40] N. Carrasco, V. Lubicz, G. Martinelli, C. T. Sachrajda, N. Tantalo, C. Tarantino and M. Testa, arXiv:1502.00257 [hep-lat].

[41] G. M. de Divitiis *et al.* [RM123 Collaboration], JHEP **1204** (2012) 124 [arXiv:1110.6294 [hep-lat]];

[42] G. M. de Divitiis *et al.* [RM123 Collaboration], Phys. Rev. D **87** (2013) 11, 114505 [arXiv:1303.4896 [hep-lat]].

[43] S. Durr *et al.*, Phys. Rev. D **81** (2010) 054507 [arXiv:1001.4692 [hep-lat]].

[44] A. Bazavov *et al.* [MILC Collaboration], Phys. Rev. Lett. **110** (2013) 172003 [arXiv:1301.5855 [hep-ph]].

[45] R. J. Dowdall, C. T. H. Davies, G. P. Lepage and C. McNeile, Phys. Rev. D **88** (2013) 074504 [arXiv:1303.1670 [hep-lat]].

[46] M. Moulson, arXiv:1411.5252 [hep-ex].

[47] P. Dimopoulos *et al.* [ETM Collaboration], PoS LATTICE **2013** (2013) 314 [arXiv:1311.3080 [hep-lat]].

[48] D. Becirevic *et al.*, Phys. Lett. B **563** (2003) 150 [hep-ph/0211271].

[49] N. Carrasco *et al.* [ETM Collaboration], JHEP **1403** (2014) 016 [arXiv:1308.1851 [hep-lat]].

[50] C. T. H. Davies, C. McNeile, E. Follana, G. P. Lepage, H. Na and J. Shigemitsu, Phys. Rev. D **82** (2010) 114504 [arXiv:1008.4018 [hep-lat]].

[51] A. Bazavov *et al.* [Fermilab Lattice and MILC Collaborations], Phys. Rev. D **85** (2012) 114506 [arXiv:1112.3051 [hep-lat]].

[52] A. Bazavov *et al.* [Fermilab Lattice and MILC Collaborations], Phys. Rev. D **90** (2014) 7, 074509 [arXiv:1407.3772 [hep-lat]].

[53] G. Colangelo, U. Wenger and J.M.S. Wu, Phys. Rev. D **82** (2010) 034502 [arXiv:1003.0847 [hep-lat]].

[54] H. Na, C. T. H. Davies, E. Follana, G. P. Lepage and J. Shigemitsu, Phys. Rev. D **86** (2012) 054510 [arXiv:1206.4936 [hep-lat]].

[55] S. R. Sharpe and Y. Zhang, Phys. Rev. D **53** (1996) 5125 [hep-lat/9510037].

[56] S. R. Sharpe, private communication.

[57] J. L. Rosner and S. Stone, arXiv:1309.1924 [hep-ex]. (See also Ref. [36]).

[58] J. Gasser and H. Leutwyler, Nucl. Phys. B **250** (1985) 517.

[59] J. Gasser and H. Leutwyler, Nucl. Phys. B **250** (1985) 465.

[60] V. Lubicz *et al.* [ETM Collaboration], PoS LATTICE **2010** (2010) 316 [arXiv:1012.3573 [hep-lat]].

[61] J. M. Flynn *et al.* [RBC and UKQCD Collaborations], Nucl. Phys. B **812** (2009) 64 [arXiv:0809.1229 [hep-ph]].

[62] C. G. Callan and S. B. Treiman, Phys. Rev. Lett. **16** (1966) 153.

[63] C. Bourrely, I. Caprini and L. Lellouch, Phys. Rev. D **79** (2009) 013008 [Phys. Rev. D **82** (2010) 099902] [arXiv:0807.2722 [hep-ph]].

[64] R. Frezzotti *et al.* [ETM Collaboration], Phys. Rev. D **79** (2009) 074506 [arXiv:0812.4042 [hep-lat]].

[65] V. Bernard, M. Oertel, E. Passemar and J. Stern, Phys. Lett. B **638** (2006) 480 [hep-ph/0603202].

[66] F. Ambrosino *et al.* [KLOE Collaboration], Eur. Phys. J. C **71** (2011) 1604 [arXiv:1011.2668 [hep-ex]].

[67] E. Abouzaid *et al.* [KTeV Collaboration], Phys. Rev. D **83** (2011) 092001 [arXiv:1011.0127 [hep-ex]].

[68] F. Ambrosino *et al.* [KLOE Collaboration], Phys. Lett. B **636** (2006) 166 [hep-ex/0601038].

[69] J. R. Batley *et al.* [NA48 Collaboration], Phys. Lett. B **544** (2002) 97 [hep-ex/0208009].

[70] V. A. Uvarov *et al.*, Phys. Atom. Nucl. **77** (2014) 725 [Yad. Fiz. **77** (2014) 765].

[71] M. Antonelli *et al.* [FlaviaNet Working Group on Kaon Decays Collaboration], Eur. Phys. J. C **69** (2010) 399 [arXiv:1005.2323 [hep-ph]].

[72] L. Widhalm *et al.* [Belle Collaboration], Phys. Rev. Lett. **97** (2006) 061804 [hep-ex/0604049].

[73] B. Aubert *et al.* [BaBar Collaboration], Phys. Rev. D **76** (2007) 052005 [arXiv:0704.0020 [hep-ex]].

[74] J. P. Lees *et al.* [BaBar Collaboration], Phys. Rev. D **91** (2015) 5, 052022 [arXiv:1412.5502 [hep-ex]].

[75] D. Besson *et al.* [CLEO Collaboration], Phys. Rev. D **80** (2009) 032005 [arXiv:0906.2983 [hep-ex]].

[76] S. Dobbs *et al.* [CLEO Collaboration], Phys. Rev. D **77** (2008) 112005 [arXiv:0712.1020 [hep-ex]].

[77] Y. Amhis *et al.* [Heavy Flavor Averaging Group Collaboration], arXiv:1207.1158 [hep-ex].